MODELAGEM E ANÁLISE DE CONECTIVIDADE EM REDES SEM FIOS OBSTRUÍDAS

MARCELO GABRIEL ALMIRON

MODELAGEM E ANÁLISE DE CONECTIVIDADE EM REDES SEM FIOS OBSTRUÍDAS

Tese apresentada ao Programa de Pós-Graduação em Ciência da Computação do Instituto de Ciências Exatas da Universidade Federal de Minas Gerais como requisito parcial para a obtenção do grau de Doutor em Ciência da Computação.

Orientadora: Olga Nikolaevna Goussevskaia
Coorientadores: Antonio A.F. Loureiro &
Alejandro C. Frery

Belo Horizonte, MG

Maio de 2014

MARCELO GABRIEL ALMIRON

MODELING AND CONNECTIVITY ANALYSIS IN OBSTRUCTED WIRELESS NETWORKS

Thesis presented to the Graduate Program in Computer Science of the Federal University of Minas Gerais in partial fulfillment of the requirements for the degree of Doctor in Computer Science.

Advisor: Olga Nikolaevna Goussevskaia
Co-Advisors: Antonio A.F. Loureiro & Alejandro C. Frery

Belo Horizonte, MG
May 2014

Ficha catalográfica elaborada pela Biblioteca do ICEx - UFMG

Almiron, Marcelo Gabriel

A449m Modelagem e Análise de Conectividade em Redes Sem Fios Obstruídas / Marcelo Gabriel Almiron. — Belo Horizonte, MG, 2014
xx, 73 f. : il. ; 29cm

Tese (Doutorado) — Universidade Federal de Minas Gerais - Departamento de Ciência da Computação

Orientadora: Olga Nikolaevna Goussevskaia
Coorientadores: Antonio Alfredo Ferreira Loureiro
Alejandro César Frery Orgambide

1. Computação - Teses. 2. Redes de computadores - Teses. 3. Sistemas de comunicação sem fios - Teses. I. Orientador. II. Coorientador. III. Título.

529.6*22(043)

UNIVERSIDADE FEDERAL DE MINAS GERAIS
INSTITUTO DE CIÊNCIAS EXATAS
PROGRAMA DE PÓS-GRADUAÇÃO EM CIÊNCIA DA COMPUTAÇÃO

FOLHA DE APROVAÇÃO

Modeling and connectivity analysis in obstructed wireless networks

MARCELO GABRIEL ALMIRON

Tese defendida e aprovada pela banca examinadora constituída pelos Senhores:

PROFA. OLGA NIKOLAEVNA GOUSSEVSKAIA - Orientadora
Departamento de Ciência da Computação - UFMG

PROF. ANTONIO ALFREDO FERREIRA LOUREIRO - Coorientador
Departamento de Ciência da Computação - UFMG

PROF. ALEJANDRO CÉSAR FRERY ORGAMBIDE - Coorientador
Departamento de Tecnologia da Informação - UFAL

PROF. JOSE D. P. ROLIM
Departamento de Ciência da Computação - University of Geneva

PROF. RENATO ANTÔNIO CELSO FERREIRA
Departamento de Ciência da Computação - UFMG

PROF. RENATO MARTINS ASSUNÇÃO
Departamento de Ciência da Computação - UFMG

PROF. VALMIR CARNEIRO BARBOSA
COPPE - UFRJ

Belo Horizonte, 16 de maio de 2014.

A mis padres, Stella Maris y Pedro José.

Acknowledgments

First, I thank my parents, Stella Maris and Pedro José, my sisters, Marité and Laura, and my brother, José. They gave me all means to achieve what I dreamed about in my life, and I will always be thankful.

Special thanks to my mentors, Profa. Olga N. Goussevskaia, Prof. Antonio A.F. Loureiro, Prof. Alejandro C. Frery and Prof. José Rolim. I was very fortunate for being surrounded by excellent people and researchers with plurality of thinking and areas of expertise.

I thank my friends from UFMG: Anderson, Anna, Alyson, Bruno (Lopes and Silva), Celso, César, Christian, Clayson, Daniel (Galinkin and Guidoni), Eduardo, Evellyn, Felipe, Fernanda, Fernando, Flávio, Guilherme, Heitor, Ilo, Izabela, John, Kássio, Laura, Leandro, Letícia, Lorena, Luciana, Max, Marcos, Pedro (Silva and Stancioli), Rafael (Colares, Santin and Siqueira), Rodolfo, Thiago, Tiago, Vinícius and Zilton. It was and will continue being a wonderful group!

My thanks also to Aubin, Cristina, Eugenio, Hakob, Kasun, Konstantinos, Marios, Orestis, Pierre and Tigran, for their friendship and shared moments during my stay in University of Geneva.

Finally, my very special thanks to Klárka for supporting me in the last and more critical moment making me feel her love at every second, on occasions, with the Atlantic Ocean between us.

Resumo

Propriedades de conectividade de redes sem fio em espaços abertos normalmente são modeladas utilizando grafos aleatórios geométricos, e já foram analisadas em profundidade em diferentes estudos. Esses cenários, no entanto, não representam, no geral, situações reais encontradas na prática, tais como ambientes urbanos ou espaços fechados, que são profundamente afetados por obstáculos. Como alternativa, propomos um modelo para redes sem fio ad hoc obstruídas, formadas por um conjunto de nós posicionados de maneira aleatória numa grade, onde todos os nós compartilham um mesmo raio de transmissão. Para o posicionamento dos nós no ambiente, todos os segmentos são considerados como sendo unidimensionais, mas para fins de comunicação, adicionamos um parâmetro ϵ para modelar a largura dos segmentos. Nós mostramos como o modelo resultante pode ser utilizado para estudar as propriedades destas redes de comunicação de maneira analítica e para simular uma variedade de topologias de rede com o intuito de avaliar o desempenho de protocolos de comunicação nos cenários acima mencionados.

Para calcular a probabilidade de conectividade em interseções de segmentos ($\Pr(I_{\text{con}})$), propomos três modelos geométricos diferentes: os modelos Max-Norm, Line-of-Sight (LoS) e Triangular. Mostramos a dificuldade de computo de $\Pr(I_{\text{con}})$ sob o modelo LoS, e calculamos limites inferiores para $\Pr(I_{\text{con}})$ sob os modelos Max-Norm e Triangular, com o respectivo limite superior no erro de aproximação.

Adicionalmente, introduzimos uma abstração na grade e aplicamos a teoria de percolação para calcular a raio mínimo de transmissão que gera conectividade, no gráfo de comunicações, com alta probabilidade. Esta solução exige um mínimo de visibilidade nos cruzamentos dentre segmentos, e esta visibilidade depende do parâmetro ϵ. Com isto, calculamos a visibilidade mínima exigida para ter conectividade quando utilizamos o raio de transmissão mínimo derivado. Este raio de transmissão especifico é conhecido como o alcance de transmissão mínimo para conectividade (em inglês, Critical Transmission Range (CTR)), e provamos que o CTR para conectividade derivado não depende do modelo geométrico em cruzamentos. Fizemos um estudo da escalabilidade

de redes obstruídas dentro do modelo proposto e desenvolvemos métodos analíticos para determinar se há possibilidade de obter conectividade com alta probabilidade em topologias homogêneas de rede para determinadas combinações de características, tais como largura dos segmentos, tamanho da grade e limite tecnológico do raio máximo de transmissão.

Abstract

Connectivity properties of wireless networks in open space are typically modeled using geometric random graphs and have been analyzed in depth in different studies. Such scenarios, however, do not often represent situations encountered in practice, like urban environments or indoor spaces, which are deeply affected by obstacles. As an alternative, we propose a model for obstructed wireless ad hoc networks consisting of a set of nodes deployed at random in a grid, all of them sharing a common transmission range. For positioning the nodes in the field, all segments are considered as being one-dimensional, but for communication purposes, we add a parameter ϵ to model the segments' width. We show how the resulting model can be used to study properties of such communication networks analytically and to simulate a variety of network topologies for performance evaluation of communication protocols in the aforementioned scenarios.

In order to compute the probability of connectivity at segments' intersections ($\Pr(I_{\text{con}})$), we propose three different geometric models, namely, the Max-Norm, LoS and Triangular models. We show the difficulty of computing $\Pr(I_{\text{con}})$ under the LoS, and we compute tight lower bounds for $\Pr(I_{\text{con}})$ under the Max-Norm and Triangular models, with the respective upper bound of the approximation error.

Additionally, we introduce an abstraction on the grid and apply percolation theory to compute the minimum transmission range that generates communication graphs that are connected with high probability (w.h.p.). The solution requires a minimal visibility at intersections, depending on the parameter ϵ. We compute the minimal visibility required to have connectivity using the derived minimum transmission range. This particular transmission range is known as the CTR for connectivity, and we prove that the derived CTR for connectivity does not depends on the geometrical model at intersections. We performed a study of the scalability of obstructed networks within the proposed model and developed analytical methods to determine the possibility of obtaining connectivity w.h.p. in homogeneous topologies for specific combinations of characteristics, e.g. segments' width, grid size and the maximum transmission range.

List of Figures

Contents

Chapter 1

Introduction

When modeling and analyzing different problems in wireless communication networks, regardless of their topology (random [Santi and Blough, 2003], regular [Gupta and Kumar, 2000], or arbitrary [Goussevskaia et al., 2009]), it has been typically assumed that communication nodes are deployed in an open space without obstacles. This assumption is quite natural, given that an open space represents the "purest" scenario of wireless communication, in which the communication channel is shared among all communication nodes, a distinguishing and challenging characteristic of wireless technology. Moreover, wireless signal propagation and interference in non-obstructed spaces can be represented by simpler, easier to analyze models [Haenggi and Ganti, 2009]. This generates possibilities for more generalized theories and results that can be applied to many network instances of large sizes.

In reality, however, wireless networks are rarely deployed in completely open spaces. Many wireless networks operate in highly obstructed environments, such as dense urban areas and indoor spaces, not to mention networks deployed in constrained spaces like tunnels and subways, or other specialized networks, like smart grid communication networks. The behavior of both wireless signal and interference when obstacles are present is more complex and, therefore, more difficult to model and analyze.

Relatively few attempts have been made to analyze obstructed wireless networks, many of which are quite complex and not easily extended to generic scenarios [Nekoui and Pishro-Nik, 2009]. The next Section 1.1 presents the more remarkable efforts in this direction, considering the gaps and discussing the requirements of a new approach. That section finish with a brief description of the model we propose, together with implications from the application and analytical point of view. Afterwards, in Section 1.2, we argue about the importance of topological characterizations of ad hoc networks and present Topology Control (TC) as an essential mechanism in this context. We dedicate

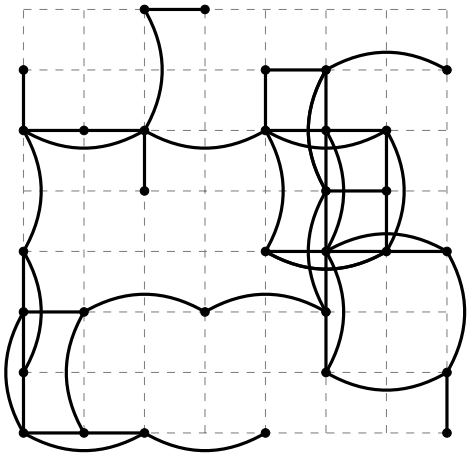

Figure 1.1. Line-of-sight network model of Frieze et al., with $p = 0.45$ and $\omega = 2$, on a grid of 8×8.

the third section of this chapter to present our contribution and explain, in a nutshell, the structure of our work.

1.1 Modeling Obstructed Networks

One interesting model for obstructed wireless networks is the so-called "line-of-sight network", proposed by Frieze et al. [2007] and further studied by Bollobás et al. [2009]. In this model, the network is represented by a grid of size $[g] \times [g]$, and a random subset of $[g]^2$ is obtained by selecting each point (x, y) with probability p, independently of the rest. Then, each vertex of the grid is assumed to be a node in the network, and each node has a deterministic communication range of ω blocks. Figure 1.1 shows an instance of the line-of-sight network. Notice that, under this model, only vertical and horizontal links are allowed. Moreover, if $\omega = 1$, i.e., a node can only see neighboring points, then the model reduces to the well-studied problem of (site) percolation[1] on a lattice square [Grimmett, 1999]. (We will see percolation models from close in Section 2.2, since we apply this theory to derive part of our results.) Among other characterizations, Frieze et al. [2009] derive asymptotic bounds for k-connectivity of such networks.

The line-of-sight network model manage to represent obstacles in a very simple way. The advantage is that the obtained random structure has place on a discrete domain and maintain similarity with a site percolation model. The drawback is that the requirement of deploying nodes only at intersections limits the application of this model.

[1] Percolation means existence of a giant connected component of infinite size.

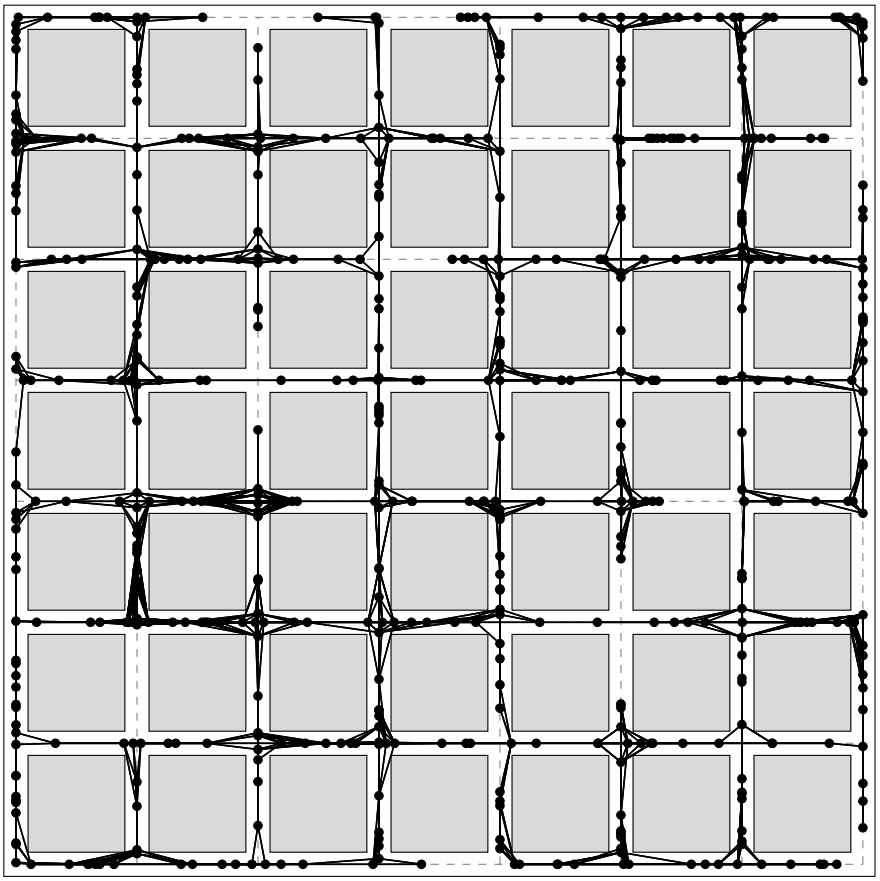

Figure 1.2. An instance of an obstructed wireless network with density $\mu = 5$ deployed in an 8×8 scenario and using transmission range $r = 0.65$. Gray areas represent the obstacles; regions in the space with infinite path loss. The communication criterion corresponds to our LoS model.

Our judgment is that more general models for obstructed wireless networks are required; models able to represent, and offer tools to characterize, ad hoc networks deployed in urban environments. In this direction, we propose an obstructed network model that considers a grid of size $[g] \times [g]$, where nodes are deployed uniformly at random over segments and intersections (see Figure 1.2). Segments and intersections have a width controlled by the parameter ϵ. Nevertheless, we consider that nodes are deployed over one-dimensional lines, whilst the density of the network is controlled by the μ parameter. Figure 1.2 shows an instance of our obstructed network model for $g = 8$. Links between nodes are allowed only for those nodes which mutual distance does not exceed r and at the same time have visual contact. Observe that the visibility restriction is reflected in the figure by the absence of links intersecting gray boxes.

This model has several appealing aspects. From the point of view of applications, it provides a realistic representation of environments with regularly spaced obstacles.

As opposed to the model in Frieze et al. [2009], for instance, where nodes are placed only at segments' intersections (and there are no nodes along the segments themselves), placing several nodes along a segment might better represent connectivity properties, especially if low-power/short-range radios are used. Therefore, this model can be potentially useful in simulating and analyzing different types of network scenarios, in particular, those that are comprised of segments of one-dimensional arrays of nodes and regularly distributed arrays of obstacles.

From the point of view of analysis, our model mixes two basic elements. On the one hand, it might be viewed as a percolation model on a lattice (see Section 2.2), where vertices and edges are random objects that occur with probabilities p_s and p_b, respectively. On the other hand, it is an intrinsically geometric model on individual segments and intersections of the grid: on the segments, we have a line topology, where connectivity is determined by node density. On the intersections, we have a two-dimensional scenario, where connectivity depends on node density and on the width parameter, ϵ, as well. This division into "percolation" and "geometry" allows us to simplify the model and analyze important properties of the network, such as local connectivity probabilities and the minimum transmission range that warrants, with high probability (w.h.p.), connectivity in the overall network.

1.2 The Role of Topology Control

The relevance of ad hoc networks in society is growing with the advances of communication technology. As a consequence, big effort from researchers in academia and industry resulted in the design and standardization of basic mechanisms that enable wireless ad hoc communication, like IEEE 802.11 and Bluetooth, among others [Santi, 2005a]. Despite this fact, applications based on ad hoc networking paradigm are still scarce. This scarcity occurs, in part, because most of the challenges to be addressed in practical implementations and real scenarios are still waiting to be solved.

In open space environments, researchers proposed methods for addressing energy conservation, interferences and scalability. These challenges, considered the most important for ad hoc networking, give place to a set of methods and techniques known as Topology Control (TC) [see Santi, 2005a,b; Labrador and Wightman, 2009]. More specifically, TC techniques were motivated by the necessity of efficient use of the scarce energy resources available in wireless ad hoc networks. Since Gilbert [1961], several studies confirmed that, from the energy-consumption point of view, it is better to communicate using short multi-hop paths between nodes in an ad hoc network. In this

context, TC techniques were developed to identify and remove energy-inefficient edges from the communication graph while maintaining some desired structural property. As a side effect, TC techniques increase the capacity of the network by eliminating high interfering long-distance links.

Under homogeneous ad hoc networks, that is, networks composed by nodes with equivalent communication hardware and configuration, the most important TC technique consists in the determine the so-called Critical Transmission Range (CTR) for Connectivity. The "CTR for Connectivity" problem consists in determining the minimal common transmission range, r_c, that warrants w.h.p. a unique connected component in the network. We will see later, in Chapter 4, what this exactly means and how we can compute r_c. Nevertheless, we anticipate here that some abstraction is required to tackle this problem, and part of this abstraction consists on characterizing local connectivity properties, and only then face the problem of connectivity in the overall network.

1.3 Contribution and Organization

After identifying a gap in contributions of researchers toward the modeling of obstructed ad hoc networks, we proposed the framework briefly described in the last part of Section 1.1. Additionally, three different modeling approaches for the communication of any two nodes, deployed in such environment, are proposed, namely, the Max-Norm, LoS, and Triangular models.

The Max-Norm is the simplest of the three models and it provides a linearization of the concept of visualization. This abstraction do not consider links between nodes which scalar coordinates difference exceed the width ϵ. For some scenario this is not a big compromise, but for some scenarios it is. The LoS model is the most realistic among the three and it is the one we use for implementing our simulations. However, it is too complex to be useful analytically, as we will see in Section 3.1.2. Basically, this model state that two nodes are able to communicate if there is a line of sight between them and, additionally, if the Euclidean distance is smaller than, or equal to, the transmission range r. The Triangular model represents a compromise between the two previous models: it is simple enough to be treated analytically and, at the same time, offers an accurate approximation to what we expect to obtain from the LoS model, especially in high-density scenarios.

Our contributions can be summarized as follows:

- We analyze an alternative model for obstructed wireless environments, based on

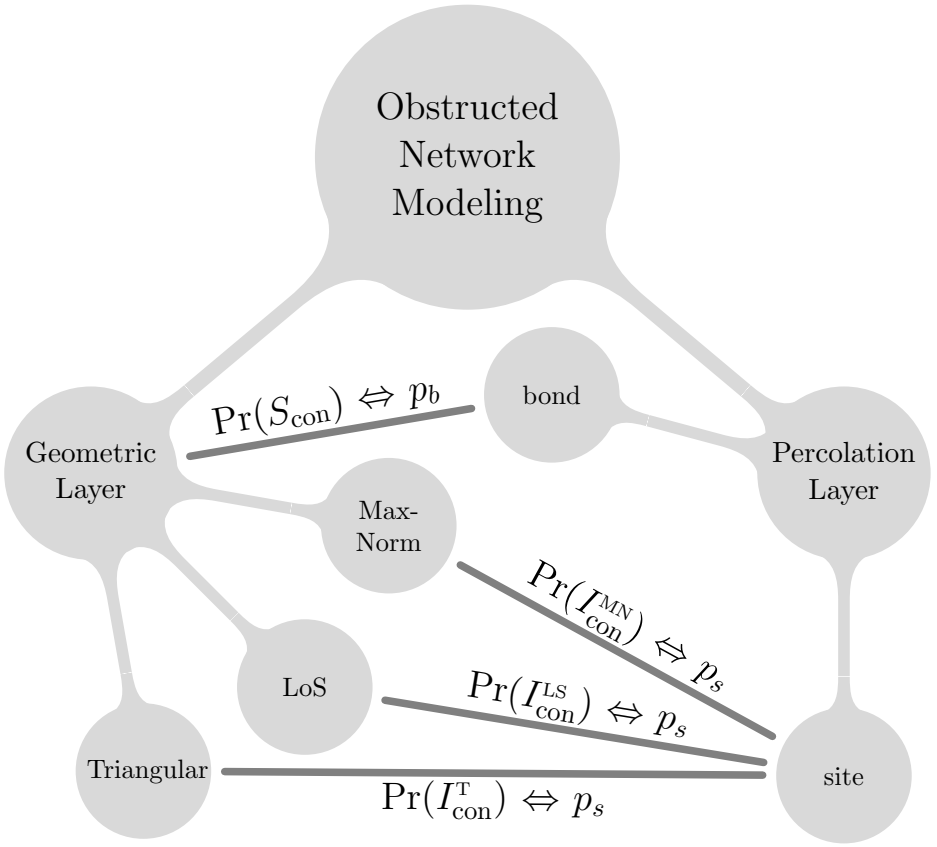

Figure 1.3. Modeling obstructed wireless networks so as to derive the CTR for Connectivity.

a grid structure of one-dimensional segments and two-dimensional intersections;

- We combine elements from percolation theory and geometry to analyze connectivity properties in this model;
- We propose three different geometric models for communication between nodes in the network;
- We derive tight approximation bounds for probability of connectivity at intersections;
- We derive the Critical Transmission Range for connectivity in the overall network;
- We discover the necessity of heterogeneous networks for large scale scenarios with low-power transmitters, and;
- We simulate different network scenarios and validate our analytical results.

The mind map of Figure 1.3 offers a visualization of how we derive the main result of this thesis, the CTR for connectivity under an obstructed environment. We model the network in two different layers, the geometric and percolation layers. In the geometric layer, we compute the probability of connectivity at segments and intersections, denoted by $\Pr(S_{\text{con}})$ and $\Pr(I_{\text{con}})$, respectively. Since differences between connectivity models occur only for the visualization criterion, connectivity at segments does not change over the models, and neither $\Pr(S_{\text{con}})$ does. On the other hand, to differentiate each case while considering connectivity at intersections, denoted by I_{con}, we specify the model under which the event is occurring by simply adding a superscript. In this sense $\Pr(I_{\text{con}}^{\text{MN}})$, $\Pr(I_{\text{con}}^{\text{LS}})$ and $\Pr(I_{\text{con}}^{\text{T}})$ denote the probabilities of connectivity at intersections for the Max-Norm, LoS and Triangular models, respectively. We find expressions for all these in Chapter 3. Section 3.1.1 presents the probabilities for connectivity at intersections for the Max-Norm model, whilst some arguments about the difficulty of computing this probability under the LoS model are presented in Section 3.1.2. Immediately after, we derive an expression for $\Pr(I_{\text{con}}^{\text{T}})$ in Section 3.1.3. We conclude Chapter 3 presenting the probability of connectivity at segments, a well known problem in one-dimensional networks for which several papers of characterization have been published already.

The (mixed) discrete percolation model is presented in Section 2.2. This model is a mixture of the site and bond percolation models. Informally, the bond percolation model consists of a grid where edges are random events that occur with probability p_b, whilst the site percolation model considers that nodes are random events that occurs with probability p_s. As showed in Figure 1.3, we associate the probability $\Pr(S_{\text{con}})$ to the parameter p_b. Similarly, we associate the probability $\Pr(I_{\text{con}})$ to the parameter p_s. These associations are done in Chapter 4, and allow us to solve the CTR for connectivity by establishing the conditions on p_b and p_s to have percolation. These conditions are, then, translated to the network by means of the model parameters, namely, the granularity g, density μ, transmission range r and width ϵ.

Chapter 2

Model

Modeling wireless ad hoc networks involves the consideration of, at least, two aspects: (i) the deployment process in an environment, and (ii) the definition of the communication rules, that is, the rules that determine whether two nodes are able to communicate directly through a link.

In one-dimensiontal networks, for instance, several works [among them, those of Desai and Manjunath, 2002; Ghasemi and Nader-Esfahani, 2006; Santi and Blough, 2003] consider an interval $[0, z]$ where n nodes are deployed uniformly at random. Additionally, they assume a common transmission range r, and consider that two nodes u and v are able to communicate if the Euclidean distance between them is smaller that or equal to r, which represents a typical deterministic communication model. This modeling describes both items above, namely (i) and (ii), and it is a convenient starting point for defining specific problems that we would like to solve, eventually.

Once we define a problem to solve, we may want to use tools and/or results from other areas in order to tackle the aforementioned problem. As a consequence, this may requires to change the model or, in the best case, to see the problem from a different point of view. An interesting example is the work of Miorandi and Altman [2006]. The authors were working toward the characterization of connectivity in one-dimensional networks, but not limited to deterministic communication models. They discover that it is possible to answer several connectivity questions by using queueing theory. In this sense, they associated the communication range in the ad hoc network with the service time in an infinite server queue. Similarly, they related a connected component in the ad hoc network with a busy period in the server. This modeling allowed the authors to compute, under a deterministic channel model, the coverage probability, node isolation probability and mean cluster size, between other metrics of interest, in addition to other results for non-deterministic channel models.

In the same direction, we present in this chapter both aspects. Our goal is to define a model for obstructed wireless networks that, on the one hand, captures some essential characteristics of obstructed environments encountered in practice and, on the other hand, maintains simplicity enough to provide a analytical path for characterizing particular network properties related to connectivity.

Section 2.1 presents the so-called *geometrical layer*, which corresponds to the actual modeling of the obstructed network. There, we define how and where nodes are deployed in an environment with obstacles, we define the shape and geometrical definition of this environment together with the rules that allow two nodes to be connected through a link. Then, we present in Section 2.2 what we call *percolation layer*. This layer is a higher abstraction on the geometric layer, and is the modeling that allowed us to solve the connectivity problem known as the CTR for connectivity. The role of this layer in our work is similar to the queueing theory approach in the work of Miorandi and Altman [2006], in the sense that it is used to take advantage of a well known theory with results ready to be applied on diverse scenarios for solving a plenty of problems.

2.1 Geometric Layer

Let us start by the definition of the environment. We consider a Manhattan-style street map with g horizontal and g vertical streets, being each street a succession of $g-1$ blocks. We refer to g as the *granularity* of the model, and each block is called a *segment*. Moreover, four adjacent segments form what we define as an *intersection*. Since we are interested in modeling an urban environment, we associate to segments a common width through the parameter ϵ.

We already introduced the environment with two parameters, namely, the granularity g and the segments' width ϵ. Before proceeding to introduce the network that will operate on this environment, let us first to take a visual representation of the environment. Figure 2.1 presents a grid of granularity $g = 4$. Notice that segments are of unitary length whilst the respective common width is 2ϵ, for all of them.

We perceive, also in Figure 2.1, that all these segments have a central dashed line. In the model, *nodes* are deployed over these lines uniformly at random with intensity enough to generate an expected amount of nodes per segment equivalent to μ. In order to warrant the desired uniformity and density, we proceed to deploy the nodes as follows:

1. Considering the total amount of segments in the environment, we compute the total amount of nodes required for the density parameter μ. The total amount

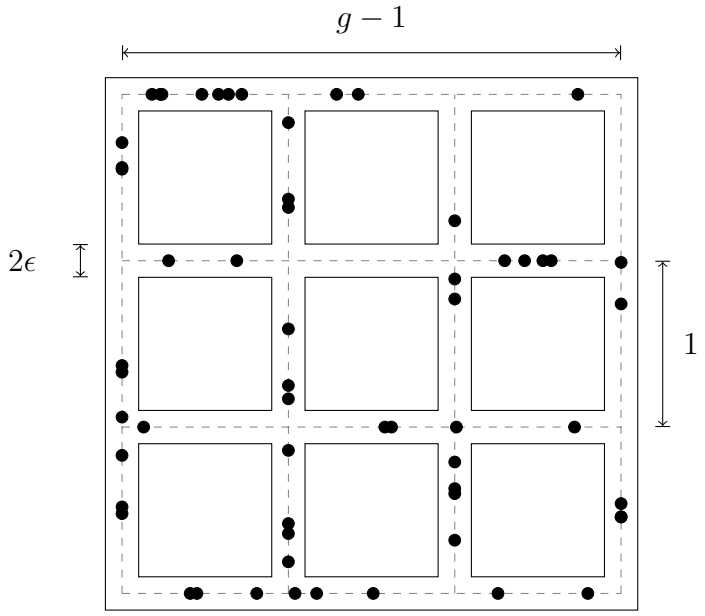

Figure 2.1. The geometrical layer: an urban obstructed environment with nodes deployed uniformly at random. The environment is defined by the granularity $g = 4$ and the segments' width parameter ϵ.

of nodes is determined by $n = 2g(g-1)\mu$;

2. We create a vector, denoted by S, of n elements coming from a uniform standard distribution. This vector represents an sample of the family $\{S_i\}_{1\leq i\leq n}$ of independent and identically distributed (i.i.d.) random variables, such that $S_i \sim \mathcal{U}(0,1)$;

3. We proceed similar as the previous step, creating a vector, denoted by N, of n elements coming from a random discrete uniform distribution defined on the set $\{1, 2, \ldots, 2g(g-1)\}$;

4. We use any bijection $f_d(.)$ from $\{1, 2, \ldots, n\}$ to the set of segments in the grid and, for all node $i \in \{1, 2, \ldots, n\}$ we deploy i in the segment $f_d(N[i])$, in the locally referenced position $S[i]$ of that specific segment.

As we anticipated at the beginning of this chapter, a second aspect for modeling a wireless ad hoc network consists on defining the rules of communication, that is, the rules that determine the existence of *links* between nodes. In general, we say that two nodes u and v are able to communicate through a link if and only if (iff) we satisfy (i) a power restriction and (ii) there exist a path for the signal to arrive from one node the the other.

The power restriction in open-space environments is typically described by the Signal-to-Interference plus Noise Ratio (SINR) model. In this model, the energy of a

signal fades with the distance to the power of the path loss. Consequently, when a node u transmit a message to node v, we say that v is able to receive it if the strength of the signal, perceived at the position of v, divided by the strength of interferences from other transmissions that occur simultaneously plus the ambient noise, exceeds some hardware dependent threshold β.

As Lotker and Peleg [2010] pointed out, a high amount of research exists on the SINR model and other variants of the so-called *physical model*, yet progress has been rather slow. This is a consequence of the non-triviality of this model for being incorporated in the analysis of communication protocols and network design. Added to these difficulties, we are in a more complex case with the presence of objects that reflect the signal in different manners.

Accordingly, we adopt a widely accepted abstraction for wireless communication, known as the Unit Disk Graph (UDG) model [Huson and Sen, 1995], and adapt it to our obstructed urban environment. The UDG model states that a message sent by node u is received by every other listening node v positioned within a disk, of radius r, centered at the position of u. Additionally, since we are considering homogeneous networks, the radius r is restricted to be a common transmission range, depending of the power with which nodes in the network transmit.

More specifically, we define three different geometric models to determine whether local communication links exist between two nodes u and v. Let us denote the positions of u and v with (x_u, y_u) and (x_v, y_v), respectively. Note that the existence of such links depends on two criteria: distance and visibility. Also, the most challenging scenario in terms of visibility is when the two nodes are located in perpendicular segments sharing an intersection. This happens because if they are in the same segment, then only the distance criterion counts, and, if they are in parallel but non-successive segments, they are never visible to each other.

We synthesize the three models as follows:

MaxNorm model: u and v are able to communicate with each other if the following two conditions are satisfied: (i) the minimum norm $\min\{\|x_u - x_v\|, \|y_u - y_v\|\}$ does not exceed ϵ, and (ii) the maximum norm $\max\{\|x_u - x_v\|, \|y_u - y_v\|\}$ does not exceed the common transmission range r (see Figure 2.2a). Informally, this model states that to satisfy the visibility criterion between nodes in perpendicular segments, at least one node of $\{u, v\}$ must be located inside the square of side 2ϵ centered at the intersection of segments.

LoS model: u and v are able to communicate with each other if the following two conditions are satisfied: (i) the Euclidean distance does not exceed the com-

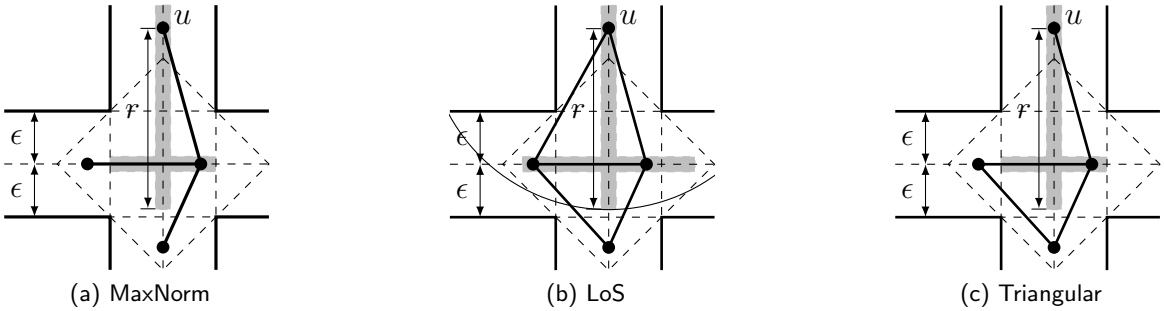

Figure 2.2. Determining the communication links present at street intersections. The gray region represents the coverage of node u.

mon transmission range r, and (ii) there is a visibility line between u and v (see Figure 2.2b). Note that this model makes no simplifications when establishing visibility between two nodes in perpendicular segments, i.e., all possible placements of $\{u, v\}$ in perpendicular (and adjacent) segments must be considered.

Triangular model: u and v are able to communicate with each other if the following two conditions are satisfied: (i) u and v are connected in the MaxNorm model, or (ii) both u and v are at most at a distance 2ϵ far from a shared intersection (see Figure 2.2c). This model greatly simplifies the definition of visibility between two nodes in perpendicular street segments. It extends the MaxNorm model by stating that if both u and v are located inside the rhombus of diagonal 4ϵ, they are visible to each other. Note that this model has a higher similarity with LoS than the MaxNorm model has, since a significantly larger area and, consequently, more links are considered.

For determining a link between two nodes located in the very same or in successive segments, there is no distinction between the variants of communication models. On the other hand, when two nodes are located at segments perpendicular to each other, then the three models above offer a different criterion to determine the existence of a link. Figure 2.2 shows an example where the communication graph, of a deployed network, changes under the different models. Observing this figure, we perceive that the LoS model tends to be the most permissive, that is, the one that "accepts" more link for a given deployment.

As we show in Chapter 3, it is difficult to compute link probability or the probability of connectivity at intersection under the LoS model. The Max-Norm model greatly simplifies the problem of determining the probability of connectivity between two nodes located at perpendicular segments sharing an intersection. This is because

we can treat connectivity by cases dividing the segments in two sectors: $[0, \epsilon]$ and $(\epsilon, 1]$. Nevertheless, having the LoS model as a reference, the main weakness of the Max-Norm model takes place when are near ϵ but in the interval $(\epsilon, 1]$, and the transmission range r is bigger than the distance between them. In this case, nodes can see each other, and they are close to each other, but the Max-Norm does not consider that link.

In response to the main weakness of the Max-Norm model, the Triangular model came for considering those links. In order to maintain a simple model for analytical treatment, we assume $r \geq \sqrt{8}\epsilon$. Consequently, we can treat connectivity by cases as before, but in this model we should divide the segments in three sectors: $[0, \epsilon]$, $(2\epsilon, \epsilon]$ and $(2\epsilon, 1]$.

2.2 Percolation Layer

As previously mentioned, we abstract the obstructed network using a *discrete percolation theory* [Grimmett, 1999]. This theory, originally introduced simply as *percolation theory*[1], was proposed by Broadbent and Hammersley [1957] after the work they had done for optimal design of filters in gas mask during the World War II. According to Franceschetti and Meester [2007], the gas mask of the time used granules of activated charcoal, and Broadbent and Hammersley perceived that the optimal functioning of the gas mask occurred while using a high charcoal surface area and tortuous paths from one extreme to the other, allowing the air flow through the canister for sufficient time and contact to absorb the toxin.

Few years later, the work of Broadbent and Hammersley was generalized by Gilbert [1961] in the context of radio communication. He introduced a model of random planar networks in continuum space, considering a network of nodes randomly distributed in the plane and connecting, through a communication link, nodes for which mutual distance is no bigger than a certain threshold. He proved the existence of a *critical* transmission range that induces and infinite chain of connected nodes. Additionally, he proved that, below this critical transmission range, any connected component of the network is bounded, that is, it is finite.

As we presented above, the discrete percolation model was introduced to study the maximum impermeability (for minimizing the penetration of toxins inside of the mask) that allows the flow of air through a canister with granules of activated charcoal. On the other hand, the continuum percolation model was introduced to study the possibility

[1]This mathematical framework was baptized under the name of *percolation theory*, since meandering paths reminded to Broadbent and Hammersley, the authors of the theory, of water trickling through a coffee percolator [Franceschetti and Meester, 2007].

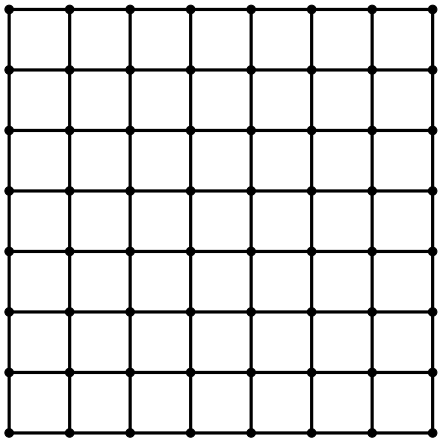

(a) An instance of the grid $\mathbb{G}_8$ for $p_b = 1$. This case contains all possible edges between vertices.

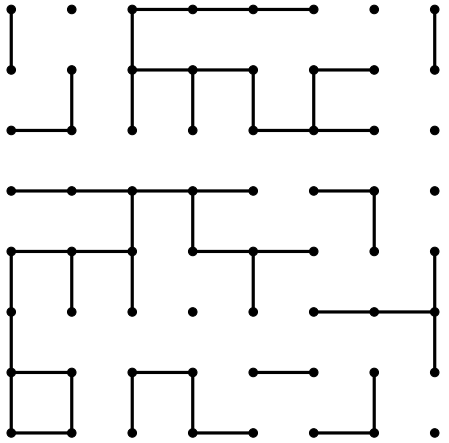

(b) An instance of the grid $\mathbb{G}_8$ for $p_b = 0.45$.

Figure 2.3. Intances of the random grid $\mathbb{G}_8$, with $\mathbb{V} = \{1, 2, \ldots, 8\}^2$, while using two different values for the probability of edges in a bond percolation model.

of providing long-distance radio connections using a large number of low-power radio transmitters. The core motivation in both percolation models was the same: provide a critical value for a parameter, $p = p_c$, beyond which connectivity is warranted w.h.p., and under which any setting $p < p_c$ generates, w.h.p., fragmentation in the system.

Technically, we abstract the obstructed network through a *discrete mixed percolation* model, which is a combination between the *bond* and *site percolation* models [Grimmett, 1999]. In the following, we start by defining the random grid for both versions (bond and site percolation). This is the regular grid structure over which percolation is defined.

Consider the graph $\mathbb{G}_g = (\mathbb{V}, \mathbb{E})$. The bond percolation model is defined on $\mathbb{G}_g$ as follows:

1. We define $\mathbb{V} = \{1, 2, \ldots, g\}^2$ as the vertices of the grid. The position of each vertex $(x, y) \in \mathbb{V}$ is defined by means of its indices (line and column in the grid) over the Euclidean plane;

2. For each pair of nodes u and v where $\|x_u - x_v\| + \|y_u - y_v\| \leq 1$, we add the edge (u, v) to the set $\mathbb{E}$ with probability p_b, independently of the rest of edges.

Figure 2.3 presents instances of the random lattice square $\mathbb{G}_8$ using two different values of p_b. Notice that, in Figure 2.3a, each one of the possible edges of the lattice occurs with maximum probability $p_b = 1$. In Figure 2.3b we show an instance of $\mathbb{G}_8$ with edge probability $p_b = 0.45$. In the discrete percolation literature, the occurrence of an edge is usually referred as "open edge", and the absence of an edge is denominated

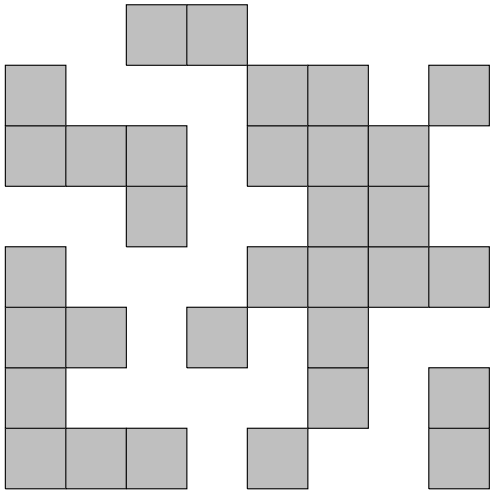

(a) An instance of a random grid for the site percolation model, constructed with $p_s = 0.45$.

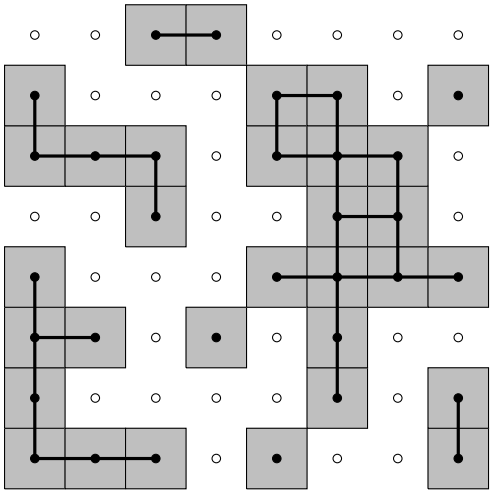

(b) Every instance of a random grid for the site percolation model can be seen as an instance of a random grid for the bond percolation model.

Figure 2.4. An instance of a random grid for the site percolation model with $g = 8$, and the relationship with an instance of a bond percolation model.

a "closed edge". The general rule of association with the "open" and "closed" words is (i) "open" means"connected" and (ii) "closed" means "disconnected".

Another kind of random grid can be obtained by considering each box of the lattice square to be occupied (or equivalently, open) with probability p_s, independently of the rest of boxes, and available (or equivalently, closed) with probability $1 - p_s$. Connections in this model have place between these open boxes, also known as "sites", and we say that two sites are connected if they share a side, that is, if they are neighbours.

Figure 2.4a shows an instance of a random grid of size 8×8 corresponding to a site percolation process with $p_s = 0.45$. Each gray square box in this figure corresponds to an open site, and white spaces represent closed sites. We can think of sites as being vertices and then, adding edges between pairs of nodes that share a side, we obtain an instance of a bond percolation model, as Figure 2.4b shows. In this figure, open sites are plotted with filled bullets and closed sites with empty bullets. We ad an edge between two vertices whenever the vertices are open and have a common side.

Notice that instances of bond percolation processes cannot, in general, be viewed as coming from a site percolation process. For example, an instance of a bond percolation process on $\mathbb{G}_2$ resulting with three edges does not represent any instance of a any site percolation process with four sites. Although it is clear that these discrete percolation models represent different random objects, the power of the relationship pictured in Figure 2.4b emerges from the possibility of combination of bond and site

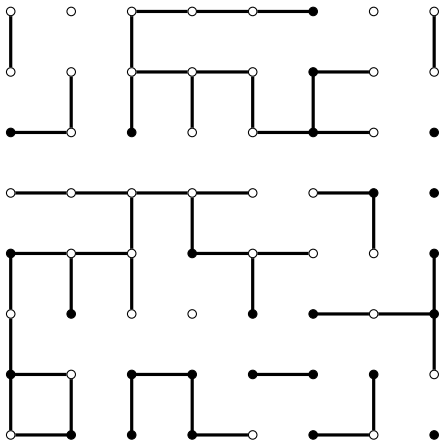

Figure 2.5. An extension of the bond percolation instance of Figure 2.3b with site probability $p_s = p_b = 0.45$.

percolation.

The discrete mixed percolation model is a bond percolation model, with parameter p_b, where the set of vertices can be open with probability p_s, independently of the rest of vertices, or closed with probability $1 - p_s$. Taking the bond percolation instance of Figure 2.3b, we obtain the mixed percolation instance of Figure 2.5 by setting the open site probability $p_s = 0.45$.

We already defined three percolation models and, in order to establish a relationship with the geometrical layer of Section 2.1, we need then to define the concept of connectivity. Under the bond percolation model the random grid is connected, for a given instance, if there exists a sequence of vertices connected successively through open edges, staring at i and finishing at j, for any pair of vertices i and j. On the other hand, under the site percolation model the random grid is connected, for a given instance, if all open sites are connected through successive open sites sharing a side. Finally, the random grid is connected under the mixed percolation model, for a given instance, if for any pair of open vertices or (equivalently) sites i and j, there exists a sequence of open vertices and open edges starting at i and finishing at j.

Figure 2.3a, in page 15, holds some similarities with the urban obstructed environment of Section 2.1. These similarities are based in two facts: (i) for each edge in the grid we have a segment in the geometric layer, and (ii) for each vertex in the grid, there is an intersection in the obstructed environment. A natural procedure is, then, to associate the occurrence of an edge in the mixed percolation model with the connectivity at segments in the obstructed environment. Similarly, we associate the event "open site" with connectivity at intersection in the obstructed network. Notice that this association is consistent in the sense that the probability of connectivity at

segments is equal in all the segments and independent of the connectivity of other segments. The same applies to the probability of connectivity at intersections.

The aforementioned similarities allow us to construct the following abstraction:

1. We compute the probability of connectivity at intersections, denoted by $\Pr(I_{\text{con}})$, and the probability of connectivity at segments, denoted by $\Pr(S_{\text{con}})$;

2. Under the mixed percolation model, we define the parameter p_s to be $\Pr(I_{\text{con}})$, and we set the parameter p_b to $\Pr(S_{\text{con}})$;

3. We determine the critical values of p_b and p_s that warrant connectivity in the random grid w.h.p.;

4. For $\Pr(I_{\text{con}})$ and $\Pr(S_{\text{con}})$, we characterize the transmission range r, density μ and segments' width parameter ϵ that generate the critical values for percolation w.h.p. in the random grid.

After step 4, the characterizations of r, μ and ϵ that generate a certain property, let us say connectivity for instance, match with the characterizations for the equivalent property under the communication network. The more relevant case, and the main for this thesis, corresponds to the characterization of critical value for connectivity, known as the critical value for percolation under the grid, and introduced as the CTR for connectivity in the communication network.

Next chapter is dedicated to the derivation of expressions for $\Pr(S_{\text{con}})$ and for $\Pr(I_{\text{con}})$ under the three communication models presented in the geometrical layer. Afterwards, in Chapter 4 we use the results of Chapter 3 to apply the abstraction of the percolation layer to find an expression for the CTR for connectivity.

Chapter 3

Local Connectivity Probabilities

Connectivity is one of the most important properties in ad hoc wireless networks since it allows basic communication between the nodes that constitute the network. There are two different instances of wireless communication: direct and multi-hop. Direct communication between two nodes occurs when they are able to exchange information without any intermediary. On the other hand, multi-hop communication has place when it is possible to find a path from one node to the other, passing through different intermediate nodes are able to exchange information, in pairs, using direct communication.

The possibility of wireless direct communication relies on complex physical phenomena, and the literature tradition is to abstract this complexity using diverse connectivity models that allow us to work analytically on different problems. As anticipated in Chapter 2, we consider a distance-based model for communication in one-dimensional problems (for connectivity at segments), and three different geometric models for two-dimensional cases (for connectivity at intersections).

In the next two sections, we derive analytical expressions for the probability of connectivity at intersections and segments, respectively. These two events are the building blocks used to solve connectivity in the overall network.

3.1 Probability of Connectivity at Intersections

As we saw in Section 2.1, we treat the problem of connectivity at intersections under three different models. Probabilities related to connectivity at intersections under the Max-Norm model are presented in Section 3.1.1. Analytical formulation for the LoS model is included in Section 3.1.2. Then, we present a derivation of the probability of connectivity at intersections under the Triangular model in Section 3.1.3.

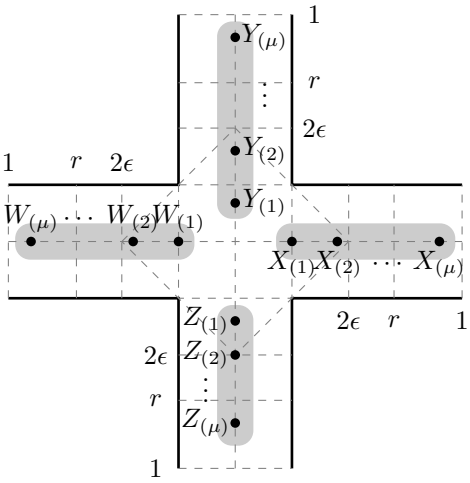

Figure 3.1. Reference scenario for connectivity at intersections

Before entering in details with any of the three models, let us first to introduce a reference scenario that defines with more precision the elements to be considered while computing connectivity at intersections.

We consider the reference scenario illustrated in Figure 3.1, where μ nodes are deployed uniformly at random, in each one of the four adjacent segments of an intersection, over imaginary lines centered in each segment. All the 4μ nodes share the same transmission range r, and segments' width is 2ϵ, where ϵ is the parameter that controls the visibility between nodes deployed in perpendicular segments.

In the aforementioned reference scenario, the communication network can be represented as a graph $G = (V, E)$, where $V = \{X_1, \ldots, X_\mu, Y_1, \ldots, Y_\mu, W_1, \ldots, W_\mu, Z_1, \ldots, Z_\mu\}$, and the set of edges E is composed by pairs of nodes that are able to communicate with each other in the network, according to each one of the three connectivity models.

Let us define now a new graph $I = (\mathbb{V}, \mathbb{E})$ with $\mathbb{V} = \{X, Y, W, Z\}$, where $X = \{X_1, \ldots, X_\mu\}$, $Y = \{Y_1, \ldots, Y_\mu\}$, $W = \{W_1, \ldots, W_\mu\}$ and $Z = \{Z_1, \ldots, Z_\mu\}$, and where $\langle A, B\rangle \in \mathbb{E}$ iff there exist $i \in A$ and $j \in B$ such that $\langle i, j\rangle \in E$, that is, iff $\langle i, j\rangle$ is an edge in G. We call this new graph the *Intersection Graph*.

Problem 1 (Connectivity at Intersections)**.** *The connectivity at intersections problem consists in determining the probability of connectivity of the intersection graph I, namely* $\Pr(I_{\text{con}})$.

Nodes under the same gray area in Figure 3.1 represent the four set of nodes X, Y, W and Z. Notice that it is possible to have a fragmented network in a particular segment, and also there is a possibility for this network to be connected at intersection

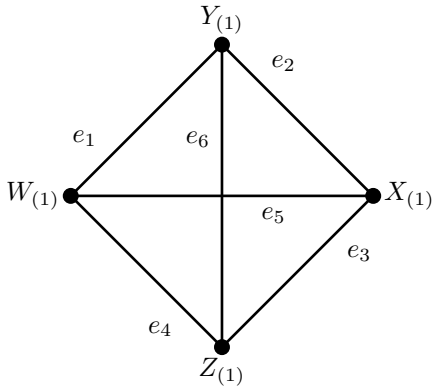

Figure 3.2. Intersection Graph

when the biggest connected component in G is smaller than four, i.e., we just need to connect the four nodes in I. Additionally, we observe that there is a link $\langle A, B\rangle$ in the intersection graph iff there is a link between the closest nodes to the intersection in the original graph G. These nodes are know to be the first order statistics, and are denoted, in this case by $A_{(1)}$ and $B_{(1)}$, respectively.

Figure 3.2 shows the intersection graph. Here, we use the "$_{(1)}$" subscript to emphasize the fact that edges between nodes in the intersection graph are present iff there exist a link between the corresponding first order statistics in the network. We number random edges from e_1 to e_6 from now on according to Figure 3.2 to simplify the treatment in the moment of computing the probability of connectivity at intersections.

In the network, we distinguish between links connecting nodes positioned in parallel and perpendicular segments. We denote by $p_{\parallel}$ the probability of existence of an link between two nodes located in parallel segments sharing an intersection. On the other hand, $p_{\perp}$ denotes the probability of existence of a link between two nodes positioned in perpendicular segments sharing an intersection. We extend these two definitions to the probability of existence of at least one link between groups of μ nodes, and we denote this extension by $p_{\parallel}(\mu)$ and $p_{\perp}(\mu)$.

3.1.1 Max-Norm Model

The Max-Norm is the simplest of the three proposed models, and we proceed to compute some connectivity probabilities having as a final goal to compute the probability of connectivity at intersections under the Max-Norm model, denoted by $\Pr(I_{\text{con}}^{\text{MN}})$.

We can think the event $I_{\text{con}}^{\text{MN}}$ as being the set instances of the intersection graph that connect the four nodes $X_{(1)}$, $Y_{(1)}$, $W_{(1)}$ and $Z_{(1)}$ (see Figure 3.2). Individually, the occurrence of edges e_1, e_2, e_3 and e_4 have the same probability, denoted by $p_{\perp}(\mu)$. Since

adjacent edges are spatially correlated,the probability of collective occurrence is not simple to compute (correlation results from the fact that adjacent *external* edges share a node). Differently, edges e_5 and e_6 are mutually independent, and the individual probability of occurrence is denoted by $p_{\parallel}(\mu)$. Although edges e_5 and e_6 are mutually independent, they are not collectively independent with any of the other edges, from e_1 to e_4.

In the following we present an accurate approximation of the probability $p_{\parallel}(\mu)$ for e_5. Since the probability of e_6 is the same as the one corresponding to e_5, Lemma 1 we presents the general result. Here, and in the rest of the work, position of nodes are relative to the origin of intersection, this means the the support for random variables is on the interval $[0, 1]$.

Lemma 1. *Let $\{X_i\}_{1\leq i\leq \mu}$ and $\{W_j\}_{1\leq j\leq \mu}$ be two families of independent random variables, such that $X_i \sim \mathcal{U}(0,1)$[§] and $W_j \sim \mathcal{U}(0,1)$, denoting the positions of μ nodes in each one of two parallel segments sharing an intersection. Let also r denote the common transmission range of all nodes, where $0 \leq r \leq 1$. The probability $p_{\parallel}(\mu)$ of existence of at least one link between two nodes in parallel adjacent segments is*

$$p_{\parallel}(\mu) \approx \frac{r}{6}\left(\mu - \mu(1-r)^{\mu} - 4\mu\left(1-\frac{r}{2}\right)^{\mu-1}\left(\left(1-\frac{r}{2}\right)^{\mu}-1\right)\right).$$

Proof. Sorting the realizations of $X_1, X_2, \ldots, X_\mu$ and $W_1, W_2, \ldots, W_\mu$ in increasing order, we obtain the order statistics[¶] $X_{(1)}, X_{(2)}, \ldots, X_{(\mu)}$ and $W_{(1)}, W_{(2)}, \ldots, W_{(\mu)}$, respectively. W.l.o.g., we consider that positions of nodes reflect the Euclidean distances from each node to the intersection point between segments.

At least one crossing link between two nodes positioned in different parallel segments exists if and only if $X_{(1)} + W_{(1)} \leq r$. Then, we can compute $p_{\parallel}(\mu)$ by

$$p_{\parallel}(\mu) = \iint_{D} f_{X_{(1)}W_{(1)}}(x,w)\,\mathrm{d}w\,\mathrm{d}x, \tag{3.1}$$

where $D = \{(x,w) \mid 0 \leq x \leq r \wedge 0 \leq w \leq r-x\}$ and $f_{X_{(1)}W_{(1)}}(x,w)$ is the joint distribution function of $X_{(1)}$ and $W_{(1)}$. Figure 3.3 draws integration region according to the restriction $X_{(1)} + W_{(1)} \leq r$.

It is well known that the k-th order statistic of a family of μ independent standard uniform random variables is a Beta random variable $U_{(k)} \sim \mathcal{B}(k, \mu+1-k)$. Consequently, we have that $f_{X_{(1)}}(x) = \mu(1-x)^{\mu-1}$ and $f_{W_{(1)}}(w) = \mu(1-w)^{\mu-1}$. Since both

[§]I.e., distributed uniformly and at random in the interval $[0, 1]$.

[¶]The k-th order statistic of a statistical sample is equal to its kth-smallest value.

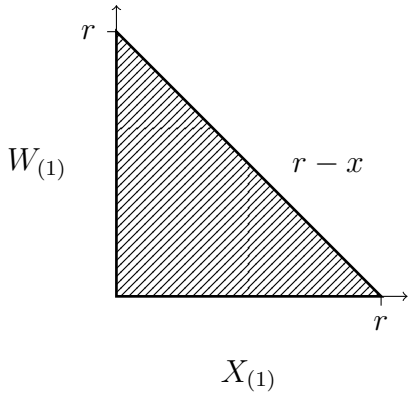

Figure 3.3. Integration region D for computing $p_{\parallel}(\mu)$

families $\{X_i\}_{1\leq i\leq \mu}$ and $\{W_j\}_{1\leq j\leq \mu}$ are independent, we have that the joint distribution function of $X_{(1)}$ and $W_{(1)}$ is $f_{X_{(1)}W_{(1)}}(x,w) = \mu^2(1-x)^{\mu-1}(1-y)^{\mu-1}$. Then, replacing $f_{X_{(1)}W_{(1)}}(x,w)$ in Equation (3.1), we have

$$\begin{aligned} p_{\parallel}(\mu) &= \int_0^r \int_0^{r-x} \mu^2(1-x)^{\mu-1}(1-w)^{\mu-1}\,\mathrm{d}w\,\mathrm{d}x \\ &= \int_0^r \mu\left(-(1-x)^{\mu-1}\right)\left((-r+x+1)^{\mu}-1\right)\,\mathrm{d}x. \end{aligned} \tag{3.2}$$

At this point, we are not able to solve the integration of Equation (3.2), so we apply an approximation method known as the Simpson's rule. Applying this Simpson's rule with two intervals, we have

$$p_{\parallel}(\mu) \approx \frac{r}{6}\left(\mu - \mu(1-r)^{\mu} - 4\mu\left(1-\frac{r}{2}\right)^{\mu-1}\left(\left(1-\frac{r}{2}\right)^{\mu}-1\right)\right).$$

□

Notice that in any moment during demonstration of Lemma 1 we assume a property that holds specifically under the Max-Norm model, which implies that $p_{\parallel}(\mu)$ is the same for the three models addressed in this manuscript.

Figure 3.4 presents the probability of crossing links between parallel segments sharing an intersection in three scenarios, determined by the parameter μ. Here we perceive that the approximation we obtained, using Simpson's rule with two intervals in (3.2), is an accurate expression for $p_{\parallel}(\mu)$.

So far, we proposed an approximation for $p_{\parallel}(\mu)$, and this is an expression that does depends only on geometric properties common to all models herein considered. In the following Lemma 2, we consider the problem of determining the probability of existence

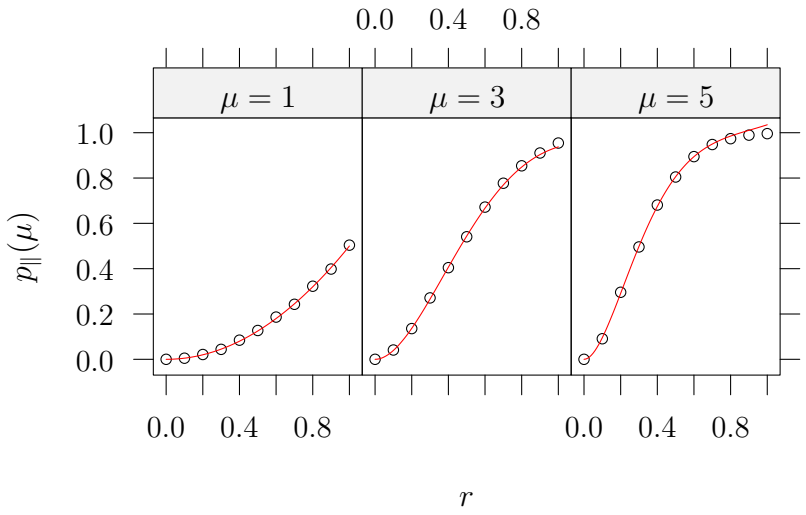

Figure 3.4. Empirical and analytical results for $p_{\|}(\mu)$ under the Max-Norm model

of at least one link between two groups of μ nodes positioned in its two respective segments sharing an intersection. In the derivation, we assume specific properties related to the Max-Norm model, and we denote the exact probability of existing at least one crossing link between perpendicular segments by $p_{\perp}^{\text{MN}}(\mu)$, emphasizing this fact.

Lemma 2. *Let* $\{X_i\}_{1\leq i\leq \mu}$, *such that* $X_i \sim \mathcal{U}(0,1)$, *and* $\{Y_j\}_{1\leq j\leq \mu}$, *such that* $Y_j \sim \mathcal{U}(0,1)$, *be two families of independent random variables denoting the position of* μ *nodes in each one of two perpendicular segments sharing an intersection. Let also* 2ϵ *be the segments' width, and* r *denote the common transmission range of all nodes, where* $\epsilon \leq r \leq 1$. *The probability* $p_{\perp}^{MN}(\mu)$ *of existence of at least one link between two nodes in different perpendicular segments, under the Max-Norm model, is*

$$p_{\perp}^{MN}(\mu) = 2\left(1-(1-r)^{\mu}\right)\left(1-(1-\epsilon)^{\mu}\right) - \left(1-(1-\epsilon)^{\mu}\right)^2.$$

Proof. Let $X_{(1)}, X_{(2)}, \ldots, X_{(\mu)}$ and $Y_{(1)}, Y_{(2)}, \ldots, Y_{(\mu)}$ be the order statistics of $X_1, X_2, \ldots, X_{\mu}$ and $Y_1, Y_2, \ldots, Y_{\mu}$, respectively. W.l.o.g., we consider that positions of nodes reflect the Euclidean distances from each node to the intersection point between segments. There exists at least one link between two nodes in different perpendicular segments if and only if there is a link between $X_{(1)}$ and $Y_{(1)}$.

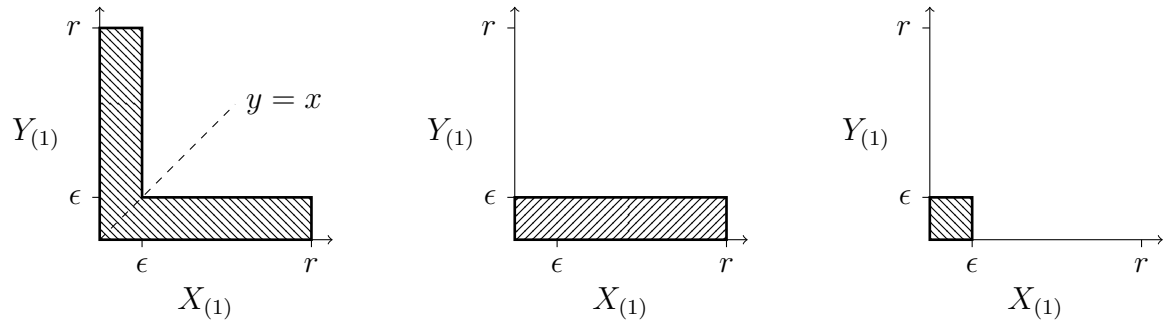

(a) General integration region D (b) Integration region R_1 (c) Integration region R_2

Figure 3.5. Integration region D, and alternative partition for computing $p_{\perp}^{\text{MN}}(\mu)$

Considering $\epsilon \leq r$, we can compute $p_{\perp}^{\text{MN}}(\mu)$ by

$$p_{\perp}^{\text{MN}}(\mu) = \iint_{D} f_{X_{(1)}Y_{(1)}}(x, y)\,\mathrm{d}y\,\mathrm{d}x, \tag{3.3}$$

where D is the region showed in Figure 3.5a and $f_{X_{(1)}Y_{(1)}}(x, y)$ is the joint distribution function of $X_{(1)}$ and $Y_{(1)}$.

It is important to highlight that the join distribution function of two equally distributed random variables is symmetric respect to the $y = x$ plane in the Euclidean space. Since region D is symmetric respect to line $y = x$ and, additionally, $f_{X_{(1)}Y_{(1)}}$ is symmetric respect to plane $y = x$, we can decompose integral of equation (3.3) into regions as follows:

$$p_{\perp}^{\text{MN}}(\mu) = 2\iint_{R_1} f_{X_{(1)}Y_{(1)}}(x, y)\,\mathrm{d}y\,\mathrm{d}x - \iint_{R_2} f_{X_{(1)}Y_{(1)}}(x, y)\,\mathrm{d}y\,\mathrm{d}x, \tag{3.4}$$

where $R_1 = \{(x, y) \mid 0 \leq x \leq r \wedge 0 \leq y \leq \epsilon\}$ and $R_2 = \{(x, y) \mid 0 \leq x \leq \epsilon \wedge 0 \leq y \leq \epsilon\}$ (see Figure 3.5).

Since $X_{(1)}, Y_{(1)} \sim \mathcal{B}(1, \mu)$ are independent, the joint distribution function is $f_{X_{(1)}Y_{(1)}} = \mu^2(1 - x)^{\mu-1}(1 - y)^{\mu-1}$. Then, from (3.4), we have

$$\begin{aligned} p_{\perp}^{\text{MN}}(\mu) &= 2\int_0^r \int_0^\epsilon \mu^2(1 - x)^{\mu-1}(1 - y)^{\mu-1}\,\mathrm{d}y\,\mathrm{d}x - \int_0^\epsilon \int_0^\epsilon \mu^2(1 - x)^{\mu-1}(1 - y)^{\mu-1}\,\mathrm{d}y\,\mathrm{d}x \\ &= 2\left((1 - (1 - r)^\mu)(1 - (1 - \epsilon)^\mu)\right) - \left(1 - (1 - \epsilon)^\mu\right)^2. \end{aligned}$$

□

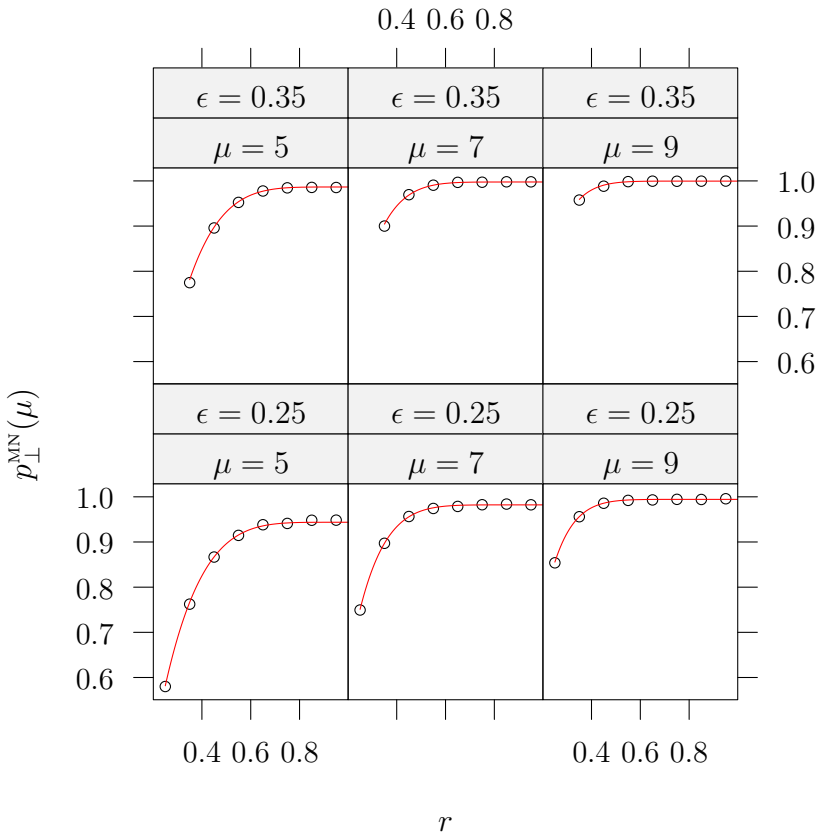

Figure 3.6. Probability of connectivity between nodes located at perpendicular segments sharing an intersection

For the case of crossing links between perpendicular segments, we have selected six scenarios, varying the segment width parameter, ϵ, and the expected number of nodes per segment, μ. Figure 3.6 presents these results considering the assumption $r \geq \epsilon$ from Lemma 2. It can be seen that the expression obtained for $p_{\perp}^{\mathrm{MN}}(\mu)$ is correct.

At this stage, we have already computed the probability of existence of at least one crossing link between parallel segments, $p_{\parallel}(\mu)$, and perpendicular segments, $p_{\perp}^{\mathrm{MN}}(\mu)$. The next step is to compute the probability of connectivity at intersections, namely $\Pr(I_{\mathrm{con}}^{\mathrm{MN}})$. Somehow, this probability can be described by a (non-trivial) function of $p_{\parallel}(\mu)$ and $p_{\perp}^{\mathrm{MN}}(\mu)$, which takes into account the geometric correlation between the existence of simultaneous links between both, parallel and perpendicular segments. Nevertheless, we perceive in Almiron et al. [2012] that the influence of $p_{\parallel}(\mu)$ on $\Pr(I_{\mathrm{con}}^{\mathrm{MN}})$ is very small in most scenarios, i.e., the probability of connectivity at an intersection is almost exclusively determined by the probability of links between perpendicular seg-

ments sharing an intersection. An exception to this behavior is when μ or ϵ are very small values, which are scenarios not so relevant in practice. An example of this occurs in the CTR problem, where we want to use the minimum radio for communication as possible while maintaining connectivity in the overall network. Clearly, in this problem, small densities and low visibility at intersections implies too large communication radios, which is not of practical interest for nowadays technological environments. For the reason above and for the sake of simplification, in Theorem 1, we compute a lower bound on $\Pr(I_{\text{con}}^{\text{MN}})$ using only $p_{\perp}^{\text{MN}}(\mu)$. After this, in Theorem 2, we present an accurate expression for $\Pr(I_{\text{con}}^{\text{MN}})$ but, at this time, considering links between both, parallel and perpendicular segments.

Theorem 1. *Let $\{X_i\}_{1\leq i\leq \mu}$, $\{Y_j\}_{1\leq j\leq \mu}$, $\{W_k\}_{1\leq k\leq \mu}$ and $\{Z_m\}_{1\leq m\leq \mu}$ be four families of independent random variables, such that $X_i \sim \mathcal{U}(0,1)$, $Y_j \sim \mathcal{U}(0,1)$, $W_k \sim \mathcal{U}(0,1)$ and $Z_m \sim \mathcal{U}(0,1)$, denoting the positions of μ nodes in four adjacent segments sharing an intersection. Let also 2ϵ be the segments' width and r denote the common transmission range of all nodes, with $\epsilon \leq r \leq 1$. A lower bound of the probability of connectivity at intersections, denoted by $\Pr(I_{con}^{MN})$, is given by*

$$\Pr(I_{con}^{MN}) \geq 2\xi^2 - \frac{\xi^4}{p^2} + p^2, \tag{3.5}$$

where $\xi = ((1-\epsilon)^{\mu} - 1)((1-r)^{\mu} - (1-\epsilon)^{\mu})$ and $p = p_{\perp}^{MN}(\mu)$.

Proof. W.l.o.g., we consider that positions of nodes reflect the Euclidean distances from each node to the intersection point between segments. Consider the order statistics $X_{(1)}$, $Y_{(1)}$, $W_{(1)}$ and $Z_{(1)}$, from the families $\{X_i\}_{1\leq i\leq \mu}$, $\{Y_j\}_{1\leq j\leq \mu}$, $\{W_k\}_{1\leq k\leq \mu}$ and $\{Z_m\}_{1\leq m\leq \mu}$, respectively. There exists a path between at least one node in a segment connecting at least one node in each one of the three other segments if and only if there exists a path between $X_{(1)}$, $Y_{(1)}$, $W_{(1)}$ and $Z_{(1)}$.

Considering only links between perpendicular segments, we can obtain a lower bound as follows. Let e_1 be the event that indicates the presence of a link between the realizations of $Y_{(1)}$ and $W_{(1)}$ (see Figure 3.2, in page 21). Additionally, let e_2, e_3 and e_4 represent the existence of a link between $X_{(1)}$ and $Y_{(1)}$, $X_{(1)}$ and $Z_{(1)}$ and finally $W_{(1)}$ and $Z_{(1)}$, respectively. Since $X_{(1)}$, $Y_{(1)}$, $W_{(1)}$ and $Z_{(1)}$ are independent, we have $e_1 \perp\!\!\!\perp e_3$ and $e_2 \perp\!\!\!\perp e_4$, where $\perp\!\!\!\perp$ indicates the stochastic independence between events. Consider now the experiment of observing the presence of e_1 and e_3 simultaneously. The sample space of this experiment can be partitioned by $\Omega = \{e_1 \cap e_3, e_1 \cap \overline{e_3}, \overline{e_1} \cap e_3, \overline{e_1} \cap \overline{e_3}\}$. Consequently, by law of total probability, we can compute the aforementioned lower

bound by

$$\Pr(I_{\text{con}}^{\text{MN}}) \geq \Pr(I_{\text{con}}^{\text{MN}} \mid e_1 \cap e_3)p^2 + 2\Pr(I_{\text{con}}^{\text{MN}} \mid e_1 \cap \overline{e_3})p(1-p) + \Pr(I_{\text{con}}^{\text{MN}} \mid \overline{e_1} \cap \overline{e_3})(1-p)^2, \quad (3.6)$$

where $p = \Pr(e_1) = \Pr(e_3) = p_{\perp}^{\text{MN}}(\mu)$.

Notice that Equation 3.6 does effectively represent a lower bound, since links between nodes positioned in parallel segments are not considered in the expression. This restriction has an immediate consequence: the third term of Equation 3.6 does not contribute to connectivity, because there is no way to have connectivity at intersections without e_1 nor e_3. Then, we only need to find expressions for $\Pr(I_{\text{con}}^{\text{MN}} \mid e_1 \cap e_3)$ and $\Pr(I_{\text{con}}^{\text{MN}} \mid e_1 \cap \overline{e_3})$. Lets consider $\Pr(I_{\text{con}}^{\text{MN}} \mid e_1 \cap e_3)$ first.

We can solve $\Pr(I_{\text{con}}^{\text{MN}} \mid e_1 \cap e_3)$ considering probabilities of three cases under which we achieve connectivity at intersections: (i) both, e_2 and e_4 occur, (ii) e_2 occurs and e_4 does not and (iii) e_2 does not occur and e_4 does. Since cases (ii) and (iii) are symmetric, we have

$$\Pr(I_{\text{con}}^{\text{MN}} \mid e_1 \cap e_3) = \Pr(e_2 \mid e_1 \cap e_3)^2 + 2\Pr(e_2 \mid e_1 \cap e_3)\left(1 - \Pr(e_2 \mid e_1 \cap e_3)\right). \quad (3.7)$$

Additionally, we have

$$\begin{aligned}\Pr(e_2 \mid e_1 \cap e_3) &= 1 - \Pr(\overline{e_2} \mid e_1 \cap e_3) \\ &= 1 - \frac{\Pr(\epsilon \leq X_{(1)} \leq r \cap \epsilon \leq Y_{(1)} \leq r \cap e_1 \cap e_3)}{\Pr(e_1 \cap e_3)}. \end{aligned} \quad (3.8)$$

Since $e_1 \perp\!\!\!\perp e_3$, we can rewrite (3.8) and solve

$$\begin{aligned}\Pr(e_2 \mid e_1 \cap e_3) &= 1 - \frac{\left(\int_{\epsilon}^{r}\int_{0}^{\epsilon} f_{X_{(1)}Z_{(1)}}(x,z)\,\mathrm{d}z\,\mathrm{d}x\right)^2}{p^2} \\ &= 1 - \frac{((1-\epsilon)^{\mu}-1)^2((1-r)^{\mu}-(1-\epsilon)^{\mu})^2}{p^2}. \end{aligned} \quad (3.9)$$

In order to solve the lower bound for $\Pr(I_{\text{con}}^{\text{MN}})$ proposed in (3.6), we still need to compute $\Pr(I_{\text{con}}^{\text{MN}} \mid e_1 \cap \overline{e_3})$. Notice that even in the case where we do not have e_3, we still need $X_{(1)} \leq r$ and $Z_{(1)} \leq r$, otherwise we are not able to achieve connectivity at intersection. Being aware of this, we know then that $\epsilon < X_{(1)} \leq r$ and $\epsilon < Z_{(1)} \leq r$. This is because we do not want to give a chance to have e_3 while we are actually conditioning on $e_1 \cap \overline{e_3}$. We all these considerations, we can then compute

$$\Pr(I_{\text{con}}^{\text{MN}} \mid e_1 \cap \overline{e_3}) = \Pr(A \mid e_1 \cap \overline{e_3}) \quad (3.10)$$

where $A = \{0 \leq Y_{(1)} \leq \epsilon \cap 0 \leq W_{(1)} \leq \epsilon \cap \epsilon \leq X_{(1)} \leq r \cap \epsilon \leq Z_{(1)} \leq r\}$. Since $Y_{(1)} \perp\!\!\!\perp \overline{e_3}$, $W_{(1)} \perp\!\!\!\perp \overline{e_3}$, $X_{(1)} \perp\!\!\!\perp e_1$ and $Z_{(1)} \perp\!\!\!\perp e_1$, from (3.10) we have

$$\Pr(I_{\text{con}}^{\text{MN}} \mid e_1 \cap \overline{e_3}) = \left(\int_0^{\epsilon} \int_0^{\epsilon} f_{Y_{(1)}W_{(1)}}(y, w)\, \mathrm{d}w\, \mathrm{d}y \right. \\ \left. \int_{\epsilon}^{r} \int_{\epsilon}^{r} f_{X_{(1)}Z_{(1)}}(x, z)\, \mathrm{d}z\, \mathrm{d}x \right) \frac{1}{p(1-p)}. \quad (3.11)$$

Solving the definite integrals in (3.11), we obtain

$$\Pr(I_{\text{con}}^{\text{MN}} \mid e_1 \cap \overline{e_3}) = \frac{((1-\epsilon)^{\mu} - 1)^2((1-r)^{\mu} - (1-\epsilon)^{\mu})^2}{p(1-p)}. \quad (3.12)$$

Finally, combining (3.7), (3.9) and (3.12) within Expression (3.6), and considering $\xi = ((1-\epsilon)^{\mu} - 1)((1-r)^{\mu} - (1-\epsilon)^{\mu})$ we finally have

$$\Pr(I_{\text{con}}^{\text{MN}}) \geq 2\xi^2 - \frac{\xi^4}{p^2} + p^2.$$

□

Although Theorem 1 considers only links between nodes located in perpendicular segments sharing an intersection, the obtained lower bound was not an expression as simple as we would like. This last fact, encouraged us to find a solution considering all links, that is, not just those between nodes in perpendicular segments, but those between nodes located in parallel segments as well.

Theorem 2 presents a tight lower bound for $\Pr(I_{\text{con}}^{\text{MN}})$ considering all links at a given intersection.

Theorem 2. *Let $\{X_i\}_{1 \leq i \leq \mu}$, $\{Y_j\}_{1 \leq j \leq \mu}$, $\{W_k\}_{1 \leq k \leq \mu}$ and $\{Z_m\}_{1 \leq m \leq \mu}$ be four families of independent random variables, such that $X_i \sim \mathcal{U}(0,1)$, $Y_j \sim \mathcal{U}(0,1)$, $W_k \sim \mathcal{U}(0,1)$ and $Z_m \sim \mathcal{U}(0,1)$, denoting the positions of μ nodes in four adjacent segments sharing an intersection. Let also 2ϵ be the segments' width and r denote the common transmission range of all nodes, with $2\epsilon \leq r \leq 1$. A lower bound of the probability of connectivity at intersections, denoted by $\Pr(I_{con}^{MN})$, is given by*

$$\Pr(I_{con}^{MN}) \geq p^2 + 2D_0^{\epsilon}(\mu)D_{\epsilon}^{r}(\mu)D_{\epsilon}^{r-\epsilon}(\mu)\left[D_0^{r}(\mu) + D_{\epsilon}^{r}(\mu)\right], \quad (3.13)$$

where $D_i^j(k) = (1-i)^k - (1-j)^k$ and $p = p_{\perp}^{MN}(\mu)$.

Proof. W.l.o.g., we consider that positions of nodes reflect the Euclidean distances from each node to the center point between streets. Consider the order statistics $X_{(1)}$, $Y_{(1)}$,

$W_{(1)}$ and $Z_{(1)}$, from the families $\{X_i\}_{1\leq i\leq \mu}$, $\{Y_j\}_{1\leq j\leq \mu}$, $\{W_k\}_{1\leq k\leq \mu}$ and $\{Z_m\}_{1\leq m\leq \mu}$, respectively. The intersection graph I is connecterd iff there exists a path between $X_{(1)}$, $Y_{(1)}$, $W_{(1)}$ and $Z_{(1)}$.

Consider events e_1, e_2, e_3, e_4, e_5 and e_6, from Figure 3.2 (page 21), as being the events that indicates the presence of a link between the realizations of $Y_{(1)}$ and $W_{(1)}$, $X_{(1)}$ and $Y_{(1)}$, $X_{(1)}$ and $Z_{(1)}$, $W_{(1)}$ and $Z_{(1)}$, $X_{(1)}$ and $W_{(1)}$, and finally $Y_{(1)}$ and $Z_{(1)}$, respectively. Let us highlight that $e_1 \perp\!\!\!\perp e_3$ and $e_2 \perp\!\!\!\perp e_4$, and that pairs of edges sharing a node are clearly not independent because of geometrical correlation. In particular, since $e_1 \perp\!\!\!\perp e_3$, we are able to construct the partition $P_e = \{e_1 \cap e_3, e_1 \cap \overline{e_3}, \overline{e_1} \cap e_3, \overline{e_1} \cap \overline{e_3}\}$ on the sample space Ω (the set of all possible combinations of nodes positions).

Consequently, applying the law of total probability and considering the symmetry between $e_1 \cap \overline{e_3}$ and $\overline{e_1} \cap e_3$, we can compute

$$\Pr(I_{\text{con}}^{\text{MN}}) = \Pr(I_{\text{con}}^{\text{MN}} \mid e_1 \cap e_3)\Pr(e_1 \cap e_3) + 2\Pr(I_{\text{con}}^{\text{MN}} \mid e_1 \cap \overline{e_3})\Pr(e_1 \cap \overline{e_3}) + \Pr(I_{\text{con}}^{\text{MN}} \mid \overline{e_1} \cap \overline{e_3})\Pr(\overline{e_1} \cap \overline{e_3}) \quad (3.14)$$

The three summands in (3.14) contain the event $I_{\text{con}}^{\text{MN}}$ conditioned on $e_1 \cap e_3$, $e_1 \cap \overline{e_3}$ or $\overline{e_1} \cap \overline{e_3}$. To solve these probabilities, we use a second partition with bounds on ϵ and r,

$$P_{\epsilon,r} = \{0 \leq W_{(1)} \leq \epsilon,\ \epsilon < W_{(1)} \leq r\} \times \{0 \leq Z_{(1)} \leq \epsilon,\ \epsilon < Z_{(1)} \leq r\}, \quad (3.15)$$

and apply the law of total probability on $e_1 \cap e_3$, $e_1 \cap \overline{e_3}$ and $\overline{e_1} \cap \overline{e_3}$, respectively. We identify two intervals, in (3.15), where $W_{(1)}$ and $Z_{(1)}$ belong to $[0, \epsilon]$ and $(\epsilon, r]$. We call these two intervals as S_1 and S_2, respectively, and define $C_{i,j}$ as being the element of partition $P_{\epsilon,r}$ where $W_{(1)} \in S_i$ and $Z_{(1)} \in S_j$. With this partition, we proceed to compute each conditional term of (3.14).

Let us consider firstly the partition $P_{\epsilon,r}$ on $e_1 \cap e_3$ for solving $\Pr(I_{\text{con}}^{\text{MN}} \mid e_1 \cap e_3)$. Figure 3.7a shows a schematic view of partition $P_{\epsilon,r}$ on $e_1 \cap e_3$, where the black balls represent instances of $W_{(1)}$ and gray balls represent instances of $Z_{(1)}$. Each pair of balls of different color represent a class $C_{i,j}$ of $P_{\epsilon,r}$. Edges, in this figure, represent the conditioning on $e_1 \cap e_3$, and the position of stars represent the worst case (farthest region from the origin) for this conditioning. Numbering in both, balls and stars, is used for identifying the intervals of instances of $W_{(1)}$ and $Z_{(1)}$, and more important, for visualizing each class $C_{i,j}$ of $P_{\epsilon,r}$. Observing the partition $P_{\epsilon,r}$ in Figure 3.7a we perceive that for each class $C_{i,j}$ it is possible to have a third edge connecting the

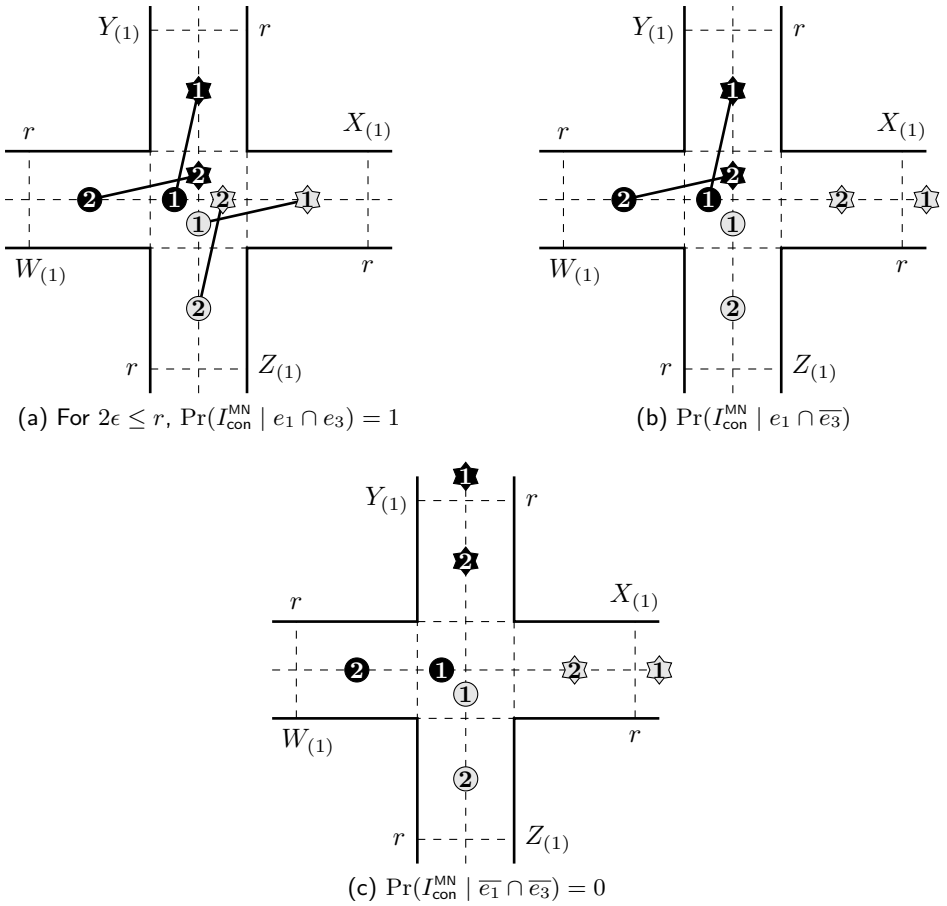

(a) For $2\epsilon \leq r$, $\Pr(I_{\text{con}}^{\text{MN}} \mid e_1 \cap e_3) = 1$

(b) $\Pr(I_{\text{con}}^{\text{MN}} \mid e_1 \cap \overline{e_3})$

(c) $\Pr(I_{\text{con}}^{\text{MN}} \mid \overline{e_1} \cap \overline{e_3}) = 0$

Figure 3.7. Computing the probability of connectivity at intersections under the Max-Norm model

connected components $\{W_{(1)}, Y_{(1)}\}$ and $\{Z_{(1)}, X_{(1)}\}$, which implies

$$\Pr(I_{\text{con}}^{\text{MN}} \mid e_1 \cap e_3) = 1. \tag{3.16}$$

Let us consider now the partition $P_{\epsilon,r}$ on $e_1 \cap \overline{e_3}$ for solving $\Pr(I_{\text{con}}^{\text{MN}} \mid e_1 \cap \overline{e_3})$. Applying law of total probability, we obtain

$$\Pr(I_{\text{con}}^{\text{MN}} \mid e_1 \cap \overline{e_3}) = \frac{\sum_{i=1}^{2}\sum_{j=1}^{2} \Pr(I_{\text{con}}^{\text{MN}} \cap C_{i,j} \cap e_1 \cap \overline{e_3})}{\Pr(e_1 \cap \overline{e_3})}. \tag{3.17}$$

Figure 3.7b shows classes $C_{i,j}$ on $e_1 \cap \overline{e_3}$. The schematic view in this figure is essentially the same as Figure3.7a, with the exception for gray stars which represent the best case positioning. The idea behind considering best cases is to identify potential edges. In the following, we analyze each one of the four terms, $\Pr(I_{\text{con}}^{\text{MN}} \cap C_{i,j} \cap e_1 \cap \overline{e_3})$, separately.

For the three classes $C_{i,1}$, we observe that random node $X_{(1)}$ is isolated even in

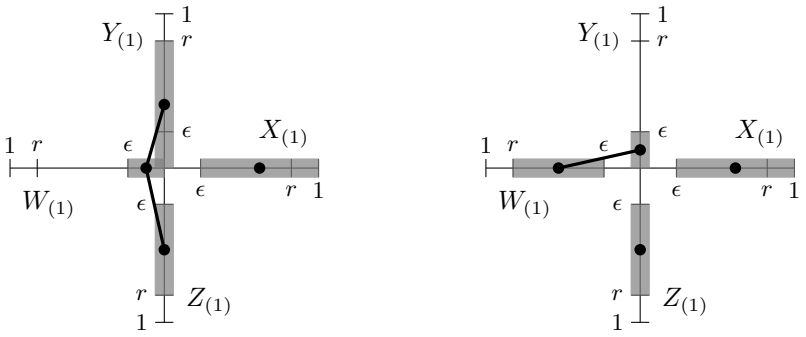

(a) $C_{1,2} \cap e_1 \cap \overline{e_3}$ (b) $C_{2,2} \cap e_1 \cap \overline{e_3}$

Figure 3.8. $C_{i,j} \cap e_1 \cap \overline{e_3}$

the best case, since $X_{(1)} > r$ (see Figure 3.7b). This means that

$$\sum_{i=1}^{2} \Pr(I_{\text{con}}^{\text{MN}} \cap C_{i,1} \cap e_1 \cap \overline{e_3}) = 0. \tag{3.18}$$

Let us consider now $\Pr(I_{con} \cap C_{1,2} \cap e_1 \cap \overline{e_3})$. Figure 3.8a shows the geometrical restrictions for $C_{1,2} \cap e_1 \cap \overline{e_3}$. Here we perceive that we need the edge $e_2 = (X_{(1)}, Y_{(1)})$ or $e_5 = (X_{(1)}, W_{(1)})$ in order to have connectivity. Since e_2 and e_5 are correlated, we compute a lower bound considering only e_5. Additionally, for the sake of simplicity, we compute a lower bound for the probability of e_5 assuming the worst case $W_{(1)} = \epsilon$, i.e., farthest away from the center. With this, we have

$$\Pr(I_{\text{con}}^{\text{MN}} \cap C_{1,2} \cap e_1 \cap \overline{e_3}) \geq \int_0^{\epsilon} f_{W_{(1)}}(w)\,\mathrm{d}w \int_0^{r} f_{Y_{(1)}}(y)\,\mathrm{d}y \int_{\epsilon}^{r} f_{Z_{(1)}}(z)\,\mathrm{d}z \int_{\epsilon}^{r-\epsilon} f_{X_{(1)}}(x)\,\mathrm{d}x \tag{3.19}$$

The last integral in (3.19) corresponds to random variable $X_{(1)}$. Note that here we restrict the domine of $X_{(1)}$ to maintain the edge $e_5 = (X_{(1)}, W_{(1)})$ given $W_{(1)} = \epsilon$, that is, we originally have $X_{(1)} \in (\epsilon, 1]$ because of condition $C_{1,2} \cap \overline{e_3}$, and afterwards we restrict $X_{(1)}$ to a smaller interval, contained in $(\epsilon, 1]$, given place to event e_5. This explain the integration intervals of (3.19).

As we saw before, the k-th order statistic of a family of μ independent standard uniform random variables is a Beta random variable $U_{(k)} \sim \mathcal{B}(k, \mu + 1 - k)$ (see David and Nagaraja [2003]). In particular, the probability density function (p.d.f.) of the first order statistic $U_{(1)}$ is $f_{U_{(1)}}(u) = \mu(1-u)^{\mu-1}$ and $\int_i^j k(1-u)^{k-1}\,\mathrm{d}u = (1-i)^k - (1-j)^k$. This last expression represents the probability of having the first order statistic of family $\{U_h\}_{1 \leq h \leq k}$ within the interval (i, j), and it is denoted by $D_i^j(k)$. Then, we can

rewrite the expression (3.19) as

$$\Pr(I_{\text{con}}^{\text{MN}} \cap C_{1,2} \cap e_1 \cap \overline{e_3}) \geq D_0^{\epsilon}(\mu) D_0^{r}(\mu) D_{\epsilon}^{r}(\mu) D_{\epsilon}^{r-\epsilon}(\mu). \tag{3.20}$$

For $\Pr(I_{\text{con}}^{\text{MN}} \cap C_{2,2} \cap e_1 \cap \overline{e_3})$ we proceed similarly. Figure 3.8b shows the restrictions for $C_{2,2} \cap e_1 \cap \overline{e_3}$. Here we observe that e_2 implies e_5, and that e_4 is an impossible event. Therefore, we need to restrict $X_{(1)} \leq r$ for having e_2 and consider the conditions for having e_6. These considerations lead to the following lower bound

$$\begin{aligned} \Pr(I_{\text{con}}^{\text{MN}} \cap C_{2,2} \cap e_1 \cap \overline{e_3}) &\geq \int_{\epsilon}^{r} f_{W_{(1)}}(w)\,\mathrm{d}w \int_{0}^{\epsilon} f_{Y_{(1)}}(y)\,\mathrm{d}y \\ &\qquad \int_{\epsilon}^{r-\epsilon} f_{Z_{(1)}}(z)\,\mathrm{d}z \int_{\epsilon}^{r} f_{X_{(1)}}(x)\,\mathrm{d}x \\ &= D_{\epsilon}^{r}(\mu) D_0^{\epsilon}(\mu) D_{\epsilon}^{r-\epsilon}(\mu) D_{\epsilon}^{r}(\mu). \end{aligned} \tag{3.21}$$

Combining (3.18), (3.20) and (3.21) into (3.17), we obtain

$$\Pr(I_{\text{con}}^{\text{MN}} \mid e_1 \cap \overline{e_3}) \geq \frac{D_0^{\epsilon}(\mu) D_{\epsilon}^{r}(\mu) D_{\epsilon}^{r-\epsilon}(\mu)\,[D_0^{r}(\mu) + D_{\epsilon}^{r}(\mu)]}{\Pr(e_1 \cap \overline{e_3})}. \tag{3.22}$$

The next step is to derive the third term of (3.14). Considering partition $P_{\epsilon,r}$ on $\overline{e_1} \cap \overline{e_3}$, we obtain four cases, namely $C_{1,1}$, $C_{1,2}$, $C_{2,1}$ and $C_{2,2}$ (see Figure 3.7c). From these four cases, just the case $C_{2,2}$ has no isolated nodes, with positions closer than r from the intersection. Additionally, we notice that no link between nodes located in perpendicular segments is possible. As a consequence, even in case we have links between nodes positioned in parallel segments, it is not possible to achieve connectivity in this scenario, therefore

$$\Pr(I_{\text{con}}^{\text{MN}} \mid \overline{e_1} \cap \overline{e_3}) = 0. \tag{3.23}$$

Finally, adding up (3.16), (3.22) and (3.23), into (3.14), and observing that $e_1 \perp\!\!\!\perp e_3$ implies $\Pr(e_1 \cap e_3) = \Pr(e_1)\Pr(e_3) = p_{\perp}^{\text{MN}}(\mu)^2$, we obtain (3.13), and this concludes the proof. □

Figure 3.9 shows the empirical probability of connectivity at intersections against the analytical lower bound derived in Theorem 1 and tight lower bound presented in Theorem 2. Red and blue curves correspond to Theorems 1 and 2, respectively. Red curves start from ϵ while blue curves start from 2ϵ in agreement with the restrictions in the corresponding analytical results. We observe that the error in the lower bound of Theorem 1 (red curves) grows when density and visibility decrease, that is, when nodes are far from the intersection due to low density (small μ), or when the visibility

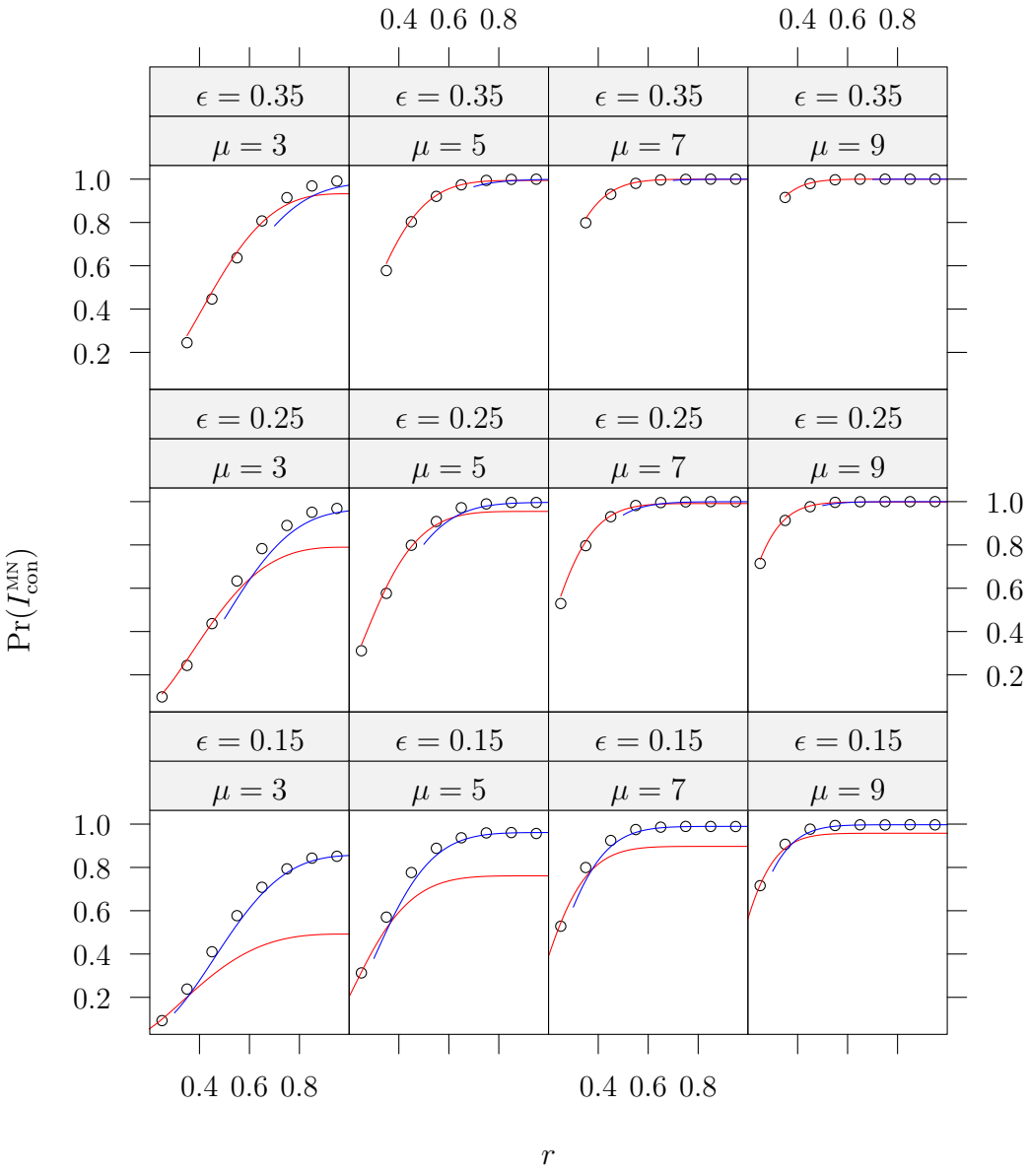

Figure 3.9. Probability of connectivity at intersection under the Max-Norm model

is restricted because of a small ϵ, the observed connectivity can be constructed, in a very small proportion, with links between nodes located in parallel segments sharing an intersection. From a different point of view, we observe that the higher the density of the network and the greater the segments' width are, the closer this lower bound is to the proper value of $\Pr(I_{\text{con}}^{\text{MN}})$. This happens because in these scenarios, links between nodes located in parallel segments are no longer needed to grant connectivity.

Differently, the result of Theorem 2 (blue curves) provides a tight lower bound independently of the scenario. In particular, we highlight two facts: (i) the error become smaller for small values of ϵ, as we expected from the proof of the analytical result, and (ii) approximations to $\Pr(I_{\text{con}}^{\text{MN}})$ are better for high probabilities.

The Max-Norm model is a simplification of a still abstract geometrical model known as the LoS model. Next section presents the formulation of local connectivity properties under this model, and the mathematical limitation for solving it analytically.

3.1.2 Line-of-Sight Model

As we saw in Section 3.1.1, for computing the probability of connectivity at intersection, we need first to compute the probability of connectivity between nodes located in perpendicular segments sharing an intersection. We already computed this for the Max-Norm model, and here we will formulate the problem for the LoS model. When we introduced the LoS model in Section 2.1, we assume that this was a convenient abstraction, comparable to the disk model for open-space networks, nevertheless this convenience is just apparent, and we will see here the limitation for analytical treatment.

Let us start considering $\{X_i\}_{1\leq i\leq \mu}$ and $\{Y_j\}_{1\leq j\leq \mu}$ as being two families of standard uniform independent random variables denoting the position of μ nodes in each one of two perpendicular segments sharing an intersection, as usual. Let also r denote the common transmission range of all nodes, where $2\epsilon \leq r \leq 1$. Additionally, let 2ϵ be the segments' width. Let us consider now the problem of determining the probability $p_{\perp}^{\text{LS}}(\mu)$ of having at least one link between μ nodes in each one of two different perpendicular segments sharing an intersection.

Let $X_{(1)}, X_{(2)}, \ldots, X_{(\mu)}$ and $Y_{(1)}, Y_{(2)}, \ldots, Y_{(\mu)}$ be the order statistics of $X_1, X_2, \ldots, X_\mu$ and $Y_1, Y_2, \ldots, Y_\mu$, respectively. We consider, as before, that positions of nodes reflect the Euclidean distances from each node to the center of intersection. With these assumptions, the problem then is to compute the probability of connectivity between $X_{(1)}$ and $Y_{(1)}$.

Under the LoS model, we need to satisfy two restrictions to have a link between $X_{(1)}$ and $Y_{(1)}$, and these restrictions are reflected in the domine of random variables $X_{(1)}$ and $Y_{(1)}$. Figure 3.10a shows the restrictions on the domine of these random variables. Here, function $y = \sqrt{r^2 - x^2}$ represents the transmission range restriction, and function $y = x\epsilon/(x - \epsilon)$ is the restriction of visibility. Since $X_{(1)}$ and $Y_{(1)}$ are i.i.d., we have that the join distribution function $f_{X_{(1)}Y_{(1)}}(x, y)$ is symmetric respect of the plane $y = x$. Consequently, we can compute $p_{\perp}^{\text{LS}}(\mu)$ as twice the value of the

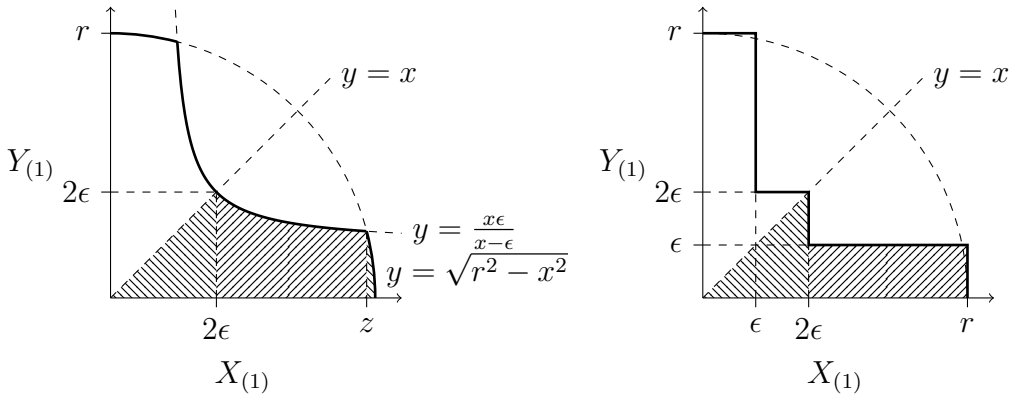

(a) LoS with $\sqrt{8}\epsilon \leq r$ (b) Triangular with $\sqrt{8}\epsilon \leq r$

Figure 3.10. Computing the probability of existence of at least one link between two nodes in perpendicular streets

volume bounded by $f_{X_{(1)}Y_{(1)}}(x,y)$ under the three filled regions of Figure 3.10a. We know from previous section that the joint distribution function of $X_{(1)}$ and $Y_{(1)}$ is $f_{X_{(1)}Y_{(1)}}(x,y) = f_{X_{(1)}}(x)f_{Y_{(1)}}(y) = \mu^2(1-x)^{\mu-1}(1-y)^{\mu-1}$, then we have

$$\begin{aligned} p_\perp(\mu) &= 2\left(\int_0^{2\epsilon}\int_0^{x} \mu^2(1-x)^{\mu-1}(1-y)^{\mu-1}\,\mathrm{d}y\,\mathrm{d}x \right. \\ &\qquad + \int_{2\epsilon}^{z}\int_0^{\frac{x\epsilon}{x-\epsilon}} \mu^2(1-x)^{\mu-1}(1-y)^{\mu-1}\,\mathrm{d}y\,\mathrm{d}x \\ &\qquad \left. + \int_z^r\int_0^{\sqrt{r^2-x^2}} \mu^2(1-x)^{\mu-1}(1-y)^{\mu-1}\,\mathrm{d}y\,\mathrm{d}x\right) \\ &= 2\left(\frac{1}{2}(1-x)^{2\mu} - (1-x)^{\mu} + \int_{2\epsilon}^{z}\mu(1-x)^{\mu-1}\left(1-\left(1-\sqrt{r^2-x^2}\right)^{\mu}\right)\mathrm{d}x\right. \\ &\qquad \left. + \int_{2\epsilon}^{z}\mu(1-x)^{\mu-1}\left(1-\left(1-\frac{x\epsilon}{x-\epsilon}\right)^{\mu}\right)\mathrm{d}x\right) \end{aligned} \tag{3.24}$$

where z is the smaller root of the system $\sqrt{r^2-x^2} - \frac{x\epsilon}{x-\epsilon} = 0$. For the two integrals in (3.24), we found no solution in terms of standard mathematical functions. And even if there exist one, we do not expect this expression to be simple.

The lack of solution for integrals in (3.24) added to the complexity of upper limit for definite integration motivate the use of a new simplified model. This model should be an abstraction capable of maintaining simplicity and accuracy at the same time, and this is the Triangular model.

3.1.3 Triangular Model

So far we derived local connectivity probabilities for the Max-Norm model, and founded elements that lead us to think about the impossibility of mathematical treatment of the LoS model. The Triangular model emerge from this impossibility and, as we will see, represents an solution with "balance" between complexity and accuracy. Naturally, for a better description of this balance, definitions of "complexity" and "accuracy" are required. We can think model complexity based on the complexity of functions, or classifying according to how easy these functions can be integrated. On the other hand, we can propose a measurement of accuracy based on distances of functions, having the LoS model as a reference. Independently of the measurements, the aforementioned balance cannot be universal; the best model can change from case to case, based on the final goal of the modeling. Nevertheless, we consider the LoS model as a reference, and we compare models with this criterion.

Herein we follow the same strategy as before, that is, we first compute, in Lemma 3 the probability of connectivity between any two nodes from two different sets of μ nodes placed at perpendicular segments sharing an intersection, and then we compute the probability of connectivity at intersection. We denote these probability by $p_{\perp}^{\mathrm{T}}(\mu)$ and $\Pr(I_{\mathrm{con}}^{\mathrm{T}})$, respectively.

We try to make proofs as self-contained as possible, although we can fall in tedious repetition. We took this decision to facilitate the reading process, allowing the reader to follow proofs with less effort.

Lemma 3. *Let $\{X_i\}_{1\leq i\leq \mu}$ and $\{Y_j\}_{1\leq j\leq \mu}$ be two families of standard uniform independent random variables denoting the position of μ nodes in each one of two perpendicular segments sharing an intersection. Let also 2ϵ be the segments' width. Additionally, let r denote the common transmission range of all nodes, where $2\epsilon \leq r \leq 1$. Assuming the Triangular model, the probability $p_{\perp}^{T}(\mu)$ of having at least one link between two nodes in different perpendicular segments is*

$$p_{\perp}^{T}(\mu) = (1-2\epsilon)^{2\mu} + 2(1-\epsilon)^{\mu}\left((1-r)^{\mu} - (1-2\epsilon)^{\mu}\right) + 2\left(1/2 - (1-r)^{\mu}\right) \qquad (3.25)$$

Proof. Let $X_{(1)}, X_{(2)}, \ldots, X_{(\mu)}$ and $Y_{(1)}, Y_{(2)}, \ldots, Y_{(\mu)}$ be the order statistics of $X_1, X_2, \ldots, X_\mu$ and $Y_1, Y_2, \ldots, Y_\mu$, respectively. We consider, without loss of generality (w.l.o.g.), that positions of nodes reflect the Euclidean distances from each node to the center point between segments. There exists at least one link between two nodes in different perpendicular segments iff there is a link between $X_{(1)}$ and $Y_{(1)}$.

For connecting $X_{(1)}$ with $Y_{(1)}$, under the Triangular model, we need to satisfy one

of the following two conditions: (i) the minimum norm $\min\{\|x_u - x_v\|, \|y_u - y_v\|\} \leq \epsilon$, and the maximum norm $\max\{\|x_u - x_v\|, \|y_u - y_v\|\} \leq r$, or (ii) both u and v are at most at a distance 2ϵ far from a shared intersection. Figure 3.10b shows the region in the domine of $f_{X_{(1)}Y_{(1)}}(x, y)$ that satisfy at least one of these conditions. Since $f_{X_{(1)}Y_{(1)}}(x, y)$ is symmetric respect of the plane $y = x$, we can compute $p_{\perp}^{\mathrm{T}}(\mu)$ as twice the value of the volume bounded by $f_{X_{(1)}Y_{(1)}}(x, y)$ under the two filled regions in the domine illustred in Figure 3.10b. Note that we assume $r \geq 2\epsilon$. This is not a strong assumption, since values of $r < \sqrt{8}\epsilon$ do not represent a scenario with obstacles. Said that, and remembering that the joint distribution function of $X_{(1)}$ and $Y_{(1)}$ is $f_{X_{(1)}Y_{(1)}}(x, y) = \mu^2(1-x)^{\mu-1}(1-y)^{\mu-1}$, we proceed to compute $p_{\perp}^{\mathrm{T}}(\mu)$ as follows:

$$
\begin{aligned}
p_{\perp}^{\mathrm{T}}(\mu) &= 2\left(\int_0^{2\epsilon}\int_0^{x} f_{X_{(1)}Y_{(1)}}(x, y)\,\mathrm{d}y\,\mathrm{d}x + \int_{2\epsilon}^{r}\int_0^{\epsilon} f_{X_{(1)}Y_{(1)}}(x, y)\,\mathrm{d}y\,\mathrm{d}x\right) \\
&= 2\left(\int_0^{2\epsilon}\int_0^{x} \mu^2(1-x)^{\mu-1}(1-y)^{\mu-1}\,\mathrm{d}y\,\mathrm{d}x \right. \\
&\qquad \left. + \int_{2\epsilon}^{r}\int_0^{\epsilon} \mu^2(1-x)^{\mu-1}(1-y)^{\mu-1}\,\mathrm{d}y\,\mathrm{d}x\right) \\
&= (1-2\epsilon)^{2\mu} + 2(1-\epsilon)^{\mu}\left((1-r)^{\mu} - (1-2\epsilon)^{\mu}\right) \\
&\qquad + 2\left(1/2 - (1-r)^{\mu}\right), \qquad (3.26)
\end{aligned}
$$

and this concludes the proof. □

Figure 3.11 shows the empirical and theoretical results for $p_{\perp}^{\mathrm{T}}(\mu)$. Red curves correspond to expression (3.26) under different densities and segments' width values. Notice that Lemma 3 presents the exact analytical solution, and all these cases in the figure are just a mechanism of validation for all the steps in the proof. Besides expression (3.26) gives the exact value for $p_{\perp}^{\mathrm{T}}(\mu)$ under the Triangular model, we highlight that under the LoS model this expression represents a lower bound for $r \geq \sqrt{8}\epsilon$, and this is why we assume the same while computing the probability of connectivity at intersections, in the following Theorem 3.

Theorem 3. *Let $\{X_i\}_{1\leq i\leq \mu}$, $\{Y_j\}_{1\leq j\leq \mu}$, $\{W_k\}_{1\leq k\leq \mu}$ and $\{Z_m\}_{1\leq m\leq \mu}$ be four families of independent random variables, such that $X_i \sim \mathcal{U}(0,1)$, $Y_j \sim \mathcal{U}(0,1)$, $W_k \sim \mathcal{U}(0,1)$ and $Z_m \sim \mathcal{U}(0,1)$, denoting the positions of μ nodes in four adjacent segments sharing an intersection. Let 2ϵ be the segments' width, and let r denote the common transmission range of all nodes, with $\sqrt{8}\epsilon \leq r \leq 1$. The probability of connectivity at intersections*

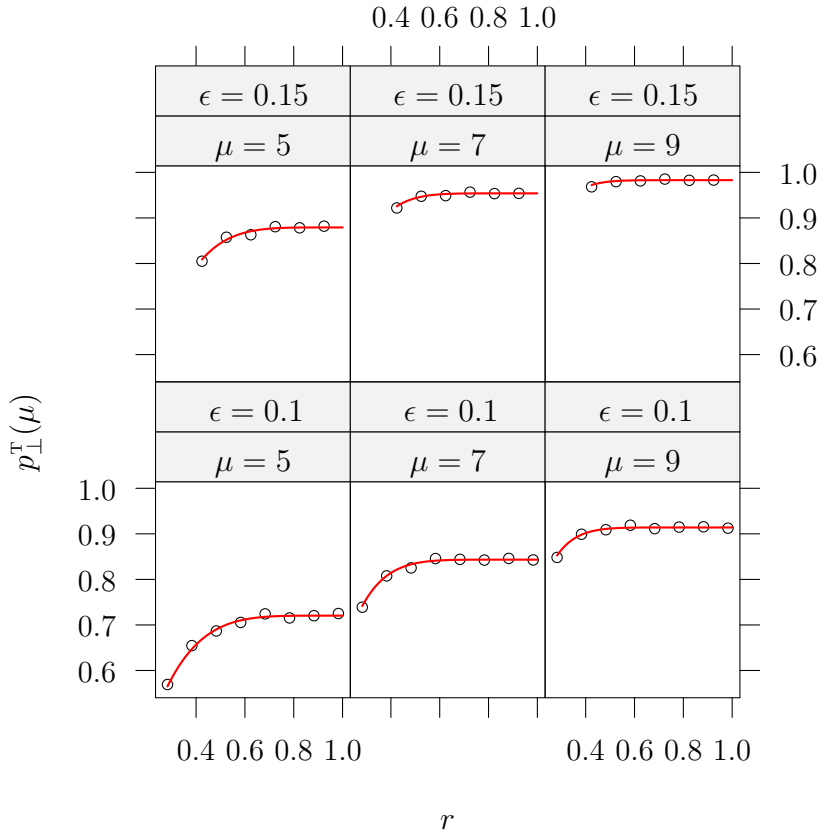

Figure 3.11. Probability of connectivity, under the Triangular model, between nodes located at perpendicular segments sharing an intersection

under the Triangular model, denoted by $\Pr(I_{con}^{T})$*, is given by*

$$\begin{aligned}\Pr(I_{con}^{T}) \geq p_{\perp}(\mu)^2 + 2\Big(&D_0^{\epsilon}(\mu)D_0^{r}(\mu)\left[D_{2\epsilon}^{r}(\mu)D_{\epsilon}^{r-\epsilon}(\mu) + D_{\epsilon}^{2\epsilon}(\mu)D_{2\epsilon}^{r-\epsilon}(\mu)\right] \\ &+D_{\epsilon}^{2\epsilon}(\mu)D_0^{2\epsilon}(\mu)\left[D_{2\epsilon}^{r-2\epsilon}(\mu)D_{\epsilon}^{r-2\epsilon}(\mu) + D_{\epsilon}^{2\epsilon}(\mu)D_{2\epsilon}^{r-2\epsilon}(\mu)\right] \\ &+D_{2\epsilon}^{r}(\mu)D_0^{\epsilon}(\mu)\left[D_{2\epsilon}^{r-\epsilon}(\mu)D_{\epsilon}^{r}(\mu) + D_{\epsilon}^{2\epsilon}(\mu)D_{2\epsilon}^{r}(\mu)\right]\Big) + 2\left(D_{\epsilon}^{2\epsilon}(\mu)D_{2\epsilon}^{r-2\epsilon}(\mu)\right)^2, \quad (3.27)\end{aligned}$$

where $D_i^j(k) = (1-i)^k - (1-j)^k$.

Proof. W.l.o.g., we consider that positions of nodes reflect the Euclidean distances from each node to the center point between segments. Consider the order statistics $X_{(1)}$, $Y_{(1)}$, $W_{(1)}$ and $Z_{(1)}$, from the families $\{X_i\}_{1\leq i\leq \mu}$, $\{Y_j\}_{1\leq j\leq \mu}$, $\{W_k\}_{1\leq k\leq \mu}$ and $\{Z_m\}_{1\leq m\leq \mu}$, respectively. The intersection graph I is connected iff there exists a path between $X_{(1)}$, $Y_{(1)}$, $W_{(1)}$ and $Z_{(1)}$.

Let e_1 be the event that indicates the presence of a link between the realizations

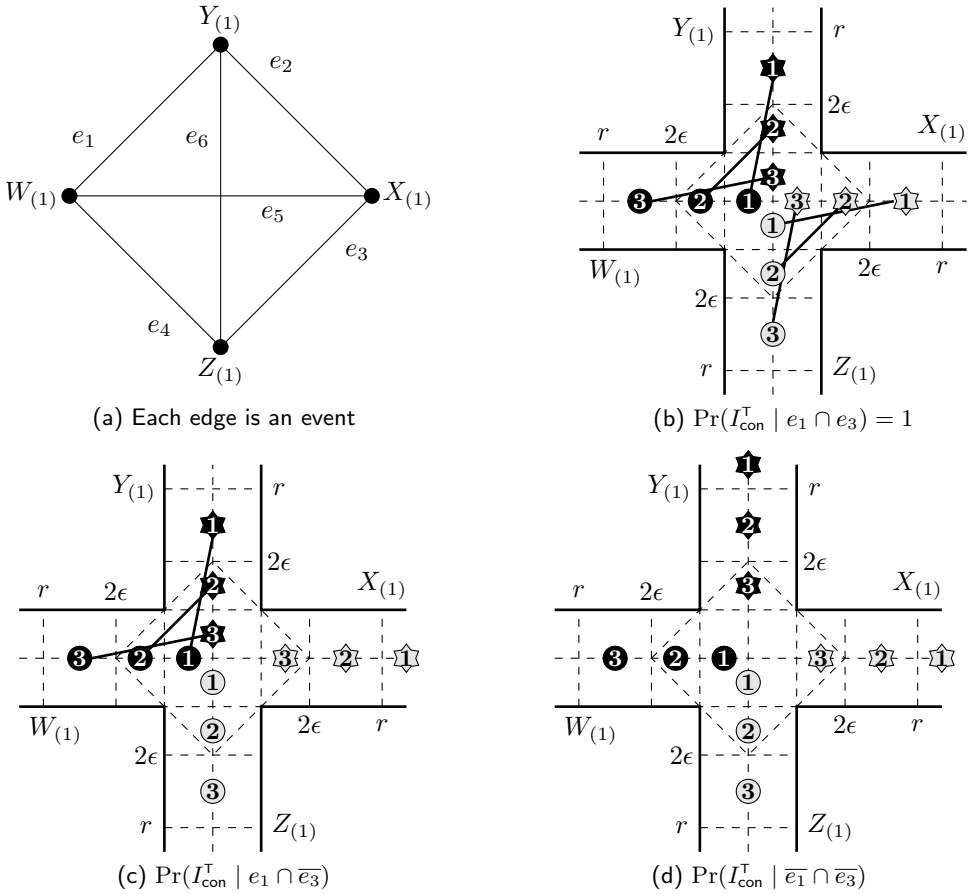

(a) Each edge is an event

(b) $\Pr(I^{\mathrm{T}}_{\mathrm{con}} \mid e_1 \cap e_3) = 1$

(c) $\Pr(I^{\mathrm{T}}_{\mathrm{con}} \mid e_1 \cap \overline{e_3})$

(d) $\Pr(I^{\mathrm{T}}_{\mathrm{con}} \mid \overline{e_1} \cap \overline{e_3})$

Figure 3.12. Computing the probability of connectivity at intersections.

of $Y_{(1)}$ and $W_{(1)}$ (see Figure 3.12a). Additionally, let e_2, e_3, e_4, e_5 and e_6 represent the existence of a link between $X_{(1)}$ and $Y_{(1)}$, $X_{(1)}$ and $Z_{(1)}$, $W_{(1)}$ and $Z_{(1)}$, $W_{(1)}$ and $X_{(1)}$ and finally $Y_{(1)}$ and $Z_{(1)}$, respectively. Then, we have $e_1 \perp\!\!\!\perp e_3$ and $e_2 \perp\!\!\!\perp e_4$, while edges that share a node are clearly not independent because of geometrical correlation. Since $e_1 \perp\!\!\!\perp e_3$, we are able to construct the partition $\tilde{P}_e = \{e_1 \cap e_3, e_1 \cap \overline{e_3}, \overline{e_1} \cap e_3, \overline{e_1} \cap \overline{e_3}\}$ on the sample space Ω.

Consequently, applying the law of total probability and considering the symmetry between $e_1 \cap \overline{e_3}$ and $\overline{e_1} \cap e_3$, we can compute

$$\Pr(I^{\mathrm{T}}_{\mathrm{con}}) = \Pr(I^{\mathrm{T}}_{\mathrm{con}} \mid e_1 \cap e_3)\Pr(e_1 \cap e_3) + 2\Pr(I^{\mathrm{T}}_{\mathrm{con}} \mid e_1 \cap \overline{e_3})\Pr(e_1 \cap \overline{e_3}) + \Pr(I^{\mathrm{T}}_{\mathrm{con}} \mid \overline{e_1} \cap \overline{e_3})\Pr(\overline{e_1} \cap \overline{e_3}) \quad (3.28)$$

The three summands in (3.28) contain the event $I^{\mathrm{T}}_{\mathrm{con}}$ conditioned on $e_1 \cap e_3$, $e_1 \cap \overline{e_3}$ or $\overline{e_1} \cap \overline{e_3}$. To solve these probabilities, we use the same technique as the one used in

Theorem 2, that is, we apply the law of total probability in the partition

$$\tilde{P}_{\epsilon,r} = \{0 \leq W_{(1)} \leq \epsilon,\ \epsilon < W_{(1)} \leq 2\epsilon,\ 2\epsilon < W_{(1)} \leq r\} \times \{0 \leq Z_{(1)} \leq \epsilon,\ \epsilon < Z_{(1)} \leq 2\epsilon,\ 2\epsilon < Z_{(1)} \leq r\} \quad (3.29)$$

on $e_1 \cap e_3$, $e_1 \cap \overline{e_3}$ and $\overline{e_1} \cap \overline{e_3}$, respectively. We identify in (3.29) three intervals where $W_{(1)}$ and $Z_{(1)}$ belong to $[0, \epsilon]$, $(\epsilon, 2\epsilon]$ and $(2\epsilon, r]$. We call these three intervals as $\tilde{S}_1$, $\tilde{S}_2$ and $\tilde{S}_3$, respectively, and define $\tilde{C}_{i,j}$ as being the element of partition $\tilde{P}_{\epsilon,r}$ where $W_{(1)} \in \tilde{S}_i$ and $Z_{(1)} \in \tilde{S}_j$. With this partition, we proceed to compute each conditional term of (3.28).

Let us consider firstly the partition $\tilde{P}_{\epsilon,r}$ on $e_1 \cap e_3$ for solving $\Pr(I^{\mathrm{T}}_{\mathrm{con}} \mid e_1 \cap e_3)$. Figure 3.12b shows a schematic view of partition $\tilde{P}_{\epsilon,r}$ on $e_1 \cap e_3$, where the black balls represent instances of $W_{(1)}$ and gray balls reprecent instances of $Z_{(1)}$. Each pair of balls of different color represent a class $\tilde{C}_{i,j}$ of $\tilde{P}_{\epsilon,r}$. Edges, in this figure, represent the conditioning on $e_1 \cap e_3$, and the position of stars represent the worst case (farthest region from the origin) for this conditioning. Numbering in both, balls and stars, is used for identifying the intervals of instances of $W_{(1)}$ and $Z_{(1)}$, and more important, for visualizing each class $\tilde{C}_{i,j}$ of $\tilde{P}_{\epsilon,r}$. Observing the partition $\tilde{P}_{\epsilon,r}$ in Figure 3.12b we perceive that for each class $\tilde{C}_{i,j}$ it is possible to have a third edge connecting the connected components $\{W_{(1)}, Y_{(1)}\}$ and $\{Z_{(1)}, X_{(1)}\}$, which implies $\Pr(I^{\mathrm{T}}_{\mathrm{con}} \mid e_1 \cap e_3) = 1$. Additionally, we have $e_1 \perp\!\!\!\perp e_3$, then the first term of (3.28) is $\Pr(e_1 \cap e_3) = \Pr(e_1)\Pr(e_3) = p^{\mathrm{T}}_{\perp}(\mu)^2$.

Let us consider now the partition $\tilde{P}_{\epsilon,r}$ on $e_1 \cap \overline{e_3}$ for solving $\Pr(I^{\mathrm{T}}_{\mathrm{con}} \mid e_1 \cap \overline{e_3})$. Applying law of total probability, we obtain

$$\Pr(I^{\mathrm{T}}_{\mathrm{con}} \mid e_1 \cap \overline{e_3}) = \frac{\sum_{i=1}^{3}\sum_{j=1}^{3} \Pr(I^{\mathrm{T}}_{\mathrm{con}} \cap C_{i,j} \cap e_1 \cap \overline{e_3})}{\Pr(e_1 \cap \overline{e_3})} \quad (3.30)$$

Figure 3.12c shows classes $C_{i,j}$ on $e_1 \cap \overline{e_3}$. The schematic view in this figure is essentially the same as Figure3.12b, with the exception for gray stars which represent the best case positioning. The idea behind considering best cases is to identify potential edges. In the following, we analyse each one of the nine terms, $\Pr(I_{con} \cap C_{i,j} \cap e_1 \cap \overline{e_3})$, separately.

For the three classes $\tilde{C}_{i,1}$, we observe that random node $X_{(1)}$ is isolated even in the best case, since $X_{(1)} > r$ (see Figure 3.12c). This means that $\sum_{i=1}^{3} \Pr(I^{\mathrm{T}}_{\mathrm{con}} \cap \tilde{C}_{i,1} \cap e_1 \cap \overline{e_3}) = 0$.

Let us consider now $\Pr(I^{\mathrm{T}}_{\mathrm{con}} \cap \tilde{C}_{1,2} \cap e_1 \cap \overline{e_3})$. Figure 3.13a shows the geometrical restrictions for $\tilde{C}_{1,2} \cap e_1 \cap \overline{e_3}$. Here we perceive that we need the edge $e_2 = (X_{(1)}, Y_{(1)})$

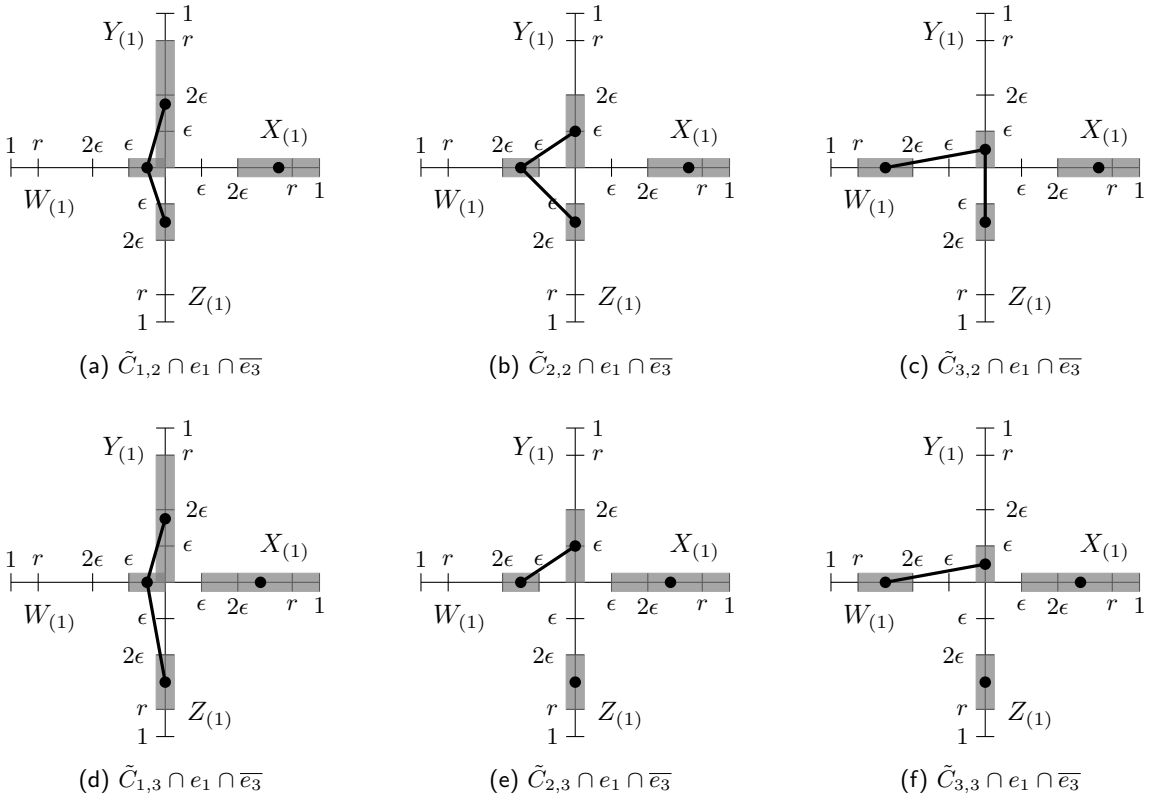

(a) $\tilde{C}_{1,2} \cap e_1 \cap \overline{e_3}$ (b) $\tilde{C}_{2,2} \cap e_1 \cap \overline{e_3}$ (c) $\tilde{C}_{3,2} \cap e_1 \cap \overline{e_3}$

(d) $\tilde{C}_{1,3} \cap e_1 \cap \overline{e_3}$ (e) $\tilde{C}_{2,3} \cap e_1 \cap \overline{e_3}$ (f) $\tilde{C}_{3,3} \cap e_1 \cap \overline{e_3}$

Figure 3.13. $\tilde{C}_{i,j} \cap e_1 \cap \overline{e_3}$

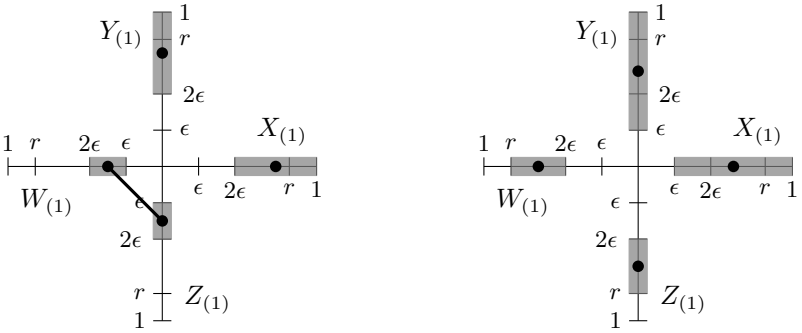

(a) $C_{2,2} \cap \overline{e_1} \cap \overline{e_3}$ (b) $C_{3,3} \cap \overline{e_1} \cap \overline{e_3}$

Figure 3.14. $C_{i,i} \cap \overline{e_1} \cap \overline{e_3}$

or $e_5 = (X_{(1)}, W_{(1)})$ in order to have connectivity. Since e_2 and e_5 are correlated, we compute a lower bound considering only e_5. Additionally, for the sake of simplicity, we compute a lower bound for the probability of e_5 assuming the worst case $W_{(1)} = \epsilon$,

i.e., farthest away from the center. With this, we have

$$\Pr(I_{\text{con}}^{\text{T}} \cap \tilde{C}_{1,2} \cap e_1 \cap \overline{e_3}) \geq \int_0^{\epsilon} f_{W_{(1)}}(w)\,\mathrm{d}w \int_0^{r} f_{Y_{(1)}}(y)\,\mathrm{d}y \int_{\epsilon}^{2\epsilon} f_{Z_{(1)}}(z)\,\mathrm{d}z \int_{2\epsilon}^{r-\epsilon} f_{X_{(1)}}(x)\,\mathrm{d}x \quad (3.31)$$

The last integral in (3.31) corresponds to random variable $X_{(1)}$. Note that here we restrict the domine of $X_{(1)}$ to maintain the edge $e_5 = (X_{(1)}, W_{(1)})$ given $W_{(1)} = \epsilon$, that is, we originally have $X_{(1)} \in (2\epsilon, 1]$ because of condition $\tilde{C}_{1,2} \cap \overline{e_3}$, and afterwards we restrict $X_{(1)}$ to a smaller interval, contained in $(2\epsilon, 1]$, given place to event e_5. This explains the integration intervals of (3.31).

We know that the p.d.f. of the first order statistic $U_{(1)}$ is $f_{U_{(1)}}(u) = \mu(1-u)^{\mu-1}$ and $\int_i^j k(1-u)^{k-1}\,\mathrm{d}u = (1-i)^k - (1-j)^k$. This last expression represents the probability of having the first order statistic of family $\{U_h\}_{1\leq h\leq k}$ within the interval (i, j), and it is denoted by $D_i^j(k)$. Then, we can rewrite the expression (3.31) as

$$\Pr(I_{\text{con}}^{\text{T}} \cap \tilde{C}_{1,2} \cap e_1 \cap \overline{e_3}) \geq D_0^{\epsilon}(\mu) D_0^{r}(\mu) D_{\epsilon}^{2\epsilon}(\mu) D_{2\epsilon}^{r-\epsilon}(\mu). \quad (3.32)$$

For $\Pr(I_{\text{con}}^{\text{T}} \cap \tilde{C}_{1,3} \cap e_1 \cap \overline{e_3})$ and $\Pr(I_{\text{con}}^{\text{T}} \cap \tilde{C}_{2,2} \cap e_1 \cap \overline{e_3})$, we have a similar scenarios as $\tilde{C}_{1,2}$, as can be observed in Figure 3.13d and Figure 3.13b. Using the same approach, we consider just e_5 and obtain the following lower bounds

$$\begin{aligned} \Pr(I_{\text{con}}^{\text{T}} \cap \tilde{C}_{1,3} \cap e_1 \cap \overline{e_3}) &\geq \int_0^{\epsilon} f_{W_{(1)}}(w)\,\mathrm{d}w \int_0^{r} f_{Y_{(1)}}(y)\,\mathrm{d}y \int_{2\epsilon}^{r} f_{Z_{(1)}}(z)\,\mathrm{d}z \int_{\epsilon}^{r-\epsilon} f_{X_{(1)}}(x)\,\mathrm{d}x \\ &= D_0^{\epsilon}(\mu) D_0^{r}(\mu) D_{2\epsilon}^{r}(\mu) D_{\epsilon}^{r-\epsilon}(\mu), \end{aligned} \quad (3.33)$$

and

$$\begin{aligned} \Pr(I_{\text{con}}^{\text{T}} \cap \tilde{C}_{2,2} \cap e_1 \cap \overline{e_3}) &\geq \int_{\epsilon}^{2\epsilon} f_{W_{(1)}}(w)\,\mathrm{d}w \int_0^{2\epsilon} f_{Y_{(1)}}(y)\,\mathrm{d}y \int_{\epsilon}^{2\epsilon} f_{Z_{(1)}}(z)\,\mathrm{d}z \int_{2\epsilon}^{r-2\epsilon} f_{X_{(1)}}(x)\,\mathrm{d}x \\ &= D_{\epsilon}^{2\epsilon}(\mu) D_0^{2\epsilon}(\mu) D_{\epsilon}^{2\epsilon}(\mu) D_{2\epsilon}^{r-2\epsilon}(\mu). \end{aligned} \quad (3.34)$$

Figure 3.13e and 3.13f present a different scenario, with just one edge. Here, for having connectivity we need at least two more edges, one of them connecting $Z_{(1)}$ to $Y_{(1)}$, and other connecting $X_{(1)}$ to $Y_{(1)}$ or $W_{(1)}$. Observe that $Z_{(1)}$ can only connect

to $Y_{(1)}$, since $W_{(1)}$ is not visible, and $X_{(1)}$ is not allowed because of condition $\overline{e_3}$. For $\tilde{C}_{2,3}$ we consider edge e_5 and e_6, obtaining a lower bound for the worst case fixing $Y_{(1)} = 2\epsilon$ and $W_{(1)} = 2\epsilon$. On the other hand, for $\tilde{C}_{3,3}$ we only fix $Y_{(1)} = \epsilon$, to compute the worst case probability of the edge $(Y_{(1)}, Z_{(1)})$ simultaneously with the probability of $(X_{(1)}, Y_{(1)})$. With this approach, we have

$$\begin{aligned}\Pr(I_{\text{con}}^{\text{T}} \cap \tilde{C}_{2,3} \cap e_1 \cap \overline{e_3}) &\geq \int_{\epsilon}^{2\epsilon} f_{W_{(1)}}(w)\,\mathrm{d}w \int_{0}^{2\epsilon} f_{Y_{(1)}}(y)\,\mathrm{d}y \\ &\qquad \int_{2\epsilon}^{r-2\epsilon} f_{Z_{(1)}}(z)\,\mathrm{d}z \int_{\epsilon}^{r-2\epsilon} f_{X_{(1)}}(x)\,\mathrm{d}x \\ &= D_{\epsilon}^{2\epsilon}(\mu) D_{0}^{2\epsilon}(\mu) D_{2\epsilon}^{r-2\epsilon}(\mu) D_{\epsilon}^{r-2\epsilon}(\mu), \end{aligned} \tag{3.35}$$

and

$$\begin{aligned}\Pr(I_{\text{con}}^{\text{T}} \cap \tilde{C}_{3,3} \cap e_1 \cap \overline{e_3}) &\geq \int_{2\epsilon}^{r} f_{W_{(1)}}(w)\,\mathrm{d}w \int_{0}^{\epsilon} f_{Y_{(1)}}(y)\,\mathrm{d}y \\ &\qquad \int_{2\epsilon}^{r-2\epsilon} f_{Z_{(1)}}(z)\,\mathrm{d}z \int_{\epsilon}^{r} f_{X_{(1)}}(x)\,\mathrm{d}x \\ &= D_{2\epsilon}^{r}(\mu) D_{0}^{\epsilon}(\mu) D_{2\epsilon}^{r-2\epsilon}(\mu) D_{\epsilon}^{r}(\mu). \end{aligned} \tag{3.36}$$

Finally, in the last case we have $\Pr(I_{\text{con}}^{\text{T}} \cap \tilde{C}_{3,2} \cap e_1 \cap \overline{e_3}) = \Pr(e_2 \cap \tilde{C}_{3,2} \cap e_1 \cap \overline{e_3})$, where $e_2 = (X_{(1)}, Y_{(1)})$ (see Figure 3.13c). Considering this, we have

$$\begin{aligned}\Pr(I_{\text{con}}^{\text{T}} \cap \tilde{C}_{3,2} \cap e_1 \cap \overline{e_3}) &= \int_{2\epsilon}^{r} f_{W_{(1)}}(w)\,\mathrm{d}w \int_{0}^{\epsilon} f_{Y_{(1)}}(y)\,\mathrm{d}y \\ &\qquad \int_{\epsilon}^{2\epsilon} f_{Z_{(1)}}(z)\,\mathrm{d}z \int_{2\epsilon}^{r} f_{X_{(1)}}(x)\,\mathrm{d}x \\ &= D_{2\epsilon}^{r}(\mu) D_{0}^{\epsilon}(\mu) D_{\epsilon}^{2\epsilon}(\mu) D_{2\epsilon}^{r}(\mu). \end{aligned} \tag{3.37}$$

Combining (3.32) to (3.37) into (3.30) and replacing in the second term of (3.28), we obtain the second term of the general result of this theorem.

The next step is to derive the third term of (3.28). Considering partition $\tilde{P}_{\epsilon,r}$ on $\overline{e_1} \cap \overline{e_3}$, we obtain four cases with no isolated nodes, namely $\tilde{C}_{2,2}$, $\tilde{C}_{2,3}$, $\tilde{C}_{3,2}$ and $\tilde{C}_{3,3}$ (see Figure 3.12d). Additionally, it is easy so perceive that it is not possible to establish connectivity for $\tilde{C}_{2,3}$ nor $\tilde{C}_{3,2}$, then

$$\Pr(I_{\text{con}}^{\text{T}} \mid \overline{e_1} \cap \overline{e_3}) = \frac{\sum_{i=1}^{2} \Pr(I_{\text{con}}^{\text{T}} \cap \tilde{C}_{i,i} \cap \overline{e_1} \cap \overline{e_3})}{\Pr(\overline{e_1} \cap \overline{e_3})}$$

Figure 3.14 presents the scenarios $\tilde{C}_{2,2}$ and $\tilde{C}_{3,3}$. For having connectivity under $\tilde{C}_{2,2} \cap \overline{e_1} \cap \overline{e_3}$, we need internal edges $(Y_{(1)}, Z_{(1)})$ and $(X_{(1)}, W_{(1)})$. We can approximate this probability, by considering the worst case $W_{(1)} = 2\epsilon$ and $Z_{(1)} = 2\epsilon$, as follows

$$\begin{aligned}\Pr(I_{\text{con}}^{\text{T}} \cap \tilde{C}_{2,2} \cap \overline{e_1} \cap \overline{e_3}) &\geq \int_{\epsilon}^{2\epsilon} f_{W_{(1)}}(w)\,\mathrm{d}w \int_{2\epsilon}^{r-2\epsilon} f_{Y_{(1)}}(y)\,\mathrm{d}y \\ &\qquad \int_{\epsilon}^{2\epsilon} f_{Z_{(1)}}(z)\,\mathrm{d}z \int_{2\epsilon}^{r-2\epsilon} f_{X_{(1)}}(x)\,\mathrm{d}x \\ &= \left(D_{\epsilon}^{2\epsilon}(\mu) D_{2\epsilon}^{r-2\epsilon}(\mu)\right)^2. \end{aligned} \tag{3.39}$$

Finally, as we can see in Figure 3.14b, we need internal edges $(Y_{(1)}, Z_{(1)})$ and $(X_{(1)}, W_{(1)})$, and external edge $(X_{(1)}, Y_{(1)})$ for grant connectivity under $\tilde{C}_{3,3} \cap \overline{e_1} \cap \overline{e_3}$, which leads to

$$\begin{aligned}\Pr(I_{\text{con}}^{\text{T}} \cap \tilde{C}_{3,3} \cap \overline{e_1} \cap \overline{e_3}) &\geq \int_{\epsilon}^{2\epsilon} f_{W_{(1)}}(w)\,\mathrm{d}w \int_{2\epsilon}^{r-2\epsilon} f_{Y_{(1)}}(y)\,\mathrm{d}y \\ &\qquad \int_{\epsilon}^{2\epsilon} f_{Z_{(1)}}(z)\,\mathrm{d}z \int_{2\epsilon}^{r-2\epsilon} f_{X_{(1)}}(x)\,\mathrm{d}x \\ &= \left(D_{\epsilon}^{2\epsilon}(\mu) D_{2\epsilon}^{r-2\epsilon}(\mu)\right)^2. \end{aligned} \tag{3.40}$$

Adding up (3.39) and (3.40), we obtain the third term of (3.28), and this concludes the proof. □

We know, by the approximation strategy, that the bigger the segments' width, the bigger the error of Theorem 3 and, indeed, Figure 3.15 shows this phenomenon. Here we visualize good approximations in all scenarios, and we also observe that approximations slightly improve as we consider denser scenarios and bigger transmission ranges.

Besides the density and transmission range clearly affect the perceived error of Theorem 3, it is really hard to determine the degree of influence of two aforementioned parameters by observing Figure 3.15. Fortunately, it is possible to compute an upper bound of this error by considering best cases for connectivity in all combinations of partitions $\tilde{P}_e$ and $\tilde{P}_{\epsilon,r}$, and this is what we do in the following Corollary 1.

Corollary 1 (Upper bound for error in Theorem 3)**.** *The upper bound of the error in Theorem 3 under the Triangular model, is given by*

$$\begin{aligned}error \leq 2\Big(&D_0^{\epsilon}(\mu) D_0^r(\mu) \left[D_{\epsilon}^{2\epsilon}(\mu) D_{r-2\epsilon}^r(\mu)\right. \\ &\left. + D_{2\epsilon}^r(\mu) D_{r-\epsilon}^r(\mu)\right] + D_{\epsilon}^{2\epsilon}(\mu) D_0^{2\epsilon}(\mu) \left[D_{\epsilon}^{2\epsilon}(\mu) D_{r-2\epsilon}^r(\mu) + D_{2\epsilon}^r(\mu) D_{r-2\epsilon}^r(\mu)\right] \\ &+ D_{2\epsilon}^r(\mu) D_0^{\epsilon}(\mu) D_{\epsilon}^r(\mu) D_{r-\epsilon}^r(\mu)\Big) + 2 D_{\epsilon}^{2\epsilon}(\mu)^2 \left[D_{2\epsilon}^{r-\epsilon}(\mu)^2 - D_{2\epsilon}^{r-2\epsilon}(\mu)^2\right] \end{aligned} \tag{3.41}$$

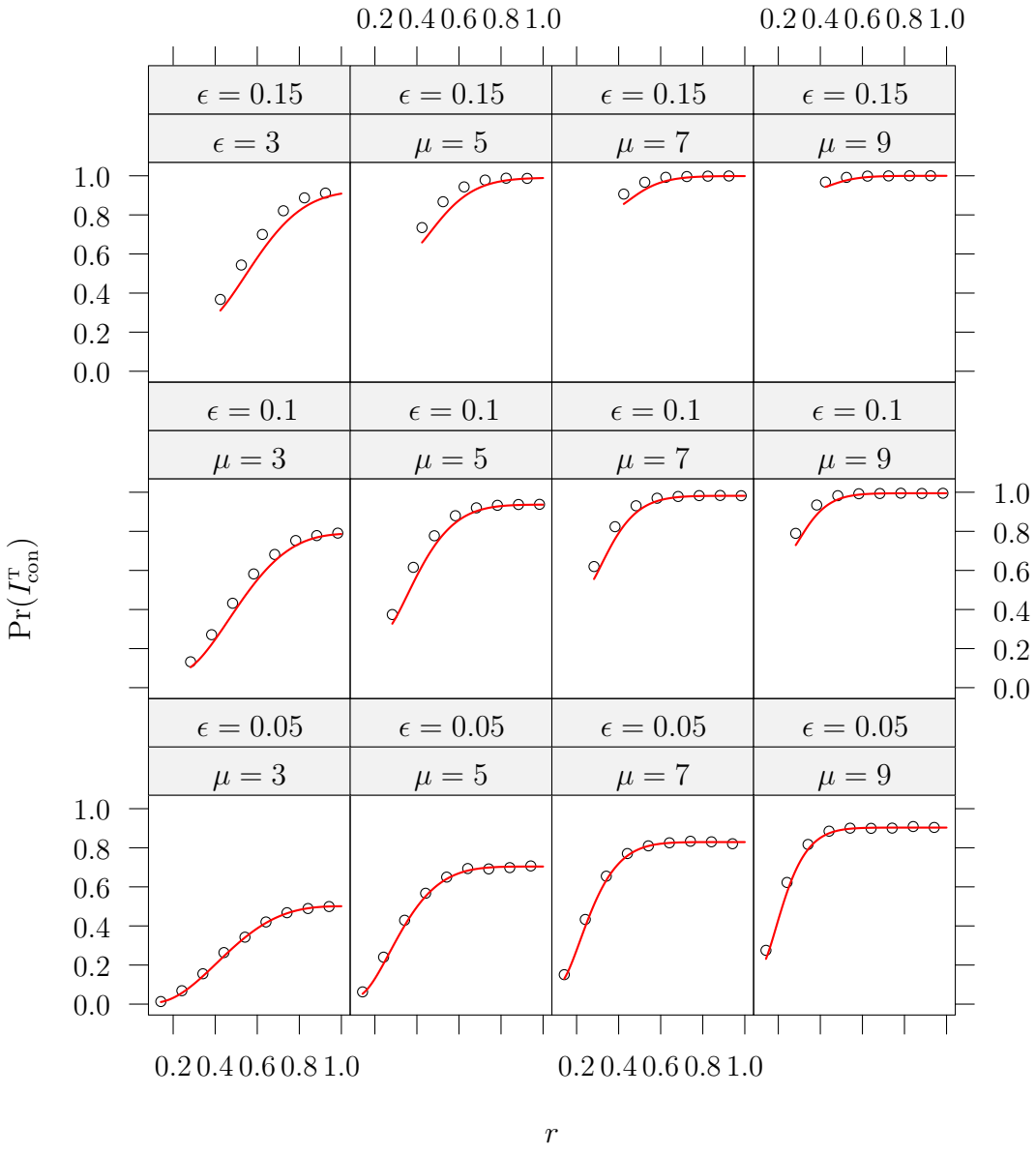

Figure 3.15. $\Pr(I^{\mathrm{T}}_{\mathrm{con}})$

Proof. In the proof of Theorem 3, we give lower bounds for the second and third summands of (3.28). The method for computing the lower bounds was to consider the worst case positions for those nodes that belong to small intervals, fixing some nodes to values as far as possible from the origin, while respecting the restrictions inherent to the class within partition $\tilde{P}_{\epsilon,r}$.

We can compute upper bounds for those two summands of (3.28) similarly as

done with the lower bounds considering, now, the best case positions. Let us start with $\Pr(I^{\mathrm{T}}_{\mathrm{con}} \mid e_1 \cap \overline{e_3})$. Following the same strategy as in Theorem 3, we consider each one of the nine term of (3.30) separately. As we showed in the proof of Theorem 3, $\sum_{i=1}^{3} \Pr(I^{\mathrm{T}}_{\mathrm{con}} \cap \tilde{C}_{i,1} \cap e_1 \cap \overline{e_3}) = 0$. Let us consider $\Pr(I^{\mathrm{T}}_{\mathrm{con}} \cap \tilde{C}_{1,2} \cap e_1 \cap \overline{e_3})$. Observing Figure 3.13a, we perceive that a tight upper bound can be obtained considering $W_{(1)} = 0$ for the occurrence of edge e_5. Then, using the same notation as in Theorem 3, we have

$$\begin{aligned}\Pr(I^{\mathrm{T}}_{\mathrm{con}} \cap \tilde{C}_{1,2} \cap e_1 \cap \overline{e_3}) &\leq \int_0^{\epsilon} f_{W_{(1)}}(w)\,\mathrm{d}w \int_0^{r} f_{Y_{(1)}}(y)\,\mathrm{d}y \\ &\qquad \int_{\epsilon}^{2\epsilon} f_{Z_{(1)}}(z)\,\mathrm{d}z \int_{2\epsilon}^{r} f_{X_{(1)}}(x)\,\mathrm{d}x \\ &= D_0^{\epsilon}(\mu) D_0^{r}(\mu) D_{\epsilon}^{2\epsilon}(\mu) D_{2\epsilon}^{r}(\mu). \end{aligned} \tag{3.42}$$

For $\Pr(I^{\mathrm{T}}_{\mathrm{con}} \cap \tilde{C}_{1,3} \cap e_1 \cap \overline{e_3})$ we fix $W_{(1)} = 0$ while computing the probability of edge e_5, and for $\Pr(I^{\mathrm{T}}_{\mathrm{con}} \cap \tilde{C}_{2,2} \cap e_1 \overline{e_3})$ we use $W_{(1)} \in [0, \epsilon]$ (see Figure 3.13d and Figure 3.13b, respectivelly). Considering this, we have

$$\begin{aligned}\Pr(I^{\mathrm{T}}_{\mathrm{con}} \cap \tilde{C}_{1,3} \cap e_1 \cap \overline{e_3}) &\leq \int_0^{\epsilon} f_{W_{(1)}}(w)\,\mathrm{d}w \int_0^{r} f_{Y_{(1)}}(y)\,\mathrm{d}y \\ &\qquad \int_{2\epsilon}^{r} f_{Z_{(1)}}(z)\,\mathrm{d}z \int_{\epsilon}^{r} f_{X_{(1)}}(x)\,\mathrm{d}x \\ &= D_0^{\epsilon}(\mu) D_0^{r}(\mu) D_{2\epsilon}^{r}(\mu) D_{\epsilon}^{r}(\mu). \end{aligned} \tag{3.43}$$

and

$$\begin{aligned}\Pr(I^{\mathrm{T}}_{\mathrm{con}} \cap \tilde{C}_{2,2} \cap e_1 \cap \overline{e_3}) &\leq \int_{\epsilon}^{2\epsilon} f_{W_{(1)}}(w)\,\mathrm{d}w \int_0^{2\epsilon} f_{Y_{(1)}}(y)\,\mathrm{d}y \\ &\qquad \int_{\epsilon}^{2\epsilon} f_{Z_{(1)}}(z)\,\mathrm{d}z \int_{2\epsilon}^{r} f_{X_{(1)}}(x)\,\mathrm{d}x \\ &= D_{\epsilon}^{2\epsilon}(\mu) D_0^{2\epsilon}(\mu) D_{\epsilon}^{2\epsilon}(\mu) D_{2\epsilon}^{r}(\mu). \end{aligned} \tag{3.44}$$

Observing Figure 3.13e we perceive that an upper bound can be obtained fixing $Y_{(1)} = 0$ while computing the probabilities of edges e_5 and e_6. On the other hand, Figure 3.13f shows that we can compute an upper bound fixing $Y_{(1)} = 0$ while computing the probability of edge e_6. Consequently, tight upper bounds for $\Pr(I^{\mathrm{T}}_{\mathrm{con}} \cap \tilde{C}_{2,3} \cap e_1 \cap \overline{e_3})$

and $\Pr(I^{\mathrm{T}}_{\mathrm{con}} \cap \tilde{C}_{3,3} \cap e_1 \cap \overline{e_3})$ are given by

$$\begin{aligned}\Pr(I^{\mathrm{T}}_{\mathrm{con}} \cap \tilde{C}_{2,3} \cap e_1 \cap \overline{e_3}) &\leq \int_{\epsilon}^{2\epsilon} f_{W_{(1)}}(w)\,\mathrm{d}w \int_{0}^{2\epsilon} f_{Y_{(1)}}(y)\,\mathrm{d}y \\ &\qquad \int_{2\epsilon}^{r} f_{Z_{(1)}}(z)\,\mathrm{d}z \int_{\epsilon}^{r} f_{X_{(1)}}(x)\,\mathrm{d}x \\ &= D^{2\epsilon}_{\epsilon}(\mu) D^{2\epsilon}_{0}(\mu) D^{r}_{2\epsilon}(\mu) D^{r}_{\epsilon}(\mu). \end{aligned} \tag{3.45}$$

and

$$\begin{aligned}\Pr(I^{\mathrm{T}}_{\mathrm{con}} \cap \tilde{C}_{3,3} \cap e_1 \cap \overline{e_3}) &\leq \int_{2\epsilon}^{r} f_{W_{(1)}}(w)\,\mathrm{d}w \int_{0}^{\epsilon} f_{Y_{(1)}}(y)\,\mathrm{d}y \\ &\qquad \int_{2\epsilon}^{r} f_{Z_{(1)}}(z)\,\mathrm{d}z \int_{\epsilon}^{r} f_{X_{(1)}}(x)\,\mathrm{d}x \\ &= D^{r}_{2\epsilon}(\mu) D^{\epsilon}_{0}(\mu) D^{r}_{2\epsilon}(\mu) D^{r}_{\epsilon}(\mu). \end{aligned} \tag{3.46}$$

The probability $\Pr(I^{\mathrm{T}}_{\mathrm{con}} \cap \tilde{C}_{3,2} \cap e_1 \cap \overline{e_3})$ was computed in the proof of Theorem 3, and the exact expression is given in (3.37).

Let L and L' be the lower and upper bounds, respectively, for $\Pr(I^{\mathrm{T}}_{\mathrm{con}})$ under the Triangular model. Then, an upper bound of the error is given by $L - L'$. Solving this, we obtain (3.41). □

Figure 3.16 shows the error curves for few combinations of ϵ and μ. Smaller values of ϵ respect to r lead to smaller errors, as expected. Higher densities of nodes also are better for decreasing the error. In all cases, we perceive that the error is almost null when r is big enough.

3.2 Probability of Connectivity at Segments

As we described in the beginning of this chapter, we are interested in computing local connectivity probabilities in both, segments and intersections. Problem 1 presented the connectivity at intersections as the problem of determining the probability of connectivity locally at intersection. This probability is used in next chapters as a building block for characterizing connectivity in the overall network, in particular, for determining bounds on the visualization restrictions in order to grant connectivity. On the other hand, we need also a characterization of connectivity at segments to have a complete description of connectivity in the network. As the intention of this work is to describe global connectivity in terms of local connectivity, we define the connectivity at segments problem as follows.

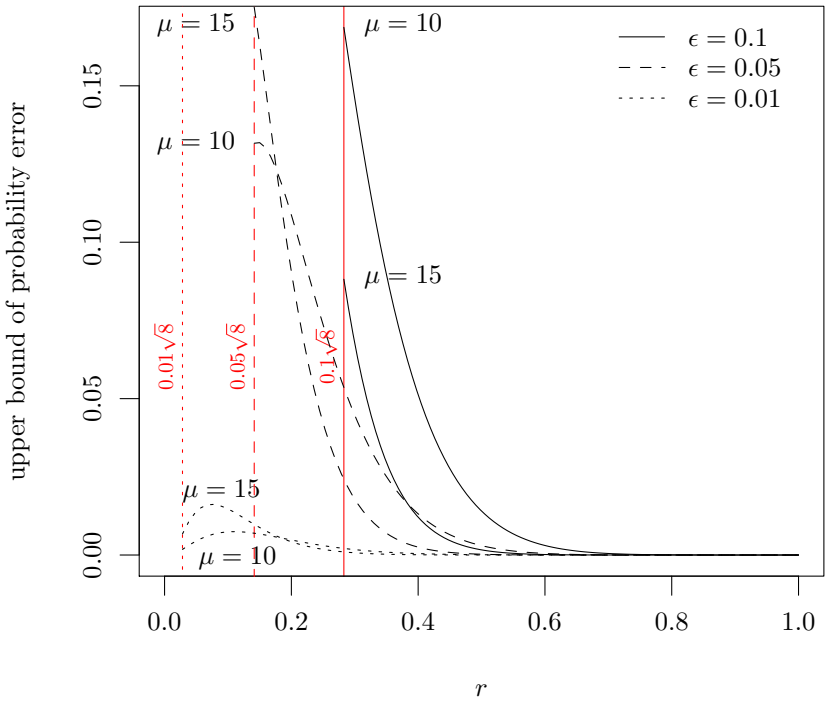

Figure 3.16. Upper bound for the error of probability of connectivity at crossroads under the Triangular model. The domain of these curves are $\sqrt{8}\epsilon \leq r \leq 1$.

Problem 2 (Connectivity at Segments)**.** *The connectivity at segments problem consists in determining the probability of having a unique connected component of μ nodes, where these μ nodes are uniformly distributed at random over the line segment* $[0, 1]$. *We denote this probability by* $\Pr(S_{con})$.

Fortunately, this is a well know problem in ad hoc wireless networks theory. To the best of out knowledge, the first exact solution of this problem was reported by Desai and Manjunath [2002]. In that paper the authors consider a finite ad hoc network with μ nodes distributed uniformly at random in the segment $[0, z]$, where all nodes have a transmission range r. Then, they expressed the probability of connectivity in the network as the fraction of volumes of polytopes induced by the order statistics of all connected networks and the order statistics of all feasible networks, respectively. With this approach, they obtained

$$\sum_{i=0}^{\mu-1} \binom{\mu-1}{i} (-1)^i \frac{(z-ir)^\mu}{z^\mu} u(z-ir),$$

where $u(.)$ is the unit step function, defined by

$$u(t-a) = \begin{cases} 0 & \text{if } t < a, \\ 1 & \text{if } t > a. \end{cases}$$

We can now consider $z = 1$, and take the case $i = 0$ separately. Then, we obtain

$$1 + \sum_{i=1}^{\min\{\mu-1, \lfloor 1/r \rfloor\}} \binom{\mu-1}{i} (-1)^i (1-ir)^\mu. \tag{3.47}$$

At this point, we perceive that formula is not simple as we wish. We need an expression able to be used inside of other complex functions, as we expect to be the case for characterizing connectivity in the overall network.

Differently to Desai and Manjunath [2002], Ghasemi and Nader-Esfahani [2006] considered a generalization of the connectivity problem. They were interested in computing the probability of having at most C connected component in the network deployed in $[0, z]$, denoted by $\Pr(S_{\text{con}}^C(z))$. The authors' strategy was to consider the problem of random division of an interval, reported in Chapter 6 of David and Nagaraja [2003]. Here, $\{U_i\}_{i=1}^{\mu}$ is a family of random variables uniformly distributed in the interval $[0, z]$. They consider the order statistics $0 \leq U_{(1)} \leq \cdots \leq U_{(\mu)} \leq z$, and define $\Delta_{i-1} = U_{(i)} - U_{(i-1)}$, for $0 \leq i \leq \mu$, where clearly $U_{(0)} = 0$. If $\Delta_{(1)} \leq \Delta_{(2)} \leq \cdots \leq \Delta_{(\mu-1)}$ denote the order statistics of the family of random variables $\{\Delta_i\}_{i=1}^{\mu-1}$, then we have $\Pr(S_{\text{con}}^C(z)) = \Pr\left(\Delta_{(\mu-C)} \leq r\right)$. Solving this, Ghasemi and Nader-Esfahani obtained

$$\Pr(S_{\text{con}}^C(z)) = 1 - \sum_{i=C}^{\min\{\mu-1, \lfloor z/r \rfloor\}} (-1)^{i-C} \binom{i-1}{C-1} \binom{n-1}{i} \left(1 - i\frac{r}{z}\right)^\mu. \tag{3.48}$$

For the special case where $C = 1$ and $z = 1$, expression (3.48) is equivalent to the previous result of Desai and Manjunath presented in (3.47). The difference with this approach, is that we know that random variables $\{\Delta_i\}_{i=1}^{\mu-1}$ have identical distributions and, assuming that they are approximately independent, we have

$$\Pr(S_{\text{con}}) = \Pr(\Delta_{(\mu-1)} \leq r) \approx \Pr(\Delta_0 \leq r)^{\mu-1}.$$

This approximation improves as μ grows, and it is the core of the next result, expressed in Theorem 4.

Theorem 4. *Let $\{X_i\}_{1 \leq i \leq \mu}$ be a family of independent random variables, such that $X_i \sim \mathcal{U}(0,1)$, denoting the positions of μ nodes in a segment. Let also r denote*

the common transmission range of all nodes, where $0 \leq r \leq 1$. *The probability of connectivity between all nodes is*

$$\Pr(S_{con}) = (1 - (1 - r)^{\mu})^{\mu - 1} + \delta$$

where $\delta \to 0$ *when* $\mu \to \infty$.

Proof. See Ghasemi and Nader-Esfahani [2006]. □

Besides the convergence to null error happens when $\mu \to \infty$, results comparing Theorem 4 with the exact theoretical solution of (3.48) and simulations in Ghasemi and Nader-Esfahani [2006], the authors show that even for small values of μ (about 10) we have accuracy, specially for high probabilities.

Next chapter presents the CTR problem, formally, and we will approach this problem using the two main building blocks we derived here; probabilities $\Pr(S_{\text{con}})$ and $\Pr(I_{\text{con}})$.

Chapter 4

Overall Connectivity

We introduced in Chapter 1 several arguments in favor of considering TC techniques in the design of wireless ad hoc networks. Here we adhere to the TC concept of Santi. Informally, we consider TC to be the "art of coordinating nodes' decisions regarding their transmitting ranges, in order to generate a network with the desired properties while reducing node energy consumption and/or increasing network capacity" [Santi, 2005a].

In homogeneous networks, which is the kind of networks we consider in this work, the simplest TC technique consists in characterize the CTR. Characterizing the CTR means to determine a common transmission range, for all nodes in the network, in such a way that we reduce node energy consumption and increase network capacity while maintaining an structural property. In this chapter we are interested in, probably, the most important structural property: connectivity. We present the so-called *CTR for Connectivity*, below, in Definition 1.

Definition 1 (CTR for Connectivity)**.** *Suppose n nodes are distributed in a region R. The Critical Transmission Range (CTR) for Connectivity is the minimum transmission range, denoted by r_c, which induces a communication graph with a unique connected component, including all the n nodes of the network.*

With this definition of the CTR for connectivity we review, in the next Section 4.1, the main results for open spaces without obstacles. Approaches and concepts introduced in that section serve to have a better understanding of the methodology applied in Section 4.2, where we compute the CTR for connectivity under our obstructed model, introduced in Chapter 2.

4.1 CTR for Connectivity in Open Spaces

Independently of the model and/or scenario, solving the CTR for Connectivity requires the knowledge of the position of each node in the network. As Santi [2005a] pointed out, once we know all position of nodes, we can compute the CTR for Connectivity by constructing an Euclidean Minimum Spanning Tree (MST) on the same set of nodes, and then computing the length of the longest edge in the tree. With this approach, as the network scales to bigger sizes the solution become impractical or not efficient in the best case. Because of this, the usual treatment consists in considering a network with n nodes deployed in a region R at random, which requires some probabilistic formulations.

In a random scenario, we consider all possible instances of deployment on a canonical region and according to some distribution. The typical assumption corresponds to model each coordinate for one-dimensional, two- and three-dimensional networks, as being uniformly distributed over the dimensions of the regions. For one-dimensional networks, we consider the region $R = [0, z]$, and nodes follow the uniform distribution in that interval, i.e., $X_i \sim \mathcal{U}(0, z)$ for $1 \leq i \leq n$. In the case of two-dimensional networks, the typical region considered by researchers is $R = [0, z]^2$. Here, nodes' coordinates follow, independently, a uniform distribution. As a consequence, nodes are positioned in the two-dimensional Euclidean space following a Poisson point process conditioned to the amount of deployed nodes. This last conditioned distribution corresponds, technically, to a Binomial distribution on $[0, z]^2$. Finally, the three-dimensional case is just an extension of the other two cases above.

From the aforementioned assumptions we perceive that it is not possible to find the CTR for connectivity in agreement with Definition 1 while considering random networks. In other words, without knowing the exact position of all nodes it is not possible to determine the CTR for connectivity. For instance, consider a one-dimensional network with two nodes deployed uniformly at random in the interval $[0, 1]$. Each pair of nodes deployed is a sample of the random network, and each sample will have a particular CTR for connectivity corresponding to the distance between the two nodes, or alternatively, corresponding to the length of the longest edge of the Euclidean MST build on the pair of nodes.

Besides we just said that there is no CTR for connectivity for random networks, it is possible to have a random approach for the CTR for connectivity by determining the CTR for connectivity w.h.p.. In this sense, we are interested in the minimum transmission range inducing connectivity w.h.p. in the overall network, that is, we analyze the network as a random object, and we compute the CTR for connectivity as

being a random event. Moreover, we are interested in characterize the conditions that make this random event to occur w.h.p. in the random network. Since all interesting results for the CTR in the literature are for random networks, we usually do not find any distinction for this specific case, we just observe assertions saying that the characterization corresponds to the CTR for connectivity. Nevertheless, it is important to have in mind what we are characterizing; an event that occurs w.h.p. in a random network. Technically, we say that a random event E_k, that depends on a parameter k, occurs w.h.p. if $\lim_{k\to\infty} \Pr(E_k) = 1$.

In random ad hoc networks, there are basically two approaches to compute the CTR for connectivity: (i) we select a fixed d-dimensional deployment region with side z and analyze the CTR for connectivity when $n/z^d \to \infty$, or (ii) we consider the deployment region side z as a parameter, expressing the transmission range r and network size n as a function of z and the nodes' distribution, and we analyze the CTR for connectivity when $z \to \infty$. Each one of these approaches has different levels of difficulty, and also has different application restrictions. In the case (i), by fixing the deployment region, we want to discover the expression $r_c = f(n, z, d)$ such that $\lim_{n/z^d\to\infty} \Pr(\text{CTR} = r_c) = 1$. Applying diverse techniques, but mainly Geometric Random Graphs (GRGs) theory [Penrose, 2003], researchers found expression for r_c in d-dimensional networks deployed over $[0, z]^d$, with $d \in \{1, 2, 3\}$. Nevertheless, all those results grant $\Pr(\text{CTR} = r_c) = 1$ only for dense networks, since we only ensure that the event of interest occurs when $n \to \infty$. For one-dimensional dense networks, the CTR for connectivity was reported by Santi [2005b]. He combined previous results from Holst [1980] and Penrose [1997, 1999a], obtaining the CTR for connectivity in $[0, 1]$:

$$r_c = \frac{\log n}{n} \tag{4.1}$$

Penrose [1997] also analyzed the length of the longest edge in the Euclidean MST induced by a Binomial deployment in $[0, 1]^2$. From that result, it is possible to deduce that the CTR for connectivity in the unit square is

$$r_c = \sqrt{\frac{\log n + f(n)}{n\pi}}, \tag{4.2}$$

where $f(n)$ is a function such that $\lim_{n\to\infty} f(n) = \infty$. Santi [2005a] combined results from Dette and Henze [1989] and Penrose [1999b], obtaining the CTR for connectivity in $[0, 1]^3$:

$$r_c = \sqrt[3]{\frac{\log n - \log\log n}{n\pi} + \frac{3}{2}\frac{1.41 + g(n)}{n\pi}}, \tag{4.3}$$

where $g(n)$ is a function as $f(n)$ above, i.e. $\lim_{n\to\infty} g(n) = \infty$.

On the other hand, the case (ii) considers a more flexible scenario, where the side of the deployment region, z, is an independent variable. With this approach, results hold for networks with arbitrary node density; not just for dense scenarios but for sparse deployments as well. Santi and Blough [2003] applied occupancy theory (see Kolchin et al. [1978]) to prove that for n nodes deployed uniformly at random in $[0, z]$, the CTR for connectivity is

$$r_c = k\frac{z \log z}{n}, \tag{4.4}$$

where k is a constant with $1 \leq k \leq 2$. The authors also analyzed two- and three-dimensional networks and they partially proved the following proposition: for n nodes deployed uniformly at random in $[0, z]^d$, with $d \in \{1, 2, 3\}$, the CTR for connectivity is

$$r_c = k\frac{z^d \log z}{n}, \tag{4.5}$$

where k is a constant such that $0 \leq k \leq 2^d d^{d/2+1}$.

Obstructed wireless ad hoc networks represent a totally different scenario, in comparison to open-space networks, and this new scenario requires a different approach. The following section presents the derivation of the CTR for connectivity on the obstructed model proposed in Chapter 2, including an analysis of limitations in terms scalability and application scenarios.

4.2 CTR for Connectivity on Obstructed Networks

Let us start by considering the percolation layer of Section 2.2. At first glance, it is reasonable to associate, on the one hand, edges of the grid with segments in the obstructed network and, on the other hand, to relate vertices of the grid with intersections in the obstructed network. Nevertheless, understanding the relationship between connectivity in the obstructed network and percolation on the grid requires a little bit more of effort.

As we commented previously, we adopt the concept of percolation on finite grids of Franceschetti and Meester [2007], which defines percolation in this context as full connectivity of all vertices of the grid (see Section 2.2).

Besides the mixed percolation model has two parameters, namely, the edge probability p_b and the vertex probability p_s, percolation in finite grids makes no sense for $p_s < 1$. This implies that under the obstructed network we need to ensure connectivity

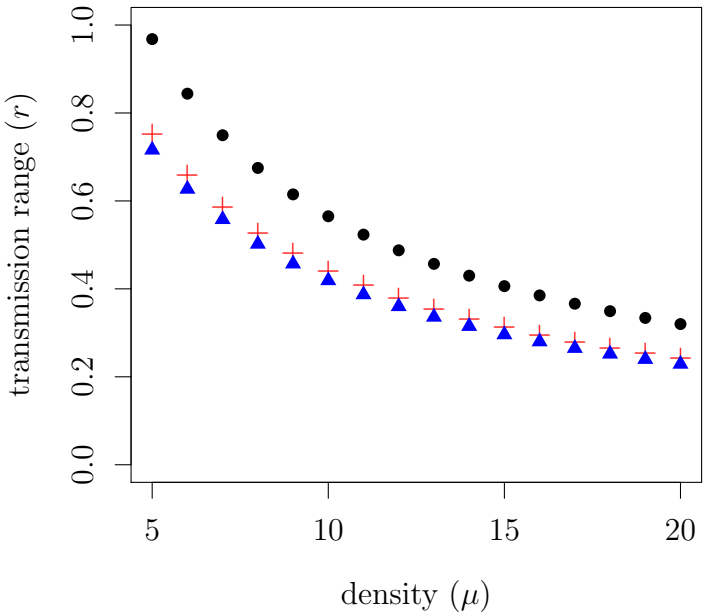

Figure 4.1. For big enough values of ϵ, connectivity at intersections is easier than at segments

at intersections with probability $p_s \to 1$. This seems to be a strong restriction, but is it? Let us analyze the implications.

The density of the network was defined, in the model, to be μ. By "density" we mean to denote the expected amount of nodes in a unit space of the deployment region of the network. Intervals at segments and intersections can be simplified to obtain the canonical intervals $[0, 1]$ and $0 \times [0, 1/2] \cup [0, 1/2] \times 0$, respectively. We can then compute, analytically, the distance between any two nodes on those two regions and compare those distances. Nevertheless, it is not hard to perceive that distances at intersections are shorter than distances at segments. We can observe this, in a simplified way, by putting a thread of unity size on a table and then lifting one of the extremes, perpendicularly to the table, in such a way that we obtain a ⌞ shape. Clearly, every interval included in the half of thread that is now in the air, is closer to the other part of the thread, the one that still is having rest on the table.

At intersections, independently of the Max-Norm, Euclidean or Triangular models, we have two requirements to meet connectivity between nodes: (i) distance below the common transmission range r and (ii) visibility. As we notice above, distances at intersections are shorter than distances at segments. Additionally, we also know that

big values of ϵ warrant visibility.

Figure 4.2 shows empirical results about the required transmission range for connectivity at intersections, while using big values of ϵ, under the Max-norm (represented by red plus signs) and Triangular (denoted with blue triangles) models. We compare this with the required transmission range for having connectivity in the overall network, represented with black balls in the figure. Notice that this last transmission range corresponds to the CTR for connectivity. Here, we perceive that $\Pr(I_{\text{con}} \mid r = r_c - \Delta) = 1$ for $\Delta > 0$, in both, the Max-Norm and Triangular models. Moreover, we observe that the CTR for connectivity does not depend on the intersection model.

These elements allow us to think that restricting $p_s \to 1$ is not a limiting condition when we look for connectivity in the overall network. Nevertheless, it is necessary to reveal which values of ϵ are big enough or, similarly, which is the minimum value of ϵ, denoted by ϵ_c (critical ϵ), that grants $p_s \to 1$ according to different settings of transmission range (r) and density (μ).

Theorems 2 and 3, presented in Chapter 3, offer a starting point toward the characterization of ϵ_c under the Max-Norm and Triangular models, respectively. Those theorems compute $\Pr(I_{\text{con}})$ in terms of the transmission range r, the density μ and the visibility parameter ϵ. Defining $F(\epsilon, r, \mu) = \Pr(I_{\text{con}})$, we can compute the critical ϵ by

$$\epsilon_c = \lim_{q \to 1^-} F^{-1}(q; r, \mu), \tag{4.6}$$

where $F^{-1}(.)$ is the inverse cumulative distribution function for $F(.)$, i.e. the quantile function for $F(.)$.

Theorem 5 presents the CTR for connectivity under the obstructed network model, independently of the intersection model adopted. We denote the value of the CTR for connectivity by r_c. Theorem 5 considers that ϵ is large enough, and that the lower bound for ϵ is determined by ϵ_c according to (4.6).

Theorem 5. *Let $\mathcal{N}$ be a set of n nodes deployed uniformly at random in a lattice square of granularity g in the area $[0, g-1]^2$, with segments' width 2ϵ. Let also μ be the expected quantity of nodes per segment. The Critical Transmission Range for Connectivity, denoted by r_c, is*

$$r_c = \frac{\ln\left(g^{a+1/2}\right) + \ln(\mu - 1)}{\mu}$$

for $a > 0$, whenever $\epsilon \geq \epsilon_c$.

Proof. Let us abstract the connectivity problem using a bond percolation model within

a random grid of $g \times g$ vertices. Here, each vertex corresponds to an intersection in the lattice square and each edge corresponds to a segment. In the percolation model, each edge occurs with probability p_b.

We know, from Theorem 4, the probability of connectivity at segments, which in the abstraction corresponds to p_b. Additionally, we know that the probability of connectivity at intersections $\Pr(I_{\text{con}})$, which in the abstraction corresponds to p_s, must approximate to one.

Franceschetti and Meester [2007] already studied the rate of convergence of p_b in order to meet percolation in a finite lattice square of $g \times g$. They found that p_b must scale slightly faster than $\sqrt{g}$ in order for the random grid to be fully connected w.h.p., which means that $p_b = 1 - C_g/\sqrt{g}$ guarantees connectivity w.h.p. if and only if the sequence $C_g \to 0$ when $g \to \infty$.

Considering the modeling presented in Chapter 2, from Theorem 4 we have

$$p_b = (1 - (1 - r)^{\mu})^{\mu - 1}, \tag{4.7}$$

while from Franceschetti and Meester [2007] we know it is necessary the convergence rate

$$p_b = 1 - \frac{C_g}{\sqrt{g}}, \tag{4.8}$$

with $C_g \to 0$ when $g \to \infty$, in order to have percolation in the finite $g \times g$ square lattice. Alternatively, we can express the result of Franceschetti and Meester [2007] by considering bond percolation under the random graph $\mathbb{G}_g$ and write

$$\lim_{g \to \infty} \Pr\left(\mathbb{G}_g \text{ percolates} \;\middle|\; p_b = 1 - \frac{C_g}{\sqrt{g}} \wedge C_g \to 0\right) = 1.$$

Let $\mathcal{N}_{\text{con}}$ be the event denoting connectivity in the overall network, with density μ, deployed in a grid with granularity g and segments' width bigger than $2\epsilon_c$. Putting (4.7) and (4.8) together, we can then obtain the CTR for connectivity, r_c, implicitly:

$$\lim_{g \to \infty} \Pr\left(\mathcal{N}_{\text{con}} \;\middle|\; 1 - \frac{C_g}{\sqrt{g}} = (1 - (1 - r_c)^{\mu})^{\mu - 1} \wedge C_g \to 0\right) = 1. \tag{4.9}$$

The conditional part of (4.9) establish the necessary and sufficient requirements for meet connectivity w.h.p. in the network. Since we are interested in the CTR for connectivity, we proceed in the next steps to write these conditions making r_c explicit.

We can start by applying the ln(.) function and simplify as follows:

$$\ln\left(1-\frac{C_g}{\sqrt{g}}\right) = \ln\left((1-(1-r_c)^{\mu})^{\mu-1}\right),$$
$$\frac{\ln\left(1-\frac{C_g}{\sqrt{g}}\right)}{\mu-1} = \ln(1-(1-r_c)^{\mu}). \tag{4.10}$$

It is well knwon that the Maclaurin series representation for $\ln(1-x)$ is $\sum_{i=0}^{\infty}\frac{-x^i}{i}$. Then, applying Maclaurin series on ln(.) for both sides of (4.10), we obtain

$$\frac{\sum_{i=1}^{\infty}-\frac{\left(\frac{C_g}{\sqrt{g}}\right)^i}{i}}{\mu-1} = \sum_{i=1}^{\infty}-\frac{(1-r_c)^{i\mu}}{i}. \tag{4.11}$$

It is reasonable to take just the first term of the series for values that are not close to 1. This is even more reasonable to apply in (4.11), since the elimination of terms occurs on both sides, achieving balanced approximations. Assuming the errors as being small enough to not be considered, we write

$$-\frac{C_g}{\sqrt{g}(\mu-1)} = -(1-r_c)^{\mu}.$$

In order make explicit r_c, we apply ln(.) and solve as follows:

$$-\ln\left(\frac{C_g}{\sqrt{g}(\mu-1)}\right) = -\ln\left((1-r_c)^{\mu}\right),$$
$$-\ln\left(\frac{C_g}{\sqrt{g}(\mu-1)}\right) = -\mu\ln\left(1-r_c\right). \tag{4.12}$$

At this point, before split the left side of (4.12), we define $C_g = \frac{1}{g^a}$. Clearly, $\lim_{g\to\infty}\frac{1}{g^a} = 0$, and depending on a we can customize to different convergence speeds. From (4.12) we proceed applying the definition of C_g above, and also using the Maclau-

rin series approximation as before. Then, we have

$$\begin{aligned}
-\ln\left(\frac{\frac{1}{g^a}}{\sqrt{g}(\mu-1)}\right) &= -\mu\ln\left(1-r_c\right), \\
-\ln\left(\frac{1}{g^{a+1/2}(\mu-1)}\right) &= \mu r_c, \\
-\left(\ln 1-\ln\left(g^{a+1/2}(\mu-1)\right)\right) &= \mu r_c, \\
\frac{\ln\left(g^{a+1/2}\right)+\ln(\mu-1)}{\mu} &= r_c. \qquad (4.13)
\end{aligned}$$

Note that (4.13) corresponds to the CTR for Connectivity whenever connectivity at intersections is guaranteed, i.e., when $\epsilon \geq \epsilon_c$. Then, replacing (4.13) on (4.9), we have

$$\lim_{g\to\infty}\Pr\left(\mathcal{N}_{\text{con}}\;\middle|\; r_c=\frac{\ln\left(g^{a+1/2}\right)+\ln(\mu-1)}{\mu}\wedge\epsilon\geq\epsilon_c\right)=1,$$

and this finish the proof. □

So far we computed the CTR for connectivity, r_c, and determined the validity for $\epsilon \geq \epsilon_c$. Recall that, according to (4.6), the critical value ϵ_c is defined as the minimum value of ϵ that warrant connectivity w.h.p. at intersections.

Notice that we are interested specifically in determining the value of ϵ_c in the context of the CTR problem. Then, by setting the transmission range to at least r_c, we are sure that the condition of distance holds for connecitivy at intersections (see Figure 4.2). Consequently, we need only to check the visibility condition for connectivity at intersections, since the distance condition for connectivity is warranted while using $r \geq r_c$. In particular, assuming $r = 1$ will allow us to find the relationship between the density μ and ϵ, and this will give us an upper bound for ϵ_c.

Let us start by the Max-Norm model. Theorem 2 showed us that

$$\Pr(I_{\text{con}}^{\text{MN}}) \geq p^2 + 2D_0^{\epsilon}(\mu)D_{\epsilon}^{r}(\mu)D_{\epsilon}^{r-\epsilon}(\mu)\left[D_0^r(\mu)+D_{\epsilon}^r(\mu)\right],$$

where $D_i^j(k) = (1-i)^k - (1-j)^k$ and $p = p_{\perp}^{\text{MN}}(\mu)$. Applying substitution $r = 1$, we have

$$\Pr(I_{\text{con}}^{\text{MN}}) \geq p_{\perp}^{\text{MN}}(\mu)^2 + 2\left(1-(1-\epsilon)^{\mu}\right)(1-\epsilon)^{\mu}\left((1-\epsilon)^{\mu}-\epsilon^{\mu}\right)\left(1+(1-\epsilon)^{\mu}\right). \qquad (4.14)$$

Additionally, by Lemma 2, we now that

$$p_{\perp}^{\text{MN}}(\mu) = 2\left(1-(1-r)^{\mu}\right)\left(1-(1-\epsilon)^{\mu}\right) - \left(1-(1-\epsilon)^{\mu}\right)^2.$$

Then, we apply also substitution $r = 1$, and solve

$$\begin{aligned} p_{\perp}^{\text{MN}}(\mu) &= 2\left(1-(1-\epsilon)^{\mu}\right) - \left(1-(1-\epsilon)^{\mu}\right)^2, \\ &= 1 - 2(1-\epsilon)^{2\mu} + (1-\epsilon)^{4\mu}. \end{aligned} \tag{4.15}$$

Finally, replacing (4.15) into (4.14) and solving, we obtain

$$\Pr(I_{\text{con}}^{\text{MN}}) \geq 1 - 2\epsilon^{\mu}(1-\epsilon)^{\mu} + 2\epsilon^{\mu}(1-\epsilon)^{3\mu} - (1-\epsilon)^{4\mu}. \tag{4.16}$$

The inequality in (4.16) does not allow us to find an expression for the critical value ϵ_c, because it represents just a lower bound for $\Pr(I_{\text{con}}^{\text{MN}})$ and consequently there is no warranty to find reasonable values of μ and ϵ such that $\Pr(I_{\text{con}}^{\text{MN}}) = 1$. Nevertheless, it is possible to tackle this problem by assuming a small error of β in the lower bound for $\Pr(I_{\text{con}}^{\text{MN}})$, and then we computationally solve

$$\Pr(I_{\text{con}}^{\text{MN}}) - \beta = 1 - 2\epsilon^{\mu}(1-\epsilon)^{\mu} + 2\epsilon^{\mu}(1-\epsilon)^{3\mu} - (1-\epsilon)^{4\mu}. \tag{4.17}$$

In a similar manner, we can obtain a characterization of the critical value ϵ_c for the Triangular model. From Theorem 3 and Lemma 3, assuming a small error $\tilde{\beta}$, we have

$$\begin{aligned} \Pr(I_{\text{con}}^{\text{T}}) - \tilde{\beta} = (1-2\epsilon)^{4\mu} - 4(1-2\epsilon)^{3\mu}\left[(1-\epsilon)^{\mu} + (2\epsilon)^{\mu}\right] + 2(1-2\epsilon)^{2\mu}\left[2(2\epsilon)^{2\mu}\right. \\ \left. +2(1-\epsilon)^{\mu}(2\epsilon)^{\mu} - (1-\epsilon)^{2\mu}\right] + 2(1-2\epsilon)^{\mu}\left\{(1-\epsilon)^{\mu}\left[2(2\epsilon)^{\mu} - 3(2\epsilon)^{2\mu} - \epsilon^{\mu}\right]\right. \\ \left. +(1-\epsilon)^{2\mu}\epsilon^{\mu} - (2\epsilon)^{2\mu}\right\} + (1-\epsilon)^{2\mu}\left[(2\epsilon)^{2\mu} + 2\epsilon^{\mu} - 4(2\epsilon)^{\mu}\right] + 2(1-\epsilon)^{\mu}\left[(2\epsilon)^{2\mu} - \epsilon^{\mu}\right] + 1. \end{aligned} \tag{4.18}$$

We implemented (4.17) and (4.18) in the `R` platform and obtained, for each model and different densities, the minimal value of ϵ for which the requirement $\Pr(I_{\text{con}}) = 1$ holds. Each minimal value ϵ corresponds, then, to the respective critical value ϵ_c. Figure 4.2 presents different critical values for $\beta = \tilde{\beta} = 0.02$, according to specific densities. The horizontal axis corresponds to the density and the vertical axis to the critical value ϵ_c. Red plus signs and blue triangles correspond to the Max-Norm and Triangular models, respectively.

We perceive from Figure 4.2 that in case of low density, the critical value ϵ_c for

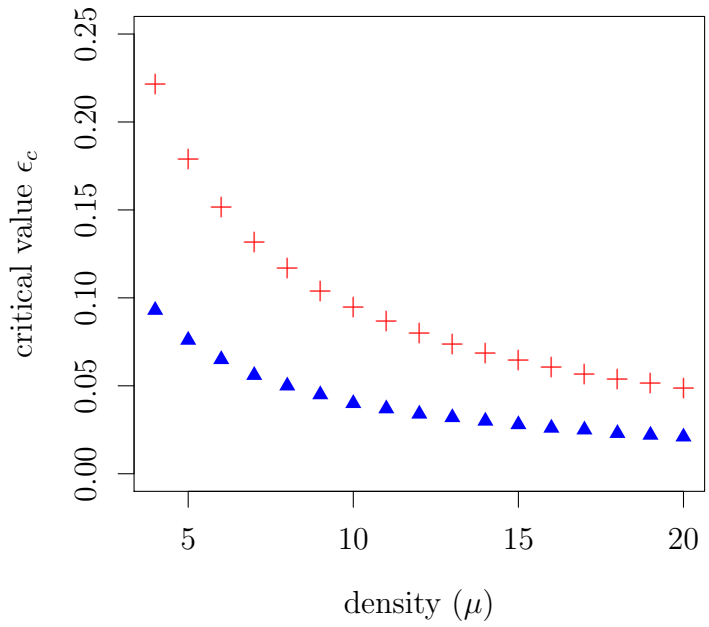

Figure 4.2. Critical value ϵ_c, according to the density μ, for the Max-Norm and Triangular models

the Triangular model is less than half of the critical value ϵ_c for the Triangular model. This difference diminish gradually as we approach big densities and has a common infimum at $\mu = \infty$, equivalent to zero.

We already know the values of ϵ (those $\epsilon \geq \epsilon_c$) that validate the result of Theorem 5. Consequently, we are able then to set up the scenarios for testing the theoretical CTR for connectivity through Monte Carlo simulation. Figure 4.3 presents ECDFs for the CTR for connectivity under different network sizes and densities, using the critical value ϵ_c for the Max-Norm and Triangular models. In both cases the result is the same, as expected, since the CTR for connectivity does not depend on the ϵ parameter. Here, we denoted the theoretical CTR for connectivity of Theorem 5 by a horizontal red line. In particular, we use $a = 1$, which warrants a fast convergence for relatively small grids. We observe that the denser the scenario, the stronger the phase transition.

Although it is not possible to visualize it in Figure 4.3, we expect to have longer phase transitions as we handle with bigger grids, even increasing the amount of nodes in order to maintain the density at a particular μ. We expect the aforementioned behavior simply because big values of granulatity (g) bring variance to the deployment of nodes, and this generate variance in the CTR for connectivity.

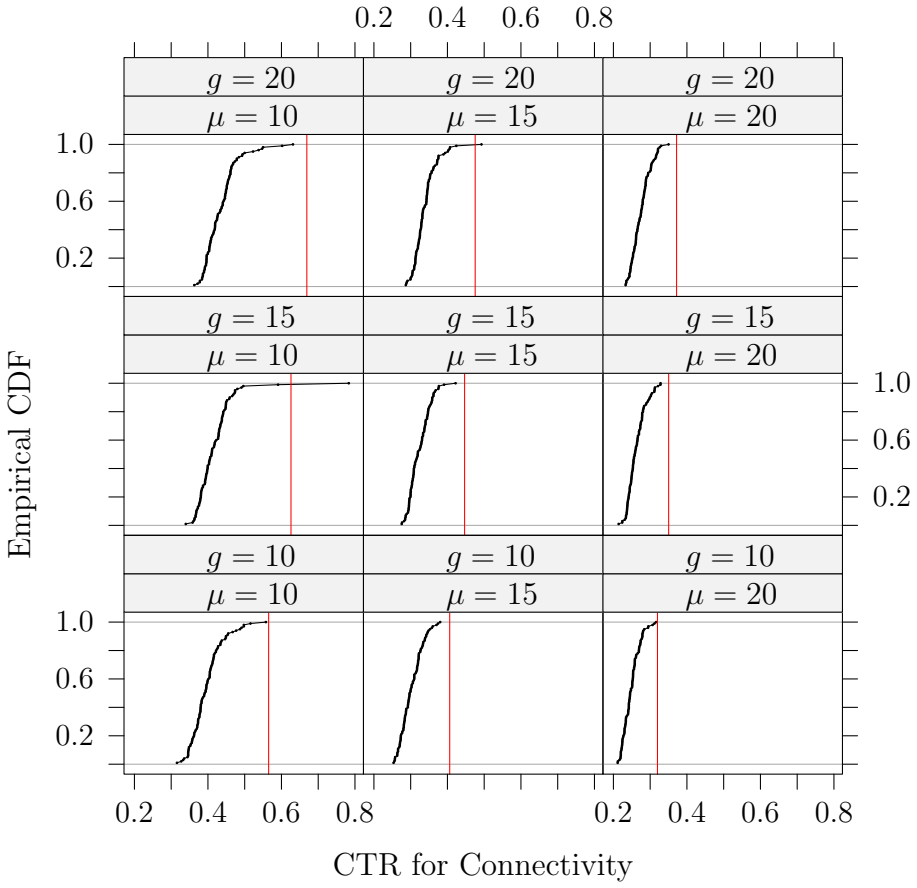

Figure 4.3. ECDFs and analytical CTRs

4.2.1 Scalability

Theorem 5 describes the CTR for connectivity in term of the granularity g and density μ. This transmission range, denoted by r_c, corresponds to the minimal transmission range that warrants connectivity w.h.p. in the overall network. Nevertheless, it is not unusual to have technological and/or market restrictions on the settings of wireless devices, invalidating the usefulness of the theorem. Alternatively, we can think about the transmission range as a constant α and determine, afterwards, the scalability of the network in terms of size.

It is clear at this point that when $g \to \infty$ an infinite amount of connected components emerges, independently of the value of α. More technically, denoting the distance between two consecutive nodes in the line by $\|X_{(i)} - X_{(i+1)}\|$, the event $\|X_{(i)} - X_{(i+1)}\| > \alpha$, for a fixed i, is a rare event. Notice that this holds because, even for big values of α, the event above occurs with positive probability, probably near

zero, but still positive. Then, applying the second Borel-Cantelli lemma[1] we have an infinite amount of i's such that $\|X_{(i)} - X_{(i+1)}\| > \alpha$, obtaining an infinite amount of connected components in the network induced by setting the transmission range to α. As a consequence, for a fixed value of α, we have a restriction on values for g and μ. More specifically, big values of g require much more higher values of μ.

In general, by fixing the transmission range to α we are obligated to maintain an equilibrium between granularity and density. The harmonious relationship between these two parameters is given by the result of Theorem 5. From there, we have

$$\begin{aligned} \alpha &= \frac{\ln(g^{a+1/2}) + \ln(\mu - 1)}{\mu}, \\ \exp\{\mu\alpha\} &= g^{a+1/2}\,(\mu - 1)\,, \\ \left(\frac{\exp\{\mu\alpha\}}{\mu - 1}\right)^{\frac{2}{3}} &= g, \end{aligned} \tag{4.19}$$

whenever we use the convergence factor $a = 1$.

Expression (4.19) give us an upper bound for the granularity according to the transmission range α and density μ. To visualize it properly, let us take as example $\alpha \in \{0.3, 0.4, 0.5\}$ and $5 \leq \mu \leq 30$. Figure 4.4 shows three curves corresponding to the upper bound, in each case, for the granularity g. We plot the relationship as continuous curves, but it is important to highlight that both, the density μ and granularity g, are discrete variables and has sense only under those conditions.

We perceive, through Figure 4.4, that extremely low-power radio devices are not suitable for medium to high scale homogeneous networks. As an example, let us make the assumption that each segment in the grid represents 100 meters in an urban scenario. We observe that a network with nodes configured to transmit up to 30 meters requires a dense deployment, about 30 nodes per segment, to be able to scale in size up to a grid of 42×42 while maintaining connectivity. In return, if we are able to give little more of power to nodes achieving a transmission range of 40 meters, with the same density above, we are able to maintain connectivity w.h.p. in much bigger scenarios, with granularities up to 315.

We just observed that small variations in the configuration of transmission range have high impact on the scalability of connectivity. This phenomenon occurs not just in the cases pictured in Figure 4.4, but in all cases included in the expression of Theorem 5. To understand this behavior, it is necessary to know how the unique

[1]The second Borel-Cantelli lemma states that if the events E_n are pairwise independent and the sum of the probabilities on the E_n diverges to infinity, then the probability that infinitely many of them occur is one.

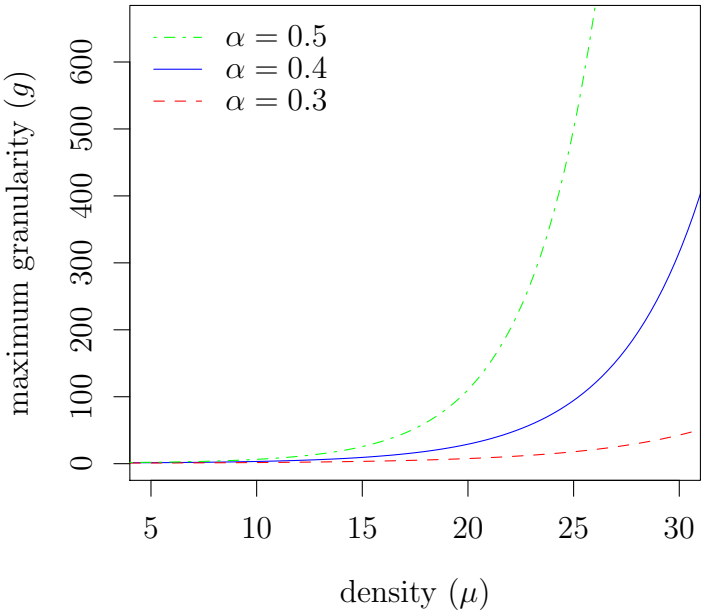

Figure 4.4. Relation between density and the upper bound for the granularity for three values of α

connected component of the network emerges as we increase the transmission range. With this knowledge we can observe the price we are paying for connecting the last two connected components in order to have connectivity in the overall network. If we are connecting with this last link two big connected components, then it is worth to pay this with extra resources (e.g. energy), otherwise, we can relax the connectivity requirement to γ-almost connectivity [Franceschetti and Meester, 2007], that is, to ensure connectivity to $\gamma \times 100$ percent of the nodes in the network, or equivalently, to contain $\gamma \times 100$ percent of nodes in the Giant component.

Figure 4.5 presents interesting evidence of how connectivity emerges as we increment the transmission range of nodes. We show two different measures: (i) the normalized quantity of connected components in the network, and (ii) the normalized size of the Giant component. We observe in this figure that the Giant component grows to a unique connected component very fast, and this phenomenon becomes faster and faster as we increment the density μ. Note that when the Giant component starts to grow, the proportion of connected components diminishes considerably. This implies that it is rare to have isolated nodes and a big Giant component in the same network.

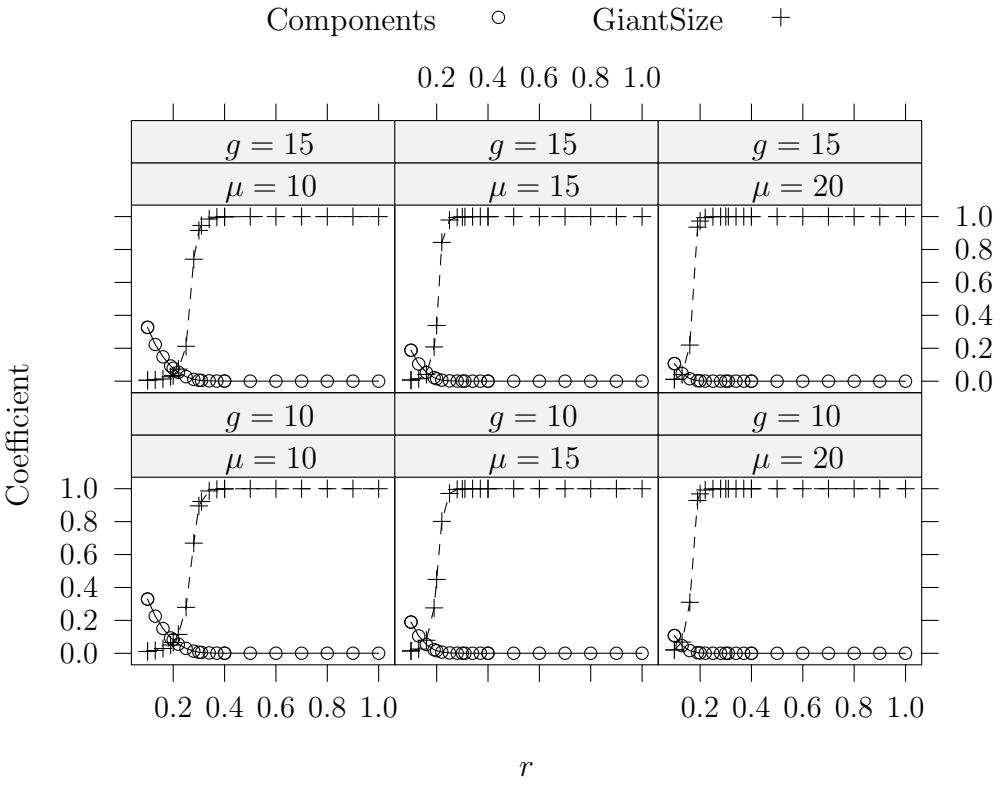

Figure 4.5. Proportion of connected components and proportional size of the Giant component.

Chapter 5

Final Remarks

In this work, we proposed and analyzed an alternative model for obstructed wireless networks, based on a grid structure of one-dimensional segments and two-dimensional intersections. This model provides a realistic representation of different network scenarios with obstacles and, at the same time, allows us to perform analythical characterizations, partly based on percolation theory and partly based on basic geometry. We analyzed three different approaches for modeling the geometric part of the network and derived tight bounds for probabilities of local connectivity at segments and intersections.

Initially, the result of Theorem 1, that computes a lower bound for $\Pr(I_{\text{con}}^{\text{MN}})$, was published in Almiron et al. [2012], together with a first version of the CTR for Connectivity presented in Theorem 5. Knowing about the difficulty for computing $\Pr(I_{\text{con}}^{\text{LS}})$, we proposed the Triangular model in Almiron et al. [2013], offering additionally a lower bound for $\Pr(I_{\text{con}}^{\text{T}})$. The tight lower bound of Theorem 3, considering all correlations while computing $\Pr(I_{\text{con}}^{\text{T}})$ was published in Almiron et al. [2014].

At this point, in Almiron et al. [2013], we added the convergence parameter, denoted by a, to the CTR for Connectivity, obtaining the result presented in Theorem 5. Notice that this result is definitive in the sense that does not depends on any visibility rule. In other words, if we consider other visibility rules or even if we take into consideration other elements (e.g. reflections on obstacles), the CTR for Connectivity does not change, it remains the same as presented in Theorem 5. What does change, in case more realistic visibility rules are added, is the critical value ϵ_c. The procedure for computing the critical value ϵ_c in any model was presented in Chapter 4, and it allows to compute new values of ϵ_c from an expression characterizing $\Pr(I_{\text{con}}^{\psi})$ for any given geometrical visibility criterion ψ.

We performed a study of the scalability of obstructed networks within the pro-

posed model and developed analytical methods to determine the possibility of obtaining connectivity with w.h.p. in homogeneous network topologies for specific combinations of characteristics, such as segments' width, the grid size and the technological limit of maximum transmission range. With that, we characterized scenarios that defy the limits of homogeneous network topologies and showed that, in sufficiently large networks deployed in obstructed environments with constrained segments' width or radio transmission range, it becomes necessary to make use of alternative topologies, such as, for example, heterogeneous topologies with auxiliary backbones of base stations connected by a wired network.

There is a number of possibilities for other future work based on our results. One might compute other connectivity properties, such as almost-connectivity and k-connectivity, and characterize several network properties, such as degree distribution of nodes. Such characterizations can assist in designing new topology-aware network algorithms. An interesting extension would be to look at other kinds of regular lattices to replace the underlying grid structure that we used.

Additionally, the PhD candidate has collaborated with some scientific works [Almiron et al., 2010; Ramos et al., 2010; Vieira et al., 2011], during the course, that even when they are not directly related to the main subject of this thesis, contributed to the maturity of ideas herein included.

Bibliography

Almiron, M. G., Goussevskaia, O., Frery, A. C., and Loureiro, A. A. (2012). Modeling and connectivity analysis in obstructed wireless ad hoc networks. In *ACM International Conference on Modeling, Analysis and Simulation of Wireless and Mobile Systems (MSWiM)*, pages 195--202.

Almiron, M. G., Goussevskaia, O., Frery, A. C., and Loureiro, A. A. (2014). Connectivity at crossroads. In *IEEE Annual International Symposium on Personal, Indoor, and Mobile Radio Communications (PIMRC)*, pages 1437--1441.

Almiron, M. G., Goussevskaia, O., Loureiro, A. A., and Rolim, J. (2013). Connectivity in obstructed wireless networks: From geometry to percolation. In *ACM International Symposium on Mobile Ad Hoc Networking and Computing (MobiHoc)*, pages 157--166.

Almiron, M. G., Ramos, H. S., Oliveira, E. M., de Menezes, J. G. M., Guidoni, D. L., Stancioli, P. O., da Cunha, F. D., de Aquino, A. L. L., Mini, R. A. F., Frery, A. C., and Loureiro, A. A. F. (2010). *Brazilian Symposium on Computer Networks and Distributed Systems (SBRC)*, chapter Redes Complexas na Modelagem de Redes de Computadores, pages 1--46. Brazilian Computer Society. Short Course.

Bollobás, B., Janson, S., and Riordan, O. (2009). Line-of-sight percolation. *Combinatorics, Probability & Computing*, 18(1–2):83--106.

Broadbent, S. R. and Hammersley, J. M. (1957). Percolation processes. *Mathematical Proceedings of the Cambridge Philosophical Society*, 53(03):629--641.

David, H. A. and Nagaraja, H. N. (2003). *Order Statistics*. Probability and Statistics. Wiley-Interscience, 3rd edition. ISBN 0-471-38926-9.

Desai, M. and Manjunath, D. (2002). On the connectivity in finite ad hoc networks. *IEEE Communications Letters*, 6(10):437--439.

Dette, H. and Henze, N. (1989). The limit distribution of the largest nearest neighbor link in the unit d-cube. *Journal of Applied Probability*, 26:67--80.

Franceschetti, M. and Meester, R. (2007). *Random Networks for Communication: From Statistical Physics to Information Systems*. Cambridge Series in Statistical and Probabilistic Mathematics. Cambridge University Press. ISBN 9780521854429.

Frieze, A., Kleinberg, J., Ravi, R., and Debany, W. (2007). Line-of-sight networks. In *ACM-SIAM Symposium on Discrete Algorithms (SODA)*, pages 968--977.

Frieze, A. M., Kleinberg, J. M., Ravi, R., and Debany, W. (2009). Line-of-sight networks. *Combinatorics, Probability & Computing*, 18(1–2):145--163.

Ghasemi, A. and Nader-Esfahani, S. (2006). Exact probability of connectivity in one-dimensional ad hoc wireless networks. *IEEE Communications Letters*, 10(4):251--253.

Gilbert, E. N. (1961). Random plane networks. *Journal of the Society for Industrial and Applied Mathematics (SIAM)*, 9(4):533--543.

Goussevskaia, O., Halldórsson, M. M., Wattenhofer, R., and Welzl, E. (2009). Capacity of arbitrary wireless networks. In *IEEE International Conference on Computer Communications (INFOCOM)*, pages 1872--1880.

Grimmett, G. (1999). *Percolation*. Springer-Verlag, second edition.

Gupta, P. and Kumar, P. R. (2000). The Capacity of Wireless Networks. *IEEE Transactions on Information Theory*, 46(2):388--404.

Haenggi, M. and Ganti, R. K. (2009). Interference in large wireless networks. *Foundations and Trends in Networking*, 3(2):127--248.

Holst, L. (1980). On multiple covering of a circle with random arcs. *Journal of Applied Probability*, 16:284--290.

Huson, M. and Sen, A. (1995). Broadcast scheduling algorithms for radio networks. In *IEEE Military Communications Conference (MILCOM)*, volume 2, pages 647--651.

Kolchin, V., Sevast'yanov, B., and Chistyakov, V. (1978). *Random Allocations*. V. H. Winston & Sons.

Labrador, M. A. and Wightman, P. M. (2009). *Topology Control in Wireless Sensor Networks*. Springer.

Lotker, Z. and Peleg, D. (2010). Structure and algorithms in the SINR wireless model. *ACM SIGACT News*, 41(2):74--84.

Miorandi, D. and Altman, E. (2006). Connectivity in one-dimensional ad hoc networks: A queueing theoretical approach. *Wireless Networks*, 12(5):573--587.

Nekoui, M. and Pishro-Nik, H. (2009). Geometrical analysis of obstructed wireless networks. In *IEEE Information Theory Workshop*, pages 589--593.

Penrose, M. (1999a). A strong law for the largest nearest-neighbour link between random points. *Journal of London Mathematical Society*, 60(2):951--960.

Penrose, M. (2003). *Random geometric graphs*. Oxford studies in probability. Oxford University Press. ISBN 9780198506263.

Penrose, M. D. (1997). The longest edge of the random minimal spanning tree. *The Annals of Applied Probability*, 7(2):340--361.

Penrose, M. D. (1999b). On k-connectivity for a geometric random graph. *Random Structures & Algorithms*, 15(2):145--164.

Ramos, H. S., Almiron, M. G., Frery, A. C., Nakamura, E. F., and Loureiro, A. A. F. (2010). Node deployment by stochastic point processes in wireless sensor networks. In *International Telecommunication Symposium (ITS)*, pages 1--5.

Santi, P. (2005a). *Topology Control in Wireless Ad Hoc and Sensor Networks*. John Wiley & Sons Ltd.

Santi, P. (2005b). Topology control in wireless ad hoc and sensor networks. *ACM Computing Surveys*, 37(2):164--194.

Santi, P. and Blough, D. (2003). The critical transmitting range for connectivity in sparse wireless ad hoc networks. *IEEE Transactions on Mobile Computing*, 2(1):25--39.

Vieira, L. F. M., Almiron, M. G., and Loureiro, A. A. F. (2011). 3d manets: Link probability, node degree, network coverage and applications. In *IEEE Wireless Communications and Networking Conference (WCNC)*, pages 2042--2047.